RSC Applied Interfaces

Accepted Manuscript

This article can be cited before page numbers have been issued, to do this please use: A. Panda, L. Nayak, T. Hati, N. Das and P. Parhi, *RSC Appl. Interfaces*, 2026, DOI: 10.1039/D6LF00096G.

ROYAL SOCIETY OF CHEMISTRY

rsc.li/RSCApplInter

View Article Online
DOI: 10.1039/D6LF00096G

Beyond Iron: Interface-Coupled Non-Ferrous Photo-Fenton-Like Catalysts for Boosted H_2O_2 Activation in Environmental Remediation

Akash Panda, [a] Lipika Nayak, [a] Tusharkanta Hati, [a] Nigamananda Das, [b] Purnendu Parhi*[a]

[a] Department of Chemistry, Ravenshaw University, Cuttack-753003, Odisha, India

[b] Department of Chemistry, Utkal University, Bhubaneswar-751004, Odisha, India

*E-mail: pparhi@ravenshawuniversity.ac.in, Phone: +91-8895193144

Abstract

The persistent presence of emerging pollutants, including antibiotics, dyes, and pharmaceutical residues in water environments, poses substantial environmental and public health risks. Conventional treatment approaches, such as Fe-based Fenton processes, are restricted by narrow pH requirements, excessive sludge formation, and poor utilization of visible light. In recent years, non-ferrous transition-metal-based catalysts, particularly those incorporating Cu, Co, Mn, Bi, and Ce, have emerged as promising alternatives due to their flexible redox chemistry, broader pH adaptability, and enhanced photo-assisted H_2O_2 activation. More importantly, interface engineering has been established as a pivotal strategy to amplify photo-Fenton-like performance by promoting interfacial charge separation, accelerating reactive oxygen species (ROS) generation, and stabilizing metal redox cycling. Approaches involving semiconductor heterojunctions, carbonaceous frameworks, layered double hydroxides, defect-rich architectures, and oxygen-vacancy modulation are systematically discussed. This review critically summarizes recent advances in the design, mechanistic understanding, and performance of interface-engineered non-ferrous photo-Fenton catalysts for environmental

View Article Online
DOI: 10.1039/D6LF00096G

remediation. We focus on structure-activity relationships, synergistic effects, and pollutant-specific degradation pathways, while also addressing challenges and opportunities toward sustainable water remediation. Current challenges and future perspectives toward scalable, sustainable, and efficient Fenton-like systems are also outlined, providing a comprehensive roadmap for the rational development of next-generation Fenton-like systems beyond iron.

1. Introduction

Since the beginning of the 21st century, water pollution has become a serious problem that exerts a significant impact on the ecological environment and human survival.[1,2] Organic dyes,[3,4] benzene-based organics,[5,6] pesticides,[7] and antibiotics[8,9] are the main pollutants of concern in wastewater due to their high toxicity and hardly degradable characteristics. Recent comprehensive analyses of Fenton and Fenton-like advanced oxidation processes (AOPs) have highlighted their effectiveness in degrading pharmaceutical and pesticide contaminants, while also emphasizing the potential formation of transformation by-products and associated environmental risks, underscoring the need for more controlled and sustainable oxidation strategies.[10] Conventional biological and physicochemical processes, though widely implemented, often prove inadequate for the degradation of emerging contaminants (ECs) due to their complex structures, low biodegradability, and persistent environmental behaviour. To overcome these drawbacks, powerful treatment technologies exploiting reactive oxygen species (ROS), notably hydroxyl radicals (•OH), achieve rapid, non-selective degradation and mineralization of refractory organic pollutants.[11–13] Among these, the homogeneous Fenton reaction, which produces highly reactive hydroxyl radicals (•OH) through the Fe^{2+}/H_2O_2 system, has been extensively applied owing to its high efficiency, low cost, and operational simplicity.[14,15] The catalytic performance can be further enhanced under solar or ultraviolet irradiation in the photo-Fenton process, where light-assisted electron transfer accelerates metal redox cycling and promotes sustained H_2O_2 activation, leading to the continuous generation of

View Article Online
DOI: 10.1039/D6LF00096G

ROS such as •OH, $^1O_2$, and $•O_2^-$.[16,17] In a typical heterogeneous photo-Fenton process, metal ions immobilized on a solid support react with H_2O_2 under UV/visible light, creating electron-hole pairs and •OH radicals, which decompose organic contaminants.[18] Despite these advantages, classical homogeneous Fenton processes suffer from intrinsic drawbacks, including the requirement for strongly acidic conditions (pH 2–3), generation of iron-containing sludge, and loss of the catalyst in the effluents, which causes secondary pollution and catalyst loss.[19,20] To address these challenges, heterogeneous Fenton catalysts, such as iron-containing solids,[21–23] have been developed as alternatives to the homogeneous Fenton process. These catalysts avoid the need for large amounts of reducing metal ions, which has been an active research area in this field. Consequently, a variety of iron-based heterogeneous photo-Fenton catalysts, such as Fe@MIL-100(Fe), Fe/Fe_3O_4 composites, Fe_3O_4@void@TiO_2, Fe–Co PBAs, and α-Fe_2O_3@g-C_3N_4 have been developed to improve catalyst recovery and stability.[24–28] However, most of these systems remain effective only under acidic conditions, exhibiting significantly diminished catalytic performance at neutral or alkaline pH, thereby limiting their practical applicability. Moreover, iron-based catalysts often suffer from sluggish charge-transfer kinetics, insufficient active-site availability, and poor visible-light utilization.[29,30]

To overcome these limitations, recent research has shifted toward the development of non-iron photo-Fenton-like catalysts capable of operating over a broader pH range with improved efficiency and stability. Alternative transition and post-transition metal systems, including Cu, Co, Mn, Bi, and Ce, have attracted increasing attention due to their favourable redox properties, more flexible operating conditions, and enhanced visible-light absorption. This paradigm shift mirrors the development of non- TiO_2 based photoanodes, where the focus has moved toward optimizing visible-light utilization and establishing clear synthesis–structure–mechanism–activity relationships to enhance practical wastewater treatment performance. In particular,

View Article Online
DOI: 10.1039/D6LF00096G

their ability to function efficiently from near-neutral to alkaline pH conditions provides a distinct advantage over Fe-based catalysts.[31] For example, Cu-based catalysts activate H_2O_2 at near-neutral pH through the Cu^+/Cu^{2+} redox cycle,[32–34] while Co- and Mn-based systems rely on multivalent redox and oxygen-vacancy-mediated pathways that are enhanced under visible light;[35–37] Bi- and Ce-based catalysts, in contrast, facilitate H_2O_2 activation primarily via photogenerated charge carriers and oxygen-vacancy-assisted interfacial electron transfer.[38,39]

However, the standalone catalytic performance of these metals is often limited by inefficient separation of photoinduced charge carriers, poor light-harvesting capability, or leaching of active species. To overcome these challenges, interface engineering strategies have gained significant attention. By constructing heterojunctions with suitable semiconductors (e.g., MoS_2, BiOBr), introducing carbonaceous supports (e.g., rGO, CNTs, biochar), or integrating porous scaffolds (e.g., MOFs, LDHs), researchers have been able to modulate the electronic structure, improve charge separation, and stabilize active species. The interfacial design is not merely structural; it fundamentally reshapes the energy band alignment, oxygen vacancies, and surface functionalities that dictate ROS generation. Importantly, interface engineering establishes built-in electric fields, suppresses charge recombination, and minimizes metal leaching, advantages not achievable through simple blending or doping.

Recent studies have demonstrated that Z-scheme and S-scheme heterojunctions integrating non-ferrous Fenton-like active components can markedly enhance photo-Fenton degradation by promoting spatial separation of photogenerated electrons and holes while preserving strong redox potentials for H_2O_2 activation. For instance, CuO/CDs/g-C_3N_4 nanocomposites exhibit superior visible-light-driven activity due to accelerated interfacial charge transfer and rapid Cu^+/Cu^{2+} cycling, which sustains continuous H_2O_2 activation.[40] Similarly, Bi_2WO_6/CoAl-LDHs S-scheme heterojunctions exhibit outstanding photo-Fenton-like activity by leveraging an interfacial electric field to drive directional charge separation while maintaining strong

View Article Online
DOI: 10.1039/D6LF00096G

redox potentials, thereby enabling efficient H_2O_2 activation and cobalt-mediated •OH generation for rapid antibiotic degradation.[41]

In parallel, the incorporation of carbonaceous matrices such as reduced graphene oxide (rGO), graphitic carbon nitride (g-C_3N_4), and biomass-derived biochar offers multifaceted advantages for non-ferrous photo-Fenton-like catalysis. These conductive frameworks promote rapid electron transport, provide abundant surface functionalities for H_2O_2 adsorption, and stabilize metal active sites, thereby facilitating efficient redox cycling. When coupled with Mn or Co-based oxides, the resulting composites demonstrate enhanced Fenton-like reactivity, often under neutral pH conditions and with low metal leaching. Moreover, the interfacial synergy between the metal oxide and the carbon support serves to suppress radical scavenging pathways and extend ROS lifetimes. Carbon-based interfaces also improve mechanical stability, surface area, and pollutant adsorption, further supporting improved photocatalytic performance. For instance, in $CuO_x{\cdot}Ag_2O$/RGO systems, the highly conductive and defect-rich carbon support acts as an efficient electron mediator and anchoring scaffold, promoting rapid charge transport, stabilizing metal active sites, and sustaining metal redox cycling for efficient H_2O_2 activation.[42]

Bismuth-based materials, particularly layered BiOX (X = Cl, Br, I) compounds, represent an emerging yet highly promising class of non-ferrous photo-Fenton-like catalysts.[36,43] Their unique internal electric fields (IEF) facilitate rapid charge separation, while their tunable band structures allow for visible-light absorption and high ROS generation. Interface engineering with materials like MOFs or g-C_3N_4 further augments their catalytic properties, enabling efficient removal of diverse organic contaminants under simulated or natural sunlight with minimal secondary pollution. Consequently, Bi-based heterostructures have emerged as powerful candidates for sunlight-driven advanced oxidation processes, particularly when combined with strategies to modulate defects and interfaces.

View Article Online
DOI: 10.1039/D6LF00096G

Despite these advances, a unified understanding of the underlying reaction pathways, advantages, and challenges of non-ferrous photo-Fenton catalysts remains fragmented. Existing reviews often focus on individual metal systems or broadly discuss Fenton-like processes without systematically addressing the synergistic role of interface engineering, such as heterojunction construction, carbon coupling, and defect modulation. Furthermore, few reviews provide a comparative perspective across different non-ferrous systems under similar conditions, nor do they sufficiently address key practical issues such as catalyst stability, reusability, pollutant selectivity, or scalability. Thus, a unified and comparative evaluation of interface-engineered non-ferrous catalysts is urgently needed to guide future material development.

This review aims to bridge these gaps by presenting a systematic and comparative analysis of non-ferrous (Cu, Co, Mn, Ce, and Bi) photo-Fenton catalysts, with a special emphasis on interface engineering approaches that have enabled performance breakthroughs. It will explore:

1. The fundamentals of redox cycling and ROS generation in non-ferrous systems.
2. Recent advances in nanocomposite design with structural and electronic interface modulation.
3. Reported degradation performance of key pollutants (antibiotics, dyes, PPCPs).
4. Mechanistic insights into charge dynamics and active species generation.
5. Current limitations, environmental considerations, and future research outlook.

In doing so, this review highlights not only the evolution of photo-Fenton chemistry "beyond iron," but also the emerging paradigm of interfacial nanoarchitectures as the foundation for next-generation water treatment technologies. An overview of this review is illustrated in Fig. 1. We aim to provide a blueprint for researchers and engineers working at the nexus of materials

View Article Online
DOI: 10.1039/D5LF00096G

chemistry, environmental catalysis, and sustainable water remediation, with a critical eye toward the practical hurdles of selectivity, long-term stability, and scalable deployment that must be overcome for real-world application.

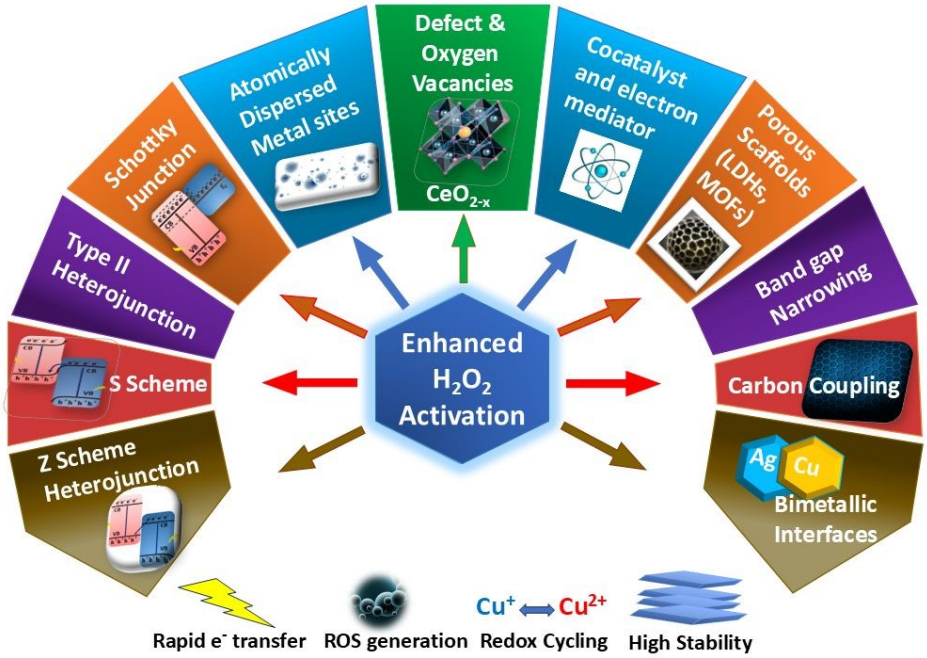

Fig. 1 Overview of interface-engineered non-ferrous photo-Fenton-like catalysis for pollutant degradation.

2. Fundamentals of Non-Ferrous Photo-Fenton Catalysis

The photo-Fenton process is a synergistic system that integrates semiconductor photocatalysis with Fenton-like redox chemistry. Its enhanced efficacy relies on multiple, often simultaneous, pathways for generating reactive oxygen species (ROS). To understand the advantages of non-ferrous catalysts, it is essential to first define the baseline mechanisms and limitations of the classic iron-based system.

2.1 Mechanism Overview of Photo-Fenton and Fenton-like Reactions

View Article Online
DOI: 10.1039/D5LF00096G

The traditional Fenton mechanism centres on Fe^{2+} activating H_2O_2 to generate hydroxyl radicals (•OH), as represented by:[44]

Fenton Reaction (Dark)

$Fe^{2+} + H_2O_2 \rightarrow Fe^{3+} + OH^- + \bullet OH$ ($k = 40 - 80 M^{-1} s^{-1}$)

$Fe^{3+} + H_2O_2 \rightarrow Fe^{2+} + H^+ + HO_2\bullet$ ($k = 0.001 - 0.01 M^{-1} s^{-1}$)

The primary limitation of the dark Fenton process is the extremely slow regeneration of Fe^{2+} from Fe^{3+}, which is the rate-determining step and requires acidic conditions to keep Fe^{3+} in solution.

Photo-Fenton Enhancement

In photo-Fenton systems, light exposure accelerates Fe^{3+} reduction and promotes additional radical formation:

$[Fe(OH)]^{2+} + h\nu \rightarrow Fe^{2+} + \bullet OH$

This photoreduction step is essential for maintaining continuous Fe^{2+} regeneration, but it is inefficient under visible light and becomes unstable at higher pH.

Non-ferrous metal-based photo-Fenton-like redox cycles

When non-ferrous metals are introduced, similar redox cycles are invoked:

- $Cu^+ + H_2O_2 \rightarrow Cu^{2+} + \bullet OH + OH^-$
- $Cu^{2+} + H_2O_2 \rightarrow Cu^+ + \bullet OOH + H^+$
- $Co^{2+} + H_2O_2 \rightarrow Co^{3+} + \bullet OH + OH^-$
- $Ce^{3+} + H_2O_2 \rightarrow Ce^{4+} + \bullet OH + OH^-$
- $Mn^{2+} + H_2O_2 \rightarrow Mn^{3+} + \bullet OH + OH^-$

View Article Online
DOI: 10.1039/D5LF00096G

- Ce^{3+}/Ce^{4+} cycles facilitate electron shuttling and oxygen-vacancy creation, although Ce-based reactions often rely more on interface-assisted H_2O_2 activation than direct Fenton reactions
- Bi-based systems typically activate H_2O_2 indirectly through oxygen vacancies and photogenerated charge carriers rather than classical redox cycling.
- Cu^+/Cu^{2+}, Co^{2+}/Co^{3+}, and Mn^{2+}/Mn^{3+} efficiently mediate ROS generation in the presence of H_2O_2 and photons.

These metals often show consistent activity and consistently maintain activity over a broader pH range, and avoid sludge formation. Their faster electron-transfer kinetics also facilitate the rapid generation of ROS under solar or visible-light illumination**.**

Photo-induced charge carrier participation

In photo-Fenton and photo-Fenton-like systems, the light-driven excitation of electrons (e^-) and holes (h^+) in semiconductors or composites further enhances radical formation:

$h^+ + H_2O \rightarrow \bullet OH + H^+$

$h^+ + OH^- \rightarrow \bullet OH$

$e^- + O_2 \rightarrow \bullet O_2^-$

$\bullet O_2^- + H^+ \rightarrow HO_2\bullet \rightarrow$ (secondary ROS)

These pathways indicate that both redox cycling and semiconductor photoexcitation contribute simultaneously, giving rise to multiple ROS species (•OH, $\bullet O_2^-$, •OOH, $^1O_2$, and even H_2O_2 regeneration in some cases).

Non-radical oxidation pathways and interface effects

In addition to conventional radical pathways dominated by •OH, increasing evidence suggests that non-radical oxidation mechanisms play a crucial role in non-ferrous photo-Fenton systems, particularly in interface-engineered catalysts. These pathways primarily involve singlet oxygen ($^1O_2$) generation and direct interfacial electron transfer, which exhibit higher selectivity and resistance to matrix interference.

Interface features such as oxygen vacancies (OVs), defect-rich surfaces, and specific exposed crystal facets significantly influence this transition. Oxygen vacancies act as electron-rich centres that facilitate the adsorption and activation of dissolved O_2 or H_2O_2, promoting the formation of surface-bound superoxide intermediates ($•O_2^-$), which can subsequently convert into $^1O_2$ via energy-transfer pathways. Unlike free •OH radicals, these processes occur on the catalyst surface, minimizing non-selective oxidation.

Moreover, facet engineering (e.g., BiOBr (010) or CeO_2 (111)) alters the local electronic structure and adsorption configuration, enabling selective electron transfer to oxygen species rather than homolytic H_2O_2 cleavage. In addition, interfacial electric fields in S-scheme and Z-scheme heterojunctions drive directional charge migration, enriching electrons at specific active sites that favour O_2 activation and $^1O_2$ generation.

Such non-radical pathways are particularly prominent in Cu–N_4 coordinated systems and oxygen-vacancy-rich Bi- and Ce-based catalysts, where strong metal–support interactions and defect-mediated charge redistribution suppress excessive •OH formation and promote surface-mediated oxidation routes. These findings highlight that rational interface design not only enhances catalytic efficiency but also fundamentally alters the dominant reaction mechanism.

Additional synergistic pathways

Synergistic mechanisms typically include:

View Article Online
DOI: 10.1039/D6LF00096G

- Direct oxidation of pollutants by h^+ (valence band holes)
- Reduction of H_2O_2 by photo-generated e^- to yield •OH or $•O_2^-$:

  $H_2O_2 + e^- \rightarrow •OH + OH^-$

  $H_2O_2 + e^- \rightarrow •O_2^- + 2H^+$
- Activation of H_2O_2 at oxygen vacancies (OVs), common in CeO_2, MnO_x, and BiOX:

  $Ov + H_2O_2 \rightarrow •OH + OH^-$
- Energy-band alignment in heterojunctions, enabling vectorial charge migration and suppressing carrier recombination.

Thus, non-ferrous photo-Fenton catalysis often involves multi-pathway ROS generation driven by both metal-centred reactions and photocatalytic charge transfer. This hybrid mechanism differentiates it from classical Fe-based systems and underpins the superior efficiency observed in interface-engineered composites (Fig. 2). Consistent with these mechanistic advantages, most non-ferrous photo-Fenton-like catalysts exhibit significantly higher degradation rates in H_2O_2-assisted systems than in H_2O_2-free photocatalytic processes, as summarized in Table 1.

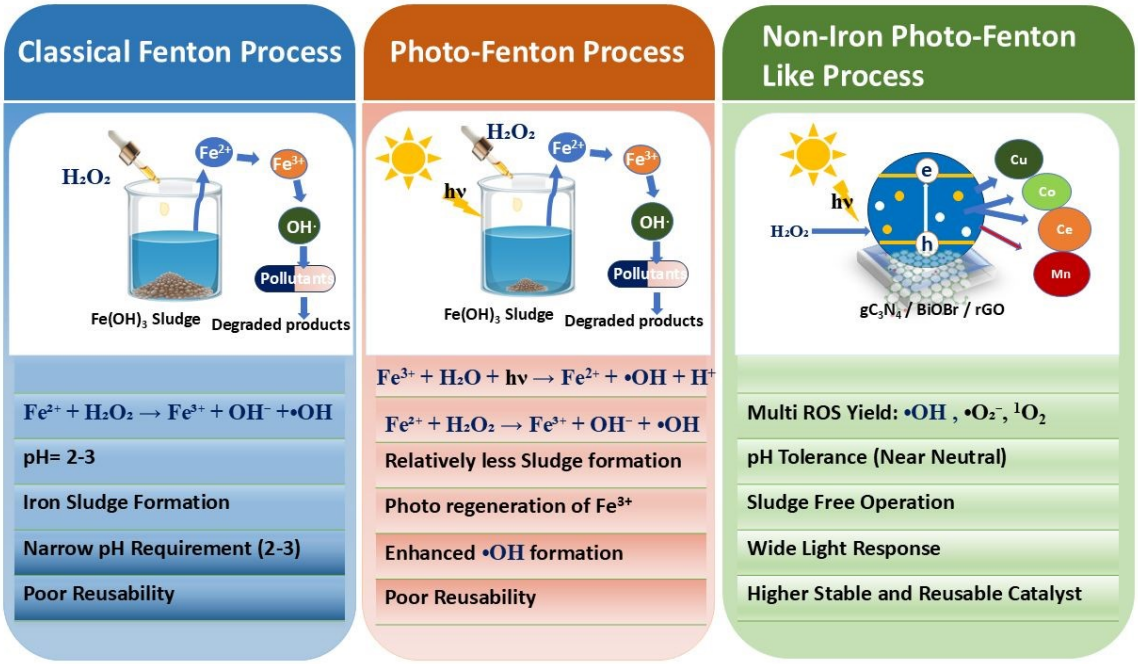

Fig. 2 Comparison of classical Fenton, photo-Fenton, and non-iron photo-Fenton-like catalytic processes.

Table 1. Photocatalytic performance of non-ferrous photo-fenton-like catalysts with and without H_2O_2

Catalyst	Pollutant	Light Source	k (min^{-1})	Degradation (%)	Main ROS	Activity Without H_2O_2 (%)	Activity With H_2O_2	Ref
V_O-Cu_2O@Cu/CN_x	Tetracycline (TC, 20 mg/L)	Visible LED (λ > 420 nm)	0.2	100	$^1O_2$	Moderate (54.4)	Strong enhancement due to Cu^0 and oxygen vacancies, which accelerates the Cu redox cycle	45
Cu-Bi_2O_2S	Tetracycline Hydrochloride (TCH, 50 mg/L)	Visible LED Lamp	0.0243	77.76	•OH	Low (18.4)	Strong due to Cu-cocatalysts, which enhance charge carrier mobility and separation	46
$BiWO_6$/CoAl LDH	Oxytetracycline (OTC, 10 mg/L)	300 W Xenon Lamp (λ > 420 nm)	-	98.47	$•O_2^-$, •OH	Moderate (41.37)	Stronger S-scheme heterojunctions facilitate cobalt-mediated H_2O_2 activation	41
$Cu_{2-x}S$/g-C_3N_4	Rhodamine B (RhB, 30 mg/L)	300 W Xenon Lamp	0.172	99.6	$•O_2^-$	Very low (2.1)	High due to Nitrogen vacancies and internal electric fields, which promote Cu^+/Cu^{2+} cycling and suppress recombination	47
BiOBr/Co_3O_4	Methylene Blue (MB, 10 mg/L)	500 W Xenon Lamp	-	96	$•O_2^-$, •OH	Moderate (27)	Significantly higher due to hierarchical nanowires and BiOBr/Co_3O_4 heterojunctions, which drive visible-light, Co-mediated H_2O_2 activation	36

Prussian Blue/Mn_3O_4	Levofloxacin (LVF)	30 W Visible LED	0.076	93.9	$^1O_2$	Moderate (74.2)	High due to Z-scheme p-n heterojunctions, which enable Fe/Mn valence cycling and continuous non-radical $^1O_2$ generation	48
Mn doped Cobalt silicate@diatomite	Methyl Orange (MO, 50 mg/L)	UV Lamp	0.0226	95	•OH	Low (20)	Stronger due to Due to manganese doping, which increases surface area and creates a Co-Mn bimetallic synergy that lowers the H_2O_2 activation energy.	35
$gC_3N_4/ZnCo_2O_4$	Rhodamine B (RhB, 10 mg/L)	40 W Visible LED	0.03	94	•OH	Moderate (39)	High due to Due to a Z-scheme heterojunction enhancing separation and enables the effective activation of H_2O_2 at neutral pH.	49

2.2 Unique Roles of Cu, Co, Mn, Bi, and Ce in Fenton-like Photocatalysis

Copper (Cu)

Copper-based photocatalysts, including CuO, Cu_2O, and Cu-modified g-C_3N_4 exhibit efficient redox cycling between Cu^+ and Cu^{2+}, enabling rapid activation of H_2O_2 through:

$$Cu^+ + H_2O_2 \rightarrow Cu^{2+} + \bullet OH + OH^-$$

This redox versatility promotes continuous ROS production, especially under visible light, where photoexcited electrons readily reduce Cu^{2+} back to Cu^+. Cu–O bonds and oxygen-

View Article Online
DOI: 10.1039/D5LF00096G

vacancy-rich CuO_x surfaces facilitate interfacial electron transfer, suppressing charge recombination and extending radical lifetimes.

Due to their suitable band gaps (1.2-2.1 eV), Cu-based catalysts exhibit strong visible-light absorption and maintain high activity near neutral pH, overcoming the acidic limitations of Fe-based Fenton systems.[50] Their performance further improves in heterojunctions with g-C_3N_4, TiO_2, or $BiVO_4$, where Z-scheme or p-n architectures enable directional charge migration.[40,51,52] Nanostructuring (e.g., hollow spheres, nanowires) and hybridization with MOFs or carbon dots enhance surface reactivity, adsorption behaviour, and long-term stability.[40,53] Collectively, Cu-based photocatalysts represent one of the most efficient and tunable non-ferrous systems for photo-Fenton water purification.

Cobalt (Co)

Cobalt-based catalysts, including Co^{2+} salts, Co_3O_4, $CoAl_2O_4$, and Co-LDHs, exhibit strong Fenton-like behaviour due to the Co^{2+}/Co^{3+} redox couple.[35,41] The primary H_2O_2 activation step occurs via:

$$Co^{2+} + H_2O_2 \rightarrow Co^{3+} + \bullet OH + OH^-$$

Under illumination, photoexcited electrons reduce Co^{3+} to Co^{2+}, sustaining continuous ROS generation. Cobalt oxides are typically p-type semiconductors, enabling strong hole-mediated oxidation pathways, especially under visible light. When integrated with carbon materials, MOFs, or semiconductors ($BiVO_4$, g-C_3N_4), Co-based composites exhibit enhanced charge transfer, broadened light absorption, and improved recyclability.[54] Their stability, tunable structure, and robust catalytic kinetics make cobalt systems excellent candidates for solar-driven Fenton-like processes.

Manganese (Mn)

View Article Online
DOI: 10.1039/D6LF00096G

Manganese-based catalysts, such as MnO_2, Mn_3O_4, MnOOH, and Mn-doped semiconductors benefit from multi-valence cycling among $Mn^{2+}/Mn^{3+}/Mn^{4+}$, enabling activation of H_2O_2 and even O_2 under illumination:[35,55]

$$Mn^{2+} + H_2O_2 \rightarrow Mn^{3+} + \bullet OH + OH^-$$

Defect-rich MnO_2 contains abundant surface hydroxyls and oxygen vacancies, which facilitate H_2O_2 adsorption, pollutant binding, and radical production. Although MnO_2 alone shows limited light absorption, its performance improves significantly when coupled with g-C_3N_4, $BiVO_4$, carbon supports, or LDHs, which enhance charge separation and visible-light utilization.[56,57] Mn-based perovskites (e.g., $LaMnO_3$) offer strong structural stability and flexible electronic configurations.[58] Due to their low toxicity, favourable redox characteristics, and cost-effectiveness, Mn-based catalysts are well-suited for the degradation of antibiotics, dyes, and phenolic pollutants under mild conditions.

Bismuth (Bi)

Bismuth-based photocatalysts BiOBr, Bi_2O_3, Bi_4MoO_9, and $BiVO_4$ are uniquely characterized by their layered structures and internal electric fields (IEFs), which strongly promote charge separation under visible light.[36,43,59] While Bi is not classically redox-active with H_2O_2, Bi-based materials can indirectly activate H_2O_2 through photogenerated h^+/e^- pairs, oxygen vacancies, and interfacial charge transfer within heterostructures.

BiOBr and $BiVO_4$ readily form type-II, S-scheme, or Z-scheme junctions with g-C_3N_4, TiO_2, or MoS_2, enabling enhanced ROS formation (•OH, $\bullet O_2^-$, $^1O_2$).[60,61] Their high visible-light response, low toxicity, and tunable band structures make Bi-based systems particularly effective for pharmaceuticals, dyes, and endocrine-disrupting chemicals under ambient or solar irradiation.

View Article Online
DOI: 10.1039/D6LF00096G

Cerium (Ce)

Cerium-based catalysts, particularly CeO_2 and Ce-doped composites, are distinguished by the Ce^{3+}/Ce^{4+} redox couple and high concentration of oxygen vacancies (OVs). Unlike Cu or Co, Ce does not strongly activate H_2O_2 via classical homogeneous Fenton reactions. Instead, Ce-based catalysis relies on:

- OV-assisted H_2O_2 adsorption and activation,
- Ce^{3+}/Ce^{4+} electron shuttling,
- surface hydroxyl-mediated ROS formation, and
- improved charge separation in heterojunctions.

CeO_2 readily forms composites with g-C_3N_4, BiOBr, or rGO, where its OVs enhance interfacial electron transfer and promote the generation of •OH and $•O_2^-$.[62–64] Ce-based photocatalysts also maintain structural stability over a wide pH range, making them attractive for practical wastewater treatment applications. These structure-activity relationships, including oxygen-vacancy-mediated H_2O_2 activation, redox shuttling behaviour, and associated challenges, are comparatively summarized in Table 2.

Table 2. Key Features, H_2O_2 Activation Mechanisms, and Challenges of Non-Ferrous (Cu, Co, Mn, Bi, Ce) Photo-Fenton-Like Catalysts.

Catalyst System	**Key Unique Features & Advantages**	**Primary H_2O_2 Activation Mechanism**	**Challenge & Interface Strategy**
Copper (Cu)	• Strong visible-light absorption • High activity at neutral pH	Direct (Fenton-like): Cu^+/Cu^{2+} redox couple	**Leaching:** Addressed by carbon supports and MOF encapsulation

Cobalt (Co)	• High intrinsic catalytic activity • Magnetic recoverability (spinels)	Direct (Fenton-like): Co^{2+}/Co^{3+} redox couple	**Toxicity/Cost:** Mitigated by doping (Ni/Mn) and core-shell structures
Manganese (Mn)	• Low toxicity • Earth-abundant • Multi-valence states	Direct (Fenton-like): $Mn^{2+}/Mn^{3+}/Mn^{4+}$ redox couple	**Low Solar Response:** Improved via Z-scheme S-scheme coupling with g-C_3N_4 or TiO_2
Bismuth (Bi)	• Strong internal electric fields (IEF) • Excellent charge separation • Low toxicity	Indirect (Photocatalytic): via h^+/e^-, Oxygen vacancies (OVs), and IEFs	**Weak Activation:** Enhanced by Oxygen Vacancy & construction of advanced heterojunctions.
Cerium (Ce)	• High oxygen-vacancy concentration • Wide pH stability • OV-mediated activation pathway	Indirect (Photocatalytic): via OVs & Ce^{3+}/Ce^{4+} shuttle	**Defect-dependence & low visible-light absorption:** Increasing OV density and forming a heterojunction with BiOBr or gC_3N_4

2.3 Key Parameters Influencing the Activity of Non-Ferrous Photo-Fenton Catalysts

The catalytic performance of non-ferrous photo-Fenton-like systems is governed by a complex interplay of intrinsic electronic properties, surface chemistry, and interfacial architecture. Optimizing these parameters is essential for efficient H_2O_2 activation, ROS generation, and visible-light-driven pollutant degradation. This section discusses the fundamental physicochemical factors redox potential, band structure, surface area and porosity, defect chemistry, and interface modulation with a specific emphasis on cerium (Ce), alongside Cu, Co, Mn, and Bi.

a. Redox Potential and Valence Flexibility

The ability of a metal centre to undergo reversible redox transformations directly influences its capacity to activate H_2O_2 and sustain ROS production. Non-ferrous metals such as Cu, Co, Mn, and Ce possess diverse valence states that enable electron exchange under light

View Article Online
DOI: 10.1039/D6LF00096G

illumination. Their standard redox potentials (E^0) determine the thermodynamic feasibility of the ROS generation process:[44,65]

- Cu^+/Cu^{2+}: +0.17 V vs. NHE
- Co^{2+}/Co^{3+}: +1.81 V vs. NHE
- Mn^{2+}/Mn^{3+}: +1.51 V vs. NHE
- Fe^{2+}/Fe^{3+}: +0.77 V vs. NHE
- Ce^{3+}/Ce^{4+}: +1.72 V vs. NHE

Copper's relatively low redox potential favours rapid Cu^{2+}/Cu^+ cycling even at near-neutral pH,[50] while Co and Mn serve as stronger oxidants capable of promoting efficient •OH generation. The Ce^{3+}/Ce^{4+} couple provides an effective electron-shuttling mechanism; photoexcited electrons readily reduce Ce^{4+} to Ce^{3+}, which enhances catalytic cycling and simultaneously promotes oxygen-vacancy formation. This valence flexibility plays a pivotal role in pollutant mineralization, particularly when these metals are incorporated into composite or heterojunction frameworks.[38]

b. Band Gap and Light Absorption

The catalyst's band gap governs its ability to absorb sunlight and generate electron–hole pairs. Representative band-gap values for key non-ferrous photocatalysts include:[66–69]

CuO: ~1.3 eV

MnO_x (e.g., alpha-MnO_2): ~1.5 eV

BiOBr: ~2.7 eV

Co_3O_4: ~1.6 eV

View Article Online
DOI: 10.1039/D6LF00096G

CeO_2: ~3.0–3.2 eV (can be narrowed by doping/defects)

While pristine CeO_2 absorbs mainly UV light due to its wide band gap, defect engineering (oxygen vacancies),[70] aliovalent doping,[71] or hybridization with visible-light-responsive semiconductors[72] (e.g., g-C_3N_4, BiOBr, WO_3) induces mid-gap or defect states. The presence of these states enables visible-light utilization and accelerates charge-carrier separation, which collectively improves ROS generation efficiency. For instance, Liu et al. developed mesoporous ceria nanoparticles (MCNs) and showed that band-gap narrowing and enhanced light absorption are the dominant factors governing their photo-Fenton activity. The optimized MCNs-240, featuring a larger pore diameter and reduced band gap, achieved >90% Acid Orange 7 dye degradation within 3 min across a wide pH (2.5–8.5) and H_2O_2 range, far outperforming conventional CeO_2. Mechanistic analysis revealed that the narrower band gap improved visible-light harvesting, while the mesoporous structure accelerated adsorption equilibrium, enabling ultrafast ROS generation. This work highlights band-gap engineering as a key strategy for boosting ceria-based photo-Fenton catalysts.[73]

c. Surface Area and Porosity

Photo-Fenton reactions occur predominantly on catalyst surfaces; therefore, increasing specific surface area and accessible porosity enhances pollutant adsorption, mass transfer, and active-site density. Nanostructuring strategies such as hollow architectures, nanosheets, nanorods, or MOF-derived frameworks considerably improve catalytic interactions.

CeO_2 nanosheets, MnO_x nanoflowers, and Co-based layered double hydroxides (LDHs) exhibit high pollutant affinity and rapid charge migration due to their accessible surfaces and layered structure. Notably, the tunable interlayer chemistry and high surface-to-volume ratio of LDH-based materials make them exceptionally effective for the advanced photocatalytic oxidation of recalcitrant pharmaceuticals, where the porous architecture facilitates the diffusion of large

View Article Online
DOI: 10.1039/D6LF00096G

medicinal molecules into active interfacial zones.[74] Ce-based MOFs, aerogels, and ordered mesoporous oxides also offer tunable porosity and high defect concentration, enabling simultaneous adsorption–oxidation pathways for improved degradation performance. For instance, it was reported that porosity and surface area are critical contributors to the superior photo-Fenton performance of supramolecularly assembled CA-Cu/TCN catalysts. The hydrogen-bond-induced self-assembly strategy generates a porous tubular g-C_3N_4 framework with high mesopore density (H4 hysteresis), enlarged pore volume, and increased specific surface area (29.3 m^2g^{-1}), markedly exceeding that of pristine CN. This hierarchical porous architecture enhances mass transport, pollutant diffusion, and accessibility of ultra-dispersed CuN_x active sites and nitrogen vacancies, while suppressing Cu aggregation. The increased interfacial contact between H_2O_2, pollutants, and active sites accelerates redox reactions and ROS generation, enabling rapid ciprofloxacin degradation (95.9%, k = 0.0948 min^{-1}). These results underscore that engineered porosity and surface accessibility are key structural parameters for maximizing active-site utilization and photo-Fenton efficiency.[75]

d. Oxygen vacancies and lattice defects

Oxygen vacancies and lattice defects critically influence both catalytic activity and charge dynamics in non-ferrous systems. These defects trap photogenerated electrons, reducing recombination, enhancing surface polarity and H_2O_2 adsorption, altering electronic structure and promoting sub-bandgap transitions, and introducing active sites for ROS production

CeO_2 is particularly noted for its CeO_{2-x} structure, where abundant OVs create Ce^{3+}-rich surface regions that facilitate H_2O_2 activation through both radical and non-radical pathways. For instance, Yang et al. reported a cerium-rich CeO_{2-x}/Bi_2MoO_6 heterojunction, non-stoichiometric CeO_{2-x} introduces abundant surface oxygen vacancies that enrich Ce^{3+} sites and promote rapid Ce^{3+}/Ce^{4+} self-circulation.[38] These vacancies create defect states that enhance

View Article Online
DOI: 10.1039/D6LF00096G

visible-light absorption, act as electron-trapping centres to suppress recombination and facilitate interfacial electron migration. Consequently, oxygen-vacancy-assisted Ce^{3+} efficiently activates H_2O_2 to generate •OH, while photogenerated electrons rapidly regenerate Ce^{3+} from Ce^{4+}, sustaining continuous ROS production. This self-circulating, OV-driven mechanism enables markedly enhanced antibiotic degradation under low-power visible light, demonstrating oxygen vacancy engineering as a key lever for high-performance non-ferrous photo-Fenton systems.

In another study, it was reported that Oxygen vacancies act as key enablers in Cu–MgO photo-Fenton systems by coupling defect-mediated charge transfer with multivalent Cu redox cycling.[76] UV photodeposition of Cu on MgO creates rich surface oxygen vacancies, which extend visible-light response, suppress electron–hole recombination, and enhance interfacial charge separation through Schottky junction formation. These vacancies work synergistically with coexisting $Cu^0/Cu^+/Cu^{2+}/Cu^{3+}$ species to facilitate efficient electron shuttling and sustained H_2O_2 activation, leading to enhanced $\bullet O_2^-$ generation. As a result, 3% Cu–MgO achieves high photo-Fenton efficiency (92.8% RhB removal, $k = 0.0436\ min^{-1}$) over a wide pH range (3.6–10), highlighting oxygen-vacancy engineering as a decisive factor for stabilizing multivalent Cu states and boosting non-ferrous photo-Fenton activity.

e. Interface Modulation and Heterojunction Engineering

Interface engineering is one of the most effective design strategies for improving photo-Fenton catalysis. Well-constructed interfaces accelerate charge separation, extend light absorption, and provide directional transport pathways for electrons and holes. Typical heterojunction architectures include:

- Type-II junctions for stepwise electron–hole migration
- Z-scheme systems that retain strong redox potentials during charge transfer

- S-scheme heterojunctions providing spatial charge separation via built-in electric fields
- p–n junctions that generate internal electric fields to accelerate electron extraction

Carbonaceous matrices such as rGO, CNTs, and biochar contribute additional conductivity and adsorption capacity, while MOFs provide ordered porous structures and abundant active sites. The synergy between redox flexibility of Ce and interfacial charge-transfer pathways allows advanced multi-component composites to achieve high degradation efficiencies even at neutral pH and under natural sunlight, surpassing the limitations of traditional Fe-based systems.

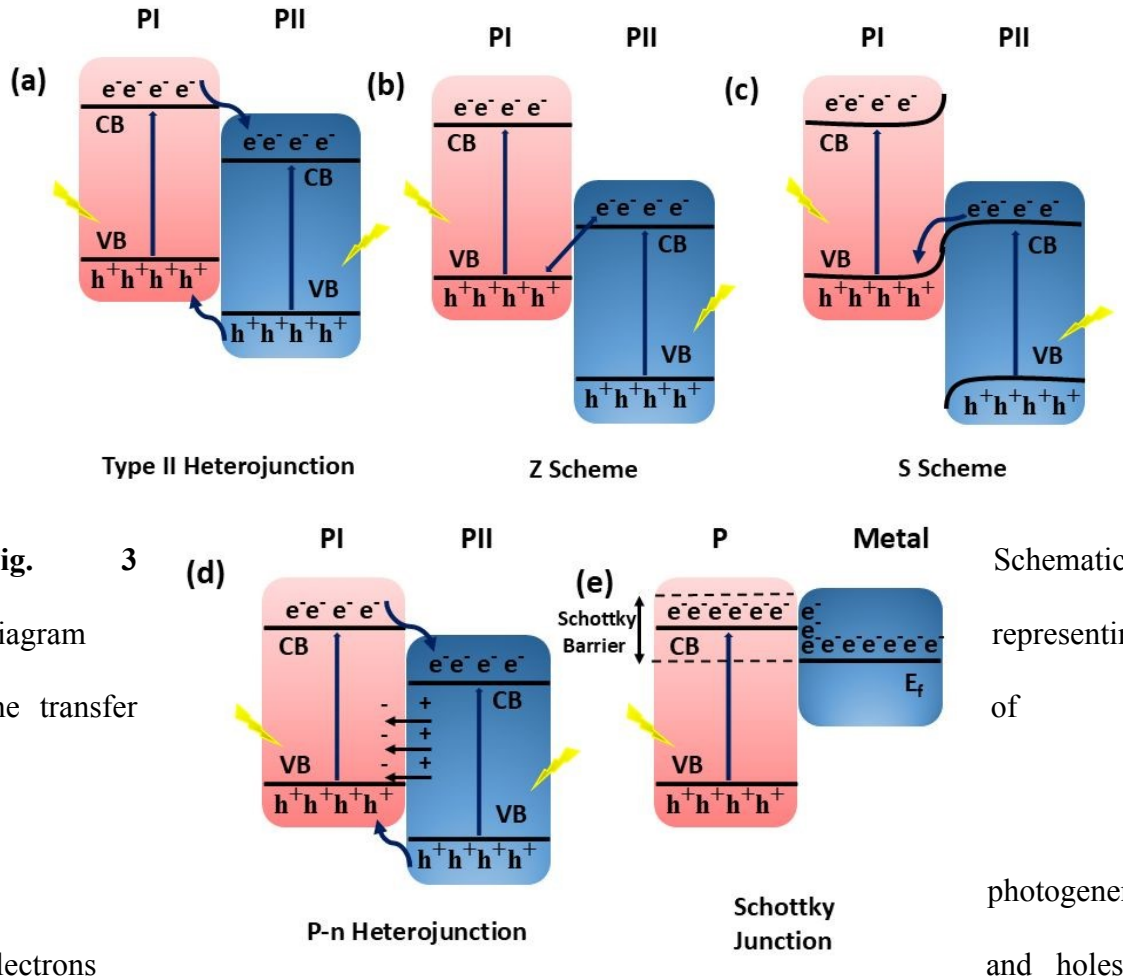

Fig. 3 Schematic diagram representing the transfer of photogenerated electrons and holes for different types of heterojunctions. (a) Type II heterojunction, (b) Z Scheme, (c) S Scheme, (d) p–n heterojunction, and (e) Schottky junction.

3. Interface Engineering Strategies for Enhanced Photo-Fenton Activity

View Article Online
DOI: 10.1039/D6LF00096G

Interface engineering plays a pivotal role in enhancing the photocatalytic performance of non-ferrous photo-Fenton catalysts. By rationally tailoring interfacial architectures, charge-carrier dynamics can be optimized, and redox activity can be modulated, leading to more efficient ROS generation. Furthermore, engineered interfaces improve pollutant adsorption, H_2O_2 activation, and structural stability. This section presents a comprehensive overview of the dominant interfacial strategies, beginning with heterojunction construction, followed by integration with carbonaceous supports, defect engineering, and the use of MOF/LDH-derived scaffolds. Different types of Interface Engineering Strategies and their applications are summarized in Table 3.

3.1 Heterojunction Engineering

Heterojunction engineering represents one of the most potent design strategies for advancing non-ferrous photo-Fenton and Fenton-like catalysis. By coupling two semiconductors with complementary band structures, heterojunctions facilitate the efficient spatial separation of photogenerated charge carriers, promote directional electron–hole migration, and minimize recombination losses. This improved charge dynamics directly enhances the redox cycling of active metal centres (Cu^{+}/Cu^{2+}, Co^{2+}/Co^{3+}, Mn^{2+}/Mn^{3+}, Ce^{3+}/Ce^{4+}) and accelerates the generation of reactive oxygen species (ROS), particularly •OH, $\bullet O_2^-$, and $^1O_2$ during H_2O_2 activation. Consequently, heterojunction construction has become indispensable in interface-engineered non-ferrous photo-Fenton systems.

A representative example of this strategy is the design of a Ce_4O_7/Bi_4MoO_9 heterojunction synthesized via molten salt-assisted synthesis strategy.[59] Transmission electron microscopy (TEM) analysis of this system demonstrated that the Ce_4O_7 nanoparticles were intimately loaded on the surface of Bi_4MoO_9 nanoblocks, creating a compact interface that reduces resistance to charge migration. Photoluminescence (PL) quenching studies revealed a drastic

View Article Online
DOI: 10.1039/D5LF00096G

suppression of electron–hole recombination, while electrochemical impedance spectroscopy (EIS) confirmed enhanced interfacial conductivity. These improvements allowed a higher density of electrons to participate in the Ce^{4+}/Ce^{3+} and Mo^{6+}/Mo^{5+} dual redox cycle, thereby accelerating H_2O_2 reduction. It is important to note that distinguishing between different heterojunction mechanisms, particularly S-scheme and Z-scheme systems, requires rigorous experimental validation. While band structure alignment provides a preliminary indication, definitive identification should be supported by complementary techniques such as in situ or operando X-ray photoelectron spectroscopy (XPS) to probe interfacial charge transfer, electron paramagnetic resonance (EPR) spin-trapping to identify active species, Mott–Schottky analysis for band structure determination, and Kelvin probe or work function measurements to verify Fermi level equilibration and internal electric field formation.

In S-scheme heterojunctions, charge transfer is governed by Fermi level differences and internal electric fields, resulting in selective recombination of low-energy electrons and holes while preserving high redox potential carriers. In contrast, Z-scheme systems involve recombination between photogenerated electrons and holes across the interface, typically mediated by direct contact or electron mediators, while retaining strong oxidative and reductive capabilities. Therefore, in this review, mechanistic assignments are made based on the available experimental evidence, and in cases where such validation is limited, the systems are described more generally as heterojunctions with enhanced charge separation.

Generally, heterojunctions used in these catalytic systems are classified into Type-II, Z-scheme, S-scheme, p–n junctions, and Schottky junctions (Fig. 3), each offering distinct charge transfer pathways.

a. Type-II Heterojunctions

View Article Online
DOI: 10.1039/D6LF00096G

As exhibited in Fig. 3a, Type-II heterojunctions form when two semiconductors with staggered band structures are coupled such that the conduction band (CB) and valence band (VB) edges of one material lie at lower energies than those of the other. This configuration directs photogenerated electrons toward the semiconductor with a more negative conduction band, while holes migrate to the component with a more positive valence band. This physical separation across the interface strongly suppresses recombination and increases the lifetime of charge carriers involved in Fenton-like reactions.[77]

Guo et al.[43] constructed a Type-II $Cu_2(OH)_3F$/BiOBr heterojunction with highly exposed BiOBr (010) facets, enabling accelerated charge transfer and efficient Cu^+/Cu^{2+} cycling in the photo-Fenton process. The (010) facet provided fast electron transport channels, allowing photogenerated electrons from BiOBr to migrate to $Cu_2(OH)_3F$ (Fig. 4a), where they rapidly reduced Cu^{2+} and boosted •OH generation from H_2O_2. Simultaneously, holes accumulated on the BiOBr oxidized surface, OH^-/H_2O to additional •OH, while electrons on $Cu_2(OH)_3F$ also reduced O_2 to $•O_2^-$. This dual-pathway ROS generation markedly enhanced the synergistic degradation of TC-HCl, achieving 98.8% removal, 4.2 and 2.5 times higher than photocatalysis and Fenton-like oxidation alone (Fig. 4b). Stable performance over five cycles (Fig. 4c) further confirmed that Type-II band alignment and facet-directed charge separation effectively overcame Cu-based recombination limitations, establishing $Cu_2(OH)_3F$/BiOBr as a robust non-ferrous photo-Fenton catalyst.[43] In another report, Wang et al.[78] constructed a 2D/2D Type-II $CuCo_2S_4/Bi_2WO_6$ heterojunction through an in-situ hydrothermal–solvothermal route, enabling intimate interfacial contact between both nanosheet components. The $CuCo_2S_4$ cocatalyst broadened visible-light absorption and accelerated electron–hole separation, while also mediating Cu^{2+}/Cu^{+1} and Co^{3+}/Co^{2+} redox cycling for efficient H_2O_2 activation. As a result, the heterojunction generated abundant •OH and $•O_2^-$ radicals and delivered markedly enhanced photo-Fenton degradation of tetracycline, with a rate constant nearly 1.8-fold higher

View Article Online
DOI: 10.1039/D5FF00096G

than pristine Bi_2WO_6. The catalyst also retained high activity over multiple cycles, confirming the stability of the interfacial charge-transfer pathway.[78]

Similarly, Guo et al.[79] synthesized a series of 2D/2D Cu_2ZnSnS_4/Bi_2WO_6 (CZTS/BWO) Type-II heterojunctions through a secondary solvothermal growth of ultrathin CZTS nanosheets onto Bi_2WO_6, forming intimate interfacial contact that was confirmed by XPS and HRTEM analysis. The optimized 2 wt% CZTS/BWO composite exhibited markedly enhanced visible-light photo-Fenton activity toward dyes and antibiotics, outperforming pristine BWO due to broadened light absorption, abundant surface active sites, and accelerated charge separation across the Type-II interface. The presence of H_2O_2 further boosted degradation efficiency by promoting rapid Cu^{2+}/Cu^{+1} cycling, enabling efficient ROS generation. ESR and radical-trapping studies verified $\bullet O_2^-$ and •OH as the dominant reactive species. The heterojunction maintained high catalytic stability over four cycles, demonstrating that coupling CZTS with BWO effectively strengthens charge mobility and redox cycling in non-ferrous photo-Fenton systems.[79]

In another study, it was reported that the superior photo-Fenton activity of cerium-rich CeO_{2-x}/Bi_2MoO_6 originates from the formation of an efficient Type-II heterojunction, which promotes directional charge separation and accelerates interfacial redox reactions.[38] Due to favourable band alignment, photogenerated electrons migrate from the conduction band of Bi_2MoO_6 to CeO_{2-x}, while holes transfer from the valence band of CeO_{2-x} to Bi_2MoO_6, resulting in efficient spatial separation of charge carriers. This directional charge transfer suppresses electron–hole recombination and enables sustained accumulation of electrons on CeO_{2-x} for rapid Ce^{3+}/Ce^{4+} self-circulation and H_2O_2 activation, while holes retained on Bi_2MoO_6 drive direct oxidation and •OH generation. The Type-II heterointerface thus couples enhanced photocatalytic charge separation with accelerated Fenton redox cycling, leading to markedly improved antibiotic degradation efficiency under low-power visible light.[38]

View Article Online
DOI: 10.1039/D6LF00096G

Overall, Type-II heterojunctions offer a robust platform for enhancing photo-Fenton-like catalysis by facilitating interfacial electron transfer and suppressing charge recombination, making them particularly attractive for non-ferrous catalytic systems. Their performance can be further strengthened when coupled with auxiliary strategies such as oxygen-vacancy engineering or LDH-based hybridization. Nevertheless, intrinsic limitations remain. The staggered band alignment in Type-II heterojunctions inevitably lowers the redox potential of photogenerated electrons and holes, weakening the oxidative and reductive driving forces required for efficient H_2O_2 activation. Moreover, the accumulation of holes on one semiconductor surface can hinder cross-interface charge migration, restricting full utilization of photogenerated carriers. These drawbacks highlight the need for more advanced charge-regulation architectures beyond conventional Type-II configurations.

b. Z-Scheme Systems

The Z-scheme heterojunction concept originates from the charge-transfer principles observed in photosynthetic systems and is regarded as an advanced alternative to conventional Type-II architectures for reactions demanding strong redox capability. Unlike Type-II heterojunctions, where charge transfer results in a net loss of redox ability, Z-scheme systems enable the spatial separation of photogenerated electron–hole pairs while preserving the strong reducing and oxidizing capabilities of the respective components. In a typical Z-scheme configuration (specifically the Direct Z-scheme, which eliminates liquid redox mediators), two semiconductors are physically coupled as shown in Fig. 3b. When exposed to light, electrons excited in the CB of the oxidation photocatalyst migrate to the interface and recombine with VB holes of the reduction photocatalyst, driven by the band potential difference.[80]

Lu et al.[51] Developed a ball-milled CPDs/$CuBi_2O_4$ Z-scheme heterojunction as an efficient photo-Fenton catalyst for antibiotic wastewater treatment. In this system, carbonized polymer

View Article Online
DOI: 10.1039/D6LF00096G

dots (CPDs) served as interfacial mediators to construct a stable Z-scheme junction with $CuBi_2O_4$, promoting extended light absorption and rapid charge-carrier separation. The optimized 20 wt% CPDs/$CuBi_2O_4$ composite showed markedly improved performance, achieving 92.3% ciprofloxacin degradation, 36% higher than pristine $CuBi_2O_4$. ESR and Scavenger experiments revealed that $^1O_2$, •OH, h^+, and $•O_2^-$ were the dominant reactive species generated through the Z-scheme pathway. Overall, this work demonstrates a scalable ball-milling strategy to engineer CPD-modified $CuBi_2O_4$ heterojunctions with enhanced redox capability for practical photo-Fenton degradation of antibiotics.[51]

Zhang et al.[81] constructed a porous Z-scheme MnO_2/Mn-modified alkalinized g-C_3N_4 (MnO_2/CNK-OH-Mn) heterojunction via a calcination–impregnation route. The optimized MnO_2/CNK-OH-Mn-15% delivered markedly higher Fenton-like photocatalytic activity, achieving 96.7% tetracycline degradation and notable TOC removal (74.9%), attributed to synergistic ROS generation. ESR and trapping studies verified •OH and $•O_2^-$ as dominant species, derived from Z-scheme charge transfer and accelerated $Mn^{4+}/Mn^{3+}/Mn^{2+}$ redox cycling for efficient H_2O_2 activation. The catalyst also maintained high stability over multiple cycles and enabled effective treatment of pharmaceutical wastewater, underscoring the role of Mn-based Z-scheme heterojunctions in enhancing Fenton-like pathways.[81]

In another study, the formation of a Z-scheme heterojunction was identified as a key factor enabling the synergistic coupling of photocatalytic processes and Fenton-like redox cycling in CuO/CDs/g-C_3N_4 systems.[40] In this ternary architecture, carbon dots act as interfacial electron-transfer bridges that reinforce the Z-scheme charge migration, enabling electrons in the conduction band of CuO to recombine with holes in the valence band of g-C_3N_4 while preserving strong redox potentials. This configuration retains highly oxidative holes on CuO for •OH generation and pollutant oxidation, while electrons accumulated on g-C_3N_4 efficiently

View Article Online
DOI: 10.1039/D6LF00096G

reduce Cu^{2+} to Cu^{+}, sustaining the Fenton-like cycle. The dual Z-scheme-assisted charge transfer pathways effectively suppress carrier recombination and accelerate Cu^{2+}/Cu^{+} conversion, resulting in synergistically enhanced •OH and $•O_2^-$ production under visible light. These findings highlight Z-scheme interface engineering as a powerful strategy to maximize redox efficiency and catalytic durability in non-ferrous photo-Fenton systems.[40]

Researchers constructed a g-C_3N_4/$ZnCo_2O_4$ Z-scheme heterojunction, which plays a crucial role in regulating charge separation and redox balance in photo-Fenton-like systems.[49] Upon visible-light illumination, electrons excited to the conduction band of g-C_3N_4 selectively recombine with valence-band holes of $ZnCo_2O_4$ via a Z-scheme charge-transfer route, preserving strongly reducing electrons on $ZnCo_2O_4$ and oxidative holes on g-C_3N_4. This charge-transfer configuration suppresses carrier recombination while enabling efficient Co^{3+}/Co^{2+} cycling, which drives the activation of both H_2O_2 and persulfate to generate •OH and $SO_4•^-$ radicals. As a result, the Z-scheme architecture ensures sustained ROS production and enhanced dye degradation under visible light, highlighting its effectiveness in coupling photocatalytic charge dynamics with Fenton-like oxidant activation.[49]

Jia et al.[55] constructed a Z-scheme MnO_x/g-C_3N_4 photo-electro-Fenton-like system in which polyvalent Mn species ($Mn^{2+}/Mn^{3+}/Mn^{4+}$) served as the core Fenton-like redox centres, fully replacing Fe in H_2O_2 activation. The MnO_x domains were uniformly anchored on g-C_3N_4 nanosheets, forming a solid Z-scheme interface that accelerated electron–hole separation and promoted the simultaneous generation of •OH, $•O_2^-$, and h^+ under visible light. The rapid $Mn^{4+}/Mn^{3+}/Mn^{2+}$ conversion cycle, strengthened by abundant oxygen vacancies generated from low-valence Mn, enabled efficient H_2O_2 decomposition and boosted electrocatalytic activity under applied bias. Benefitting from these features, the MnO_x/g-C_3N_4 catalyst achieved 96.2% CIP removal in 120 min with widened pH applicability and excellent

View Article Online
DOI: 10.1039/D6LF00096G

durability. This study highlights the indispensable role of Mn multivalence and OV-induced electronic modulation in enabling Fe-free Z-scheme PEF systems with high oxidative efficiency and rapid Mn valence transitions, enabling efficient H_2O_2 activation even under visible light.[55]

Yang et al.[42] constructed a $CuO_x \cdot Ag_2O$/RGO multiphase heterostructure via electrochemical post-treatment of a bimetallic ICP/RGO precursor, in which the intimate CuO_x–Ag_2O coupling on conductive RGO established a direct Z-scheme charge transfer pathway. In this configuration, photogenerated electrons with strong reducing power and holes with high oxidation potential are spatially retained on their respective components, avoiding the redox loss typical of type-II junctions. This Z-scheme-driven charge migration not only accelerates electron–hole separation but also sustains efficient Cu-based redox cycling and H_2O_2 activation, leading to robust •OH generation during photo-Fenton degradation. The study highlights that Z-scheme architectures are highly advantageous for integrating bimetallic oxides with carbon mediators, enabling stable, recyclable, and high-efficiency photo-Fenton catalysis under visible light.

It was reported that the Z-scheme p–n heterojunction is critical for maintaining redox capability while enhancing charge separation in Prussian blue (PB)/Mn_3O_4 photo-Fenton systems.[48] In the p-Mn_3O_4/n-PB heterostructure, the built-in electric field drives Z-scheme charge migration, where photogenerated electrons in the conduction band of PB recombine with holes in the valence band of Mn_3O_4. This process suppresses carrier recombination while retaining highly oxidative holes on PB and strongly reductive electrons on Mn_3O_4, enabling simultaneous •OH and $\bullet O_2^-$ generation. Such charge regulation also facilitates efficient Fe^{3+}/Fe^{2+} and $Mn^{4+}/Mn^{3+}/Mn^{2+}$ redox cycling, sustaining H_2O_2 activation and favouring a non-radical pathway dominated by $^1O_2$. Consequently, the Z-scheme architecture enhances photo-Fenton

View Article Online
DOI: 10.1039/D6LF00096G

efficiency, stability, and resistance to environmental interference, underscoring its importance in advanced non-ferrous photo-Fenton catalyst design.

c. S scheme systems

While the Direct Z-scheme model effectively describes the vectoral charge transfer pathway, it often lacks a rigorous physical explanation regarding the driving forces at the atomic level. To address this, the S-scheme (Step-scheme) mechanism was recently proposed to clarify the charge transfer dynamics based on Fermi level differences and work functions. This design preserves the high redox potential of the photogenerated carriers while simultaneously achieving spatial separation, making it exceptionally effective for driving the demanding redox cycles in non-ferrous photo-Fenton catalysis. Structurally, an S-scheme heterojunction is composed of a reduction photocatalyst (RP) with a high conduction band (CB) position and an oxidation photocatalyst (OP) with a deep valence band (VB) as shown in Fig. 3c. When these materials come into contact, electrons flow from the material with the higher Fermi level to the one with the lower Fermi level until equilibrium is reached. This creates an electron-depletion layer and an electron-accumulation layer, resulting in a built-in internal electric field (IEF) at the interface. Under irradiation, the IEF and band bending drive the "useless" electrons (those in the lower CB of the OP) to recombine with the "useless" holes (those in the higher VB of the RP). Consequently, the photogenerated electrons with the highest reducing power are retained in the CB of the RP, and the holes with the highest oxidizing power are retained in the VB of the OP.[82]

For non-ferrous photo-Fenton systems, this mechanism is vital. For instance, Li et al.[53] synthesized AgAu–C/N–CeO_2@C/N–CuO S-scheme nanohybrids from a Ce/Cu-MOF precursor via sequential hydrothermal growth, calcination, and photoreduction. The MOF-derived 1D/2D C/N–CeO_2/C/N–CuO heterostructure provided abundant surface defects and

View Article Online
DOI: 10.1039/D6LF00096G

intimate interfacial contact, while plasmonic AgAu nanoparticles were uniformly anchored onto the composite. Comprehensive XRD, XPS, TEM, ESR, and trapping experiments confirmed the formation of a compact S-scheme interface that preserved strong redox potentials and enhanced exciton separation. Owing to the synergistic contributions of LSPR-induced hot-electron injection, defect-mediated charge trapping, and accelerated S-scheme charge transfer, the catalyst delivered a remarkable H_2O_2 production rate (3289.3 μmol g^{-1} h^{-1}) and efficient in-situ photo-Fenton degradation of ofloxacin (91% in 1 h), maintaining excellent photostability across multiple cycles.[53]

In another work, Shao et al.[41] constructed hortensia-like Bi_2WO_6/CoAl-LDHs nanohybrids via a hydrothermal route to engineer an S-scheme heterojunction for strengthened photo-Fenton-like activity. The intimate Bi_2WO_6/CoAl-LDH interface established a robust internal electric field that accelerated directional charge migration while preserving strong oxidizing holes on Bi_2WO_6 and reducing electrons on CoAl-LDHs (Fig. 4d). The photocurrent and EIS results (Fig. 4e,f) suggested that the existence of heterojunction of Bi_2WO_6/CoAl-LDHs-20 nanohybrid, which was benefit for the electron transfer process, thus effectively decreased the recombination of photoexcited e^--h^+ pairs and promoted the H_2O_2 activation, enabling rapid •OH formation. Benefiting from this S-scheme charge-transfer pathway and cobalt-mediated Fenton-like reaction, the composite achieved 98.47% oxytetracycline removal under visible light and H_2O_2, significantly outperforming the individual components. DFT calculations confirmed improved H_2O_2 adsorption and optimized band alignment as key contributors to its superior photo-Fenton-like performance.

Kumar et al.[83] synthesized a $gC_3N_{4x}/AgO_y@Co_{1-x}Bi_{0.1-y}O_7$ composite, in which the S-scheme heterojunction plays an important role in preserving redox potential while suppressing charge recombination in photo-Fenton catalysis. Unlike conventional Type-II or Z-scheme pathways that compromise reduction or oxidation capability, the S-scheme configuration enables

View Article Online
DOI: 10.1039/D6LF00096G

selective recombination of low-energy charge carriers while retaining highly oxidative holes on g-C_3N_4 and strongly reductive electrons on the cobalt–bismuth oxide component. This charge-selective migration maintains a continuous supply of high-energy electrons and holes under visible light, promoting efficient O_2 reduction to $\bullet O_2^-$ and subsequent H_2O_2/•OH generation. As a result, the S-scheme heterointerface synergistically enhances ROS production and Fenton-assisted oxidation, leading to high degradation efficiencies of methylene blue and oxytetracycline under neutral pH with improved stability and reusability.

Researchers reported that the formation of an S-scheme heterojunction is essential for maintaining strong redox capability and promoting efficient charge migration in 2D/2D MgO/g-C_3N_4 photo-Fenton catalysts.[84] Owing to the large work-function difference between MgO and g-C_3N_4, an internal electric field is established at the tightly bonded MgO/g-C_3N_4 interface, which promotes the recombination of energetically unfavourable charge carriers while preserving highly reductive electrons on MgO and strongly oxidative holes on g-C_3N_4. This S-scheme charge regulation effectively suppresses electron–hole recombination and sustains high redox potential for ROS generation. Notably, the formation of interfacial Mg–N bonds strengthen the S-scheme contact, accelerates interfacial charge transfer, and simultaneously induces oxygen vacancies in MgO, which further promote H_2O_2 activation and •OH formation. The synergistic coupling of S-scheme charge migration and oxygen-vacancy-enhanced Fenton-like reactions enables markedly improved pollutant degradation under visible light.

Wang et al.[85] synthesized S-scheme $CuInS_2$/WO_3 hybrid heterostructures, in which the S-scheme heterojunction plays a key role in maintaining strong redox capability while enabling efficient charge separation during photo-Fenton degradation. Owing to the Fermi-level difference between p-type $CuInS_2$ and n-type WO_3, an internal electric field is established at the interface, driving selective recombination of low-energy electrons in WO_3 with holes in

View Article Online
DOI: 10.1039/D6LF00096G

$CuInS_2$. This S-scheme charge migration preserves highly reductive electrons on $CuInS_2$ and strongly oxidative holes on WO_3, which are essential for generating $\bullet O_2^-$ and •OH radicals, respectively. Consequently, the S-scheme architecture suppresses charge recombination while sustaining efficient photo-Fenton redox reactions, leading to enhanced tetracycline degradation under visible light.

S-scheme and Z-scheme heterojunctions, although often used interchangeably in the literature, are fundamentally distinct in their charge transfer mechanisms. In S-scheme systems, charge migration is governed by Fermi level equilibration and the formation of an internal electric field, which drives the recombination of low-energy electrons and holes while preserving high-energy charge carriers with strong redox potential. In contrast, Z-scheme heterojunctions involve the recombination of photogenerated electrons and holes across the interface, either through direct contact or via an electron mediator, while maintaining strong oxidative and reductive capabilities on the respective semiconductors. Therefore, careful differentiation between these mechanisms is necessary when interpreting photocatalytic behaviour.

d. p–n Junctions

The construction of p-n junctions represents a distinct heterojunction strategy that exploits the contrasting electronic characteristics of p-type (hole-rich) and n-type (electron-rich) semiconductors. Unlike conventional heterojunctions, where charge separation is driven primarily by band-edge offsets, p–n junctions operate through the formation of a strong internal electric field (IEF) created by carrier diffusion. When a p-type material contacts an n-type counterpart, majority carriers, holes from the p-side and electrons from the n-side, diffuse across the interface until their Fermi levels align (Fig. 3d). This diffusion produces a depletion layer and a built-in electric field directed from the n-region toward the p-region.[86] Under illumination, this internal field acts as an efficient driving force for rapid electron–hole

View Article Online
DOI: 10.1039/D6LF00096G

separation: electrons drift toward the n-type conduction band, while holes migrate toward the p-type valence band. Such field-assisted separation markedly increases carrier lifetimes and accelerates interfacial charge transport. This behaviour is particularly advantageous in non-ferrous photo-Fenton and Fenton-like systems, where prolonged carrier lifetimes are crucial for sustaining multistep H_2O_2 activation and ROS generation.

Wang et al.[87] synthesised a Cu_2O/Bi_2MoO_6 (CBM) p–n heterojunction, in which the tightly coupled interface generated a strong built-in electric field that directed photogenerated electrons from p-Cu_2O to n-Bi_2MoO_6. This interfacial field greatly enhanced charge separation and created an efficient pathway for electron-driven H_2O_2 activation, producing abundant ·OH through both photoinduced reduction and accelerated Cu^{2+}/Cu^{+} cycling. The optimized CBM-25% catalyst leveraged this engineered p–n interface to deliver nearly complete ciprofloxacin degradation within 120 min, far outperforming single-component catalysts, and retained >92% efficiency over multiple cycles, demonstrating the critical role of p-n junction interface design in boosting non-iron photo-Fenton-like reactivity.

Shi et al.[88] constructed a $Bi_4Ti_3O_{12}/CuBi_2O_4$ p–n heterojunction piezo-photocatalyst that markedly enhanced photo-Fenton degradation of dyes and antibiotics. The intimate n-$Bi_4Ti_3O_{12}$/p-$CuBi_2O_4$ interface generated a strong built-in electric field, while piezoelectric polarisation further intensified carrier drift under ultrasonic excitation, jointly suppressing recombination. This interfacial driving force enabled rapid electron migration to $Bi_4Ti_3O_{12}$ and hole accumulation in $CuBi_2O_4$, thereby accelerating Cu^{2+}/Cu^{1+} cycling and H_2O_2 activation. As a result, the composite achieved superior degradation of MB, LEV, and OTC, outperforming single-component catalysts and maintaining high stability. This work highlights how robust p–n junctions coupled with piezoelectric polarization can dramatically boost charge separation and Fenton-like reactivity.[88]

View Article Online
DOI: 10.1039/D6LF00096G

Researchers developed a $Cu_2(OH)_3F/Cu_2O$ p–n heterojunction that plays a critical role in accelerating charge separation and facilitating the Cu^{2+}/Cu^{+} redox cycle in photo-Fenton-like systems.[89] In this n-type $Cu_2(OH)_3F$ and p-type Cu_2O composite, the built-in electric field at the p–n interface drives directional migration of photogenerated electrons toward $Cu_2(OH)_3F$ and holes toward Cu_2O, effectively suppressing electron–hole recombination. This charge redistribution enriches Cu^{+} species and facilitates rapid Cu^{2+}/Cu^{+} interconversion, thereby enhancing H_2O_2 activation and continuous •OH and $•O_2^-$ generation. Consequently, the p–n heterojunction synergistically couples efficient photocatalytic charge transport with Fenton-like redox kinetics, leading to near-complete tetracycline degradation and improved stability over a wide pH range.

Researchers reported that the $Cu_{2-x}S/g\text{-}C_3N_4$ system forms a p–n heterojunction in which the internal electric field promotes efficient charge separation, while redox preservation plays a secondary role.[47] Mott–Schottky analysis confirms the formation of a p–n junction between p-type $Cu_{2-x}S$ and n-type $g\text{-}C_3N_4$, which promotes directional migration of photogenerated electrons and holes and effectively suppresses charge-carrier recombination. This interfacial electric field stabilizes Cu^{2+}/Cu^{+} cycling and enables complementary enhancement between photocatalysis and Fenton-like reactions, even though the band structure of $Cu_{2-x}S$ alone is not highly favourable for ROS generation. Consequently, the p–n heterojunction mainly functions as a charge-regulation and redox-stabilization interface, supporting efficient $•O_2^-$-dominated degradation and high TOC removal under photo-Fenton conditions.

Guo et al.[90] synthesized a 2D in-plane CuS/Bi_2WO_6 p–n heterojunction, which plays a key role in enhancing charge separation and stabilizing Cu-based photo-Fenton activity. The intimate coupling of p-type CuS with n-type Bi_2WO_6 establishes an internal electric field that promotes directional migration of photogenerated electrons and holes, thereby suppressing carrier

View Article Online
DOI: 10.1039/D6LF00096G

recombination under visible light. This charge redistribution enables efficient electron transfer from Bi_2WO_6 to CuS, facilitating H_2O_2 activation and sustaining Cu^{2+}/Cu^{+} cycling, while holes retained on Bi_2WO_6 directly participate in pollutant oxidation. Consequently, the p–n heterointerface synergistically couples photocatalytic charge regulation with heterogeneous Fenton reactions, resulting in rapid degradation, improved stability, and excellent reusability.

e. Schottky Junctions

As exhibited in Fig. 3e, Schottky junctions arise at metal–semiconductor interfaces due to differences in Fermi levels and work functions, leading to the formation of a Schottky barrier and an interfacial space-charge region. In such systems, metallic cocatalysts serve both as electron sinks and as active reaction sites. Under light irradiation, photogenerated electrons in the semiconductor conduction band are preferentially transferred to the cocatalyst with a lower Fermi level, while holes remain in the semiconductor, resulting in efficient charge separation and suppressed recombination. This directional electron migration is particularly advantageous in non-ferrous photo-Fenton-like catalysis, as the accumulated electrons facilitate continuous redox cycling of active metal species and promote H_2O_2 activation. Consequently, Schottky interface engineering provides an effective strategy for enhancing charge-transfer kinetics and overall photocatalytic efficiency.[91]

Zhong et al.[92] reported in situ formed Ti^{3+}-self-doped TiO_2/Ti_3C_2 MXene Schottky heterojunctions exhibiting highly efficient photo-Fenton-like degradation of cationic dyes over a wide pH range (3–10). The Schottky barrier arising from the work-function mismatch between TiO_2 and metallic Ti_3C_2 promoted directional charge separation, enabling effective utilization of photogenerated electrons and holes for H_2O_2 activation. Negligible degradation was observed without light or H_2O_2, whereas nearly complete dye removal (~99%) occurred

under visible light in the Ti_3C_2/H_2O_2 system, confirming a synergistic photo-Fenton pathway. Radical quenching, EPR, and DFT analyses revealed that the Schottky interface not only enhanced carrier separation but also weakened –OH adsorption, facilitating H_2O_2 decomposition and boosting •OH and $•O_2^-$ generation. This work underscores the dual role of Schottky junctions in regulating both charge-transfer dynamics and surface reaction kinetics in non-ferrous photo-Fenton-like systems.

In another study, it was reported that the metal semiconductor Schottky junction is central to efficient charge separation and accelerated H_2O_2 activation, leading to enhanced photo-Fenton activity in Ag/g-C_3N_4–H_2O_2 systems.[93] Deposited Ag nanoparticles act as electron sinks due to their lower Fermi level, establishing a Schottky barrier at the Ag/g-C_3N_4 interface that promotes directional transfer of photogenerated electrons from g-C_3N_4 to Ag. This interfacial electron trapping effectively inhibits charge recombination and extends carrier lifetimes, allowing a greater fraction of electrons to participate in H_2O_2 and O_2 reduction to generate •OH and $•O_2^-$ radicals. Simultaneously, the retained holes on g-C_3N_4 contribute to direct oxidation pathways. As a result, the Schottky junction synergistically couples photocatalytic charge regulation with oxidant activation, leading to accelerated ROS production, enhanced degradation kinetics, and improved stability in photo-Fenton-like dye removal.

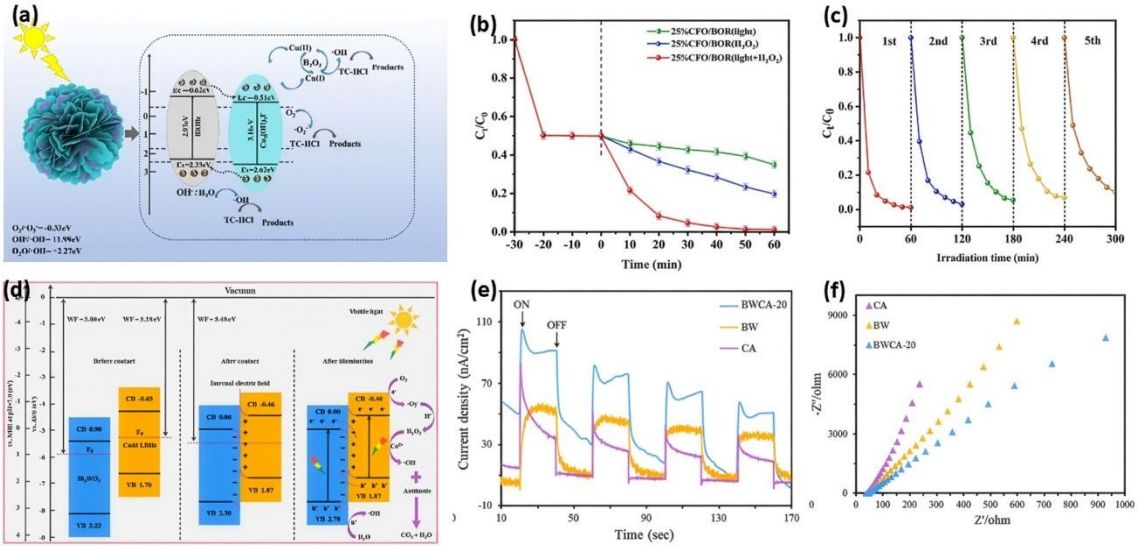

View Article Online
DOI: 10.1039/D6LF00096G

Fig. 4 (a) A type II heterojunction for charge transfer between $Cu_2(OH)_3F$ and BiOBr in 25% CFO/BOR catalyst, (b) catalyst activity under different situations over 25% CFO/BOR, and (c) Stability performance over 5 cycles. Reproduced from ref. 43 with permission from Elsevier, Guo, Y.; Liu, Y.; Hao, S.; Zhang, X.; Yu, Y. *Journal of Water Process Engineering,* **2023**, *55*, 104140. Copyright 2023. (d) Schematic diagram for photo-Fenton-like catalytic mechanism of S-scheme heterojunction of Bi_2WO_6/CoAl-LDHs, (e) Photocurrent, and (f) EIS study of Bi_2WO_6/CoAl-LDHs-20 nanohybrid. Reproduced from ref. 41 with permission from Elsevier, Shao, B.; Liu, Z.; Tang, L.; Liang, Q.; He, Q.; Wu, T.; Pan, Y.; Cheng, M.; Liu, Y.; Tan, X. *Chemosphere* **2022**, *291*, 133001. Copyright 2021.

3.2 Cocatalyst and Electron Mediator Incorporation

Cocatalyst incorporation is an effective strategy for accelerating charge transfer, suppressing recombination, and promoting H_2O_2 activation in non-ferrous photo-Fenton systems. By integrating conductive nanoparticles or carbonaceous electron mediators, the interfacial electron mobility is significantly enhanced, enabling more efficient ROS generation during visible-light irradiation.

a. Noble and Transition Metal Nanoparticles

Metallic nanoparticles such as Cu^0, Ag^0, Au^0, and Pd^0 are frequently employed as cocatalysts due to their high electrical conductivity and strong electron-capturing capability. When deposited onto semiconductor surfaces, they form Schottky junctions that facilitate directional electron trapping. This process serves two major functions:

- Suppressing photogenerated electron–hole recombination, thereby extending charge-carrier lifetimes.
- Enhancing H_2O_2 activation through accelerated electron transfer to catalytic sites.

View Article Online
DOI: 10.1039/D6LF00096G

For instance, Xiong et al.[94] developed a CNNS/Ni–Ag heterostructure in which dual-metal cocatalysts were interfacially anchored to regulate charge flow and enable sacrificial-agent-free H_2O_2 production and self-photo-Fenton degradation. The bimetallic interface generated a strong built-in electric field that directed photogenerated electrons from CNNS and LSPR-derived hot electrons from Ag toward Ni centres, markedly suppressing recombination. Ni acted as the primary electron mediator, optimizing O_2 adsorption and the two-electron ORR pathway, while Ag broadened visible-light absorption. This engineered interface delivered a high H_2O_2 production rate (1541.3 μmol g^{-1} h^{-1} with IPA) and enabled efficient in-situ Fenton degradation of metronidazole (92.9% in 60 min), demonstrating the power of dual-metal synergy and interfacial electric-field tuning in boosting non-ferrous Fenton-like catalysis.[94]

Dihingia et al.[95] green-synthesized a bimetallic (Cu^0 + Ag^0) @Bentonite heterojunction using *Psidium guajava* leaf extract to anchor zero-valent Cu and Ag nanoparticles onto bentonite. The resulting Cu–Ag interface lowered the band gap (2.32 eV), enhanced visible-light absorption, and promoted efficient •OH- and peroxy-radical generation under photo-Fenton-like conditions. The catalyst achieved 84% AMX and 74% SMZ degradation (UV-A), with significant mineralisation and minimal Cu^{2+} leaching, and retained stability over repeated cycles. The study demonstrates that a simple bio-assisted route can yield a robust Cu–Ag heterojunction with strong antibiotic-removal capability.[95]

Guo et al.[46] reported a Cu nanoparticle-modified Bi_2O_2S nanosheet, where surface-anchored Cu nanoparticles act as electron sinks, rapidly extracting photogenerated electrons from the semiconductor and thereby suppressing electron–hole recombination. This interfacial charge separation facilitates efficient reduction of Cu^{2+} to Cu^{+}, enabling continuous Cu^{2+}/Cu^{+} redox cycling that is essential for sustained H_2O_2 activation. Meanwhile, Cu^{+} directly catalyses H_2O_2 decomposition to generate abundant •OH radicals, while excess electrons reduce dissolved O_2 to $•O_2^-$, jointly accelerating pollutant mineralization. Importantly, the noble-metal-free nature

View Article Online
DOI: 10.1039/D5LF00096G

of Cu nanoparticles offers a cost-effective alternative to Au or Ag cocatalysts while retaining key functionalities such as enhanced charge mobility, increased surface adsorption, and durable redox mediation. This dual role electron mediator and Fenton active centre- highlights metal nanoparticles as pivotal components for boosting both efficiency and stability in advanced photo-Fenton processes.

In the Cu-decorated C@Bi/Bi_2MoO_6 heterojunction reported by Hu et al.[96], metallic Cu and Bi nanoparticles act as plasmonic and redox-active centres that enhance visible-light absorption through surface plasmon resonance (SPR) while simultaneously promoting interfacial charge separation. The SPR-excited electrons generated on metallic Bi nanoparticles are efficiently transferred to dissolved O_2, producing reactive intermediates ($\bullet O_2H$ and $^1O_2$), whereas Cu species facilitate H_2O_2 activation to yield abundant •OH radicals. Meanwhile, the carbon-anchored metal nanoparticles serve as electron mediators, suppressing electron–hole recombination and sustaining rapid metal redox cycling during the Fenton process. This dual functionality—plasmon-induced charge generation and metal-assisted oxidant activation-highlights how noble and transition metal nanoparticles synergistically bridge photocatalysis and Fenton chemistry, enabling ultrafast pollutant degradation under mild conditions.

b. Carbon-Based Mediators

Carbonaceous materials, including reduced graphene oxide (rGO), carbon nanotubes (CNTs), carbon quantum dots (CQDs), and biochar, serve as highly conductive electron mediators due to their delocalized Π electron systems and large surface areas. Their advantages include:

- Rapid electron transport through conjugated networks.
- Improved H_2O_2 reduction kinetics.
- Enhanced pollutant adsorption through Π-Π interactions.

- Stabilization of metal species through strong interfacial bonding.

View Article Online
DOI: 10.1039/D6LF00096G

Zhang et al.[97] engineered a $Cu_2(OH)_3F$/CQDs–$BiVO_4$ photo-Fenton-like catalyst in which 0D carbon quantum dots acted as an electron mediator between $BiVO_4$ and $Cu_2(OH)_3F$, enabling rapid and directional charge shuttling (Fig. 5a). As shown in Fig. 5(b-e), SEM analyses reveal decahedral $BiVO_4$ crystals uniformly decorated with $Cu_2(OH)_3F$ nanosheets confirming successful construction of a hierarchical heterointerface. Crystal-facet tuning of $BiVO_4$ (highly exposed (010) facet) enhanced its electron-donor capability, while CQDs bridged electron transfer and regenerated Cu^+, thereby strengthening H_2O_2 activation. Benefiting from accelerated carrier separation and intensified ROS generation, the CQDs-bridged heterojunction achieved 98.1% ciprofloxacin removal within 1 h, maintained stable activity over pH 3–11, as shown in Fig. 5f, and exhibited excellent structural stability across five cycles. This work highlights how electron mediators and cocatalyst interfaces synergistically overcome recombination limits and significantly boost non-ferrous photo-Fenton efficiency.

N-doped carbon matrices derived from MOF precursors function as active carbon mediators rather than inert supports in photo-Fenton systems by regulating electron transfer, stabilizing metal redox sites, and enhancing H_2O_2 activation. In the Cu–Cu_2O/N-doped carbon catalyst reported by Tan et al.[98], the graphitized N-doped carbon framework serves as an efficient electron-transfer highway, as shown in Fig. 5g, facilitating rapid migration of photogenerated electrons from Cu/Cu_2O heterojunctions to adsorbed H_2O_2 molecules. Pyridinic- and graphitic-N sites introduce additional electron-rich centres that lower the activation barrier for H_2O_2 decomposition, thereby accelerating •OH generation. Consistently, the addition of tert-butanol (TBA) suppressed DY degradation by 73.5%, confirming •OH as the dominant reactive species (Fig. 5h). Meanwhile, the carbon matrix spatially confines Cu/Cu_2O domains, suppressing metal aggregation and leaching while maintaining stable Cu^{2+}/Cu^+ redox cycling under visible light. As a result, the optimized Cu–N–C-500 catalyst achieved 93.3% DY

View Article Online
DOI: 10.1039/D6LF00096G

removal within 30 min under visible light, with complete degradation observed by 45 min, as shown in Fig. 5i, showing the best performance in the photo-Fenton catalytic system. This work highlights that carbon mediators play a decisive role in coupling photocatalysis with Fenton chemistry by synchronizing charge transport, redox stability, and oxidant activation.

Metal-free platforms can also act as electron mediators; Taha et al.[99] synthesized N-doped porous carbon nanofibers with abundant pyridinic-N/graphitic-N sites that efficiently activated H_2O_2 and mediated multi-electron transfer pathways. Their high conductivity and porous 1D architecture enabled a solar-Fenton-like reaction active across pH 3-11, without metal leaching.[100]

Carbon-based semiconductors such as graphitic carbon nitride (g-C_3N_4) play a dual mediator role in Cu-based photo-Fenton systems by simultaneously facilitating charge transport and stabilizing metal redox cycling. In the CuO/g-C_3N_4/H_2O_2 system reported by Sharma *et al.*, g-C_3N_4 acts as an efficient electron reservoir under visible-light irradiation, promoting rapid transfer of photogenerated electrons to CuO and thereby accelerating the Cu^{2+}/Cu^{+} redox cycle essential for H_2O_2 activation. This interfacial electron mediation suppresses charge recombination, enhances •OH generation, and significantly improves pollutant degradation efficiency. Moreover, the strong CuO–g-C_3N_4 interaction stabilizes surface Cu species, effectively minimizing Cu^{2+} leaching during repeated photo-Fenton cycles. These findings highlight that carbon mediators do not merely serve as photocatalytic supports but actively regulate electron flow, oxidant activation, and catalyst durability in non-ferrous photo-Fenton-like systems.

Carbon-based mediators such as reduced graphene oxide (RGO) play a pivotal role in photo-Fenton systems by acting as conductive charge bridges and structural stabilizers at multicomponent interfaces. Yang et al.[42] fabricated an ultra-fine Z-scheme $CuO_x \cdot Ag_2O$/RGO

View Article Online
DOI: 10.1039/D6LF00096G

heterostructure via electrochemical post-treatment of a bimetallic ICP/RGO precursor, in which RGO provided a highly conductive platform for rapid electron transport and interfacial charge redistribution. The exposed oxygenated functional groups and defect sites on RGO facilitated intimate anchoring of CuO_x and Ag_2O nanoparticles while suppressing aggregation, thereby enhancing catalyst stability and recyclability. More importantly, rGO functioned as an efficient electron shuttle, facilitating Z-scheme charge separation while preserving the redox reactivity of photogenerated carriers, thereby sustaining Cu-based redox cycling and effective H_2O_2 activation during the photo-Fenton process. This study highlights that integrating metal oxides with carbon mediators such as RGO is an effective strategy to couple efficient charge transport, interfacial stability, and high photo-Fenton activity under visible light.

Carbon-based architectures such as active carbon fibres (ACFs) play a multifunctional mediator role in advanced photo-Fenton-like systems by simultaneously regulating electron transfer, reactant enrichment, and catalyst dispersion. In the Mn_3O_4@ZnO/ACFs micromotor system reported by Cui et al.[101], the 3D hierarchical ACF framework acts as an efficient electron-transfer bridge, promoting rapid migration of photogenerated electrons from the semiconductor heterojunction to Mn-based Fenton-active sites, thereby accelerating H_2O_2 activation and •OH generation. In parallel, the high surface area and porous nature of ACFs enhance pollutant adsorption, increasing local reactant concentration near reactive oxygen species. Importantly, ACFs stabilize and uniformly disperse Mn_3O_4@ZnO heterostructures, maximizing accessible active sites and light utilization. These functions collectively demonstrate that carbon mediators extend beyond passive supports, actively governing charge flow, ROS formation, and catalytic efficiency in non-ferrous photo-Fenton systems.These carbon-based mediators not only enhance charge-separation efficiency but also increase the structural durability of non-ferrous catalysts, enabling stable operation under continuous photo-Fenton cycles.

View Article Online
DOI: 10.1039/D6LF00096G

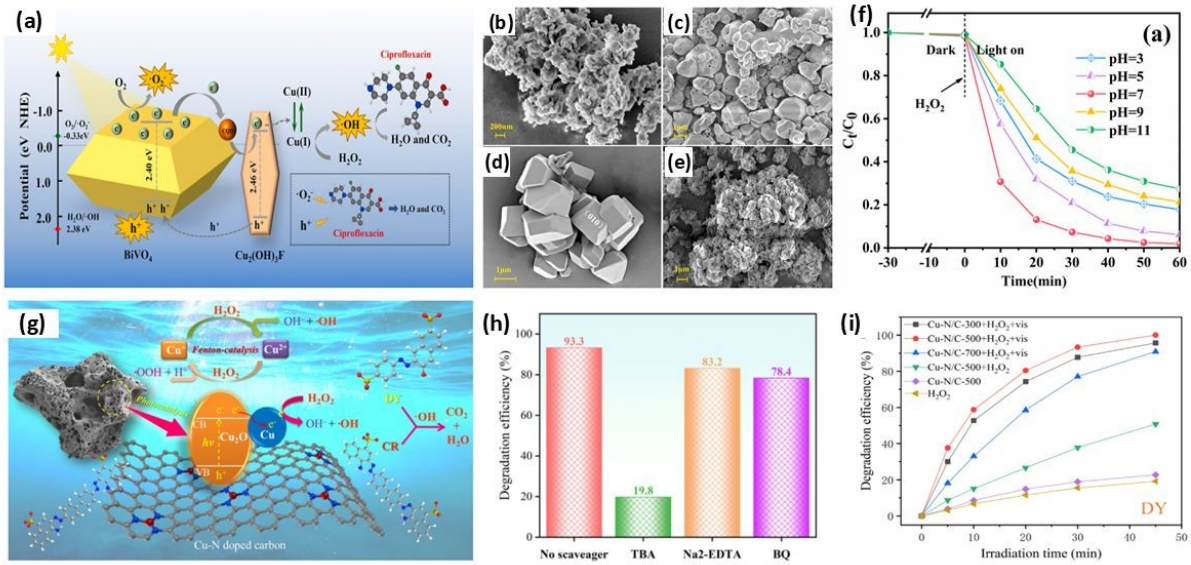

Fig. 5 (a) A schematic illustration showing carbon quantum dots acting as an electron mediator between $BiVO_4$ and $Cu_2(OH)_3F$ in CFO/CQDs (3)-BVO, SEM images of $Cu_2(OH)_3F$ (b), $BiVO_4$(c), CQDs (3)-BVO(d), and CFO/CQDs (3)-BVO(e), and (f) Stability performance over wide pH of 3-11. Reproduced from ref. 97 with permission from Elsevier, Zhang, X.; Liu, Y.; Zhai, Y.; Yu, Y.; Guo, Y.; Hao, S. *Environ. Res.* **2023**, *222*, 115347. Copyright 2023. (g) Proposed mechanism for CR and DY degradation in Cu-N/C-500/H_2O_2 system, (h) Effect of different reactive species scavengers on the degradation efficiencies of DY, and (i) degradation efficiencies of DY under different catalytic conditions. Reproduced from ref. 98 with permission from Elsevier, Tan, Z.; Wang, R.; Yang, S.; Shi, Z.; Wang, D. *J. Mol. Struct.* **2025**, *1337*, 142248. Copyright 2025.

3.3 Oxygen Vacancy and Defect Engineering at Interfaces

Oxygen vacancies (OVs) and defect-rich surfaces are powerful tools for enhancing interfacial charge dynamics and catalytic reactivity in non-ferrous photo-Fenton systems. OVs, in particular, function as powerful catalytic hotspots by modulating the local electronic and coordination environment.

View Article Online
DOI: 10.1039/D6LF00096G

Their primary functions at the interface are to:

- Act as electron-rich centres that can trap photogenerated electrons, suppressing e- and h+ recombination.
- Modulate the electronic structure by creating mid-gap states, which often extends light absorption into the visible region.
- Facilitate H_2O_2 adsorption and dissociation by altering surface polarity and providing active binding sites.
- Modulate the Fermi level at the interface, lowering the activation energy for subsequent redox reactions.

Guo et al.[102] constructed a CeO_2/Bi_4TaO_8Cl (CE-BTC) heterojunction via a molten-salt-mediated defect-engineering route, yielding highly dispersed CeO_2 nanodots and abundant oxygen vacancies (OVs) without damaging the perovskite morphology. The coexistence of OVs and the Ce^{4+}/Ce^{3+} redox pair markedly strengthened charge separation and H_2O_2 activation, enabling a 7.78-fold higher photo-Fenton degradation rate of ofloxacin compared to pristine Bi_4TaO_8Cl. OVs served as crucial electron-trapping and activation centres, boosting •OH and $•O_2^-$ generation while facilitating rapid Ce^{3+}/Ce^{4+} cycling. The CE-BTC catalyst also degraded multiple antibiotics with excellent stability, demonstrating OV-driven enhancement as the key factor governing its superior photo-Fenton performance.[102]

Zhan et al.[103] developed an aeration-free in-situ Fenton-like system by integrating $TiO_{2-x}/W_{18}O_{49}$ heterophase oxygen-vacancy structures with floating rGO-modified polyurethane foam, enabling continuous solar-driven H_2O_2 production (4.2 ppm h^{-1}) and >90% antibiotic removal. In this catalyst, interfacial oxygen vacancies act as powerful electron mediators, tuning the d-band centre to selectively adsorb and activate O_2, weakening the O–O bond, and accelerate the hydrogenation of $•O_2^-$/•OOH intermediates. These vacancies also enhance

View Article Online
DOI: 10.1039/D6LF00096G

spontaneous H_2O_2 adsorption and ROS formation, thereby eliminating the need for external aeration. The work highlights oxygen-vacancy engineering as a critical cocatalytic pathway for enabling self-sustained Fenton-like reactions with drastically reduced energy inputs.[103]

Gao et al.[84] constructed a 2D/2D MgO/g-C_3N_4 S-scheme heterojunction in which MgO nanosheets were in-situ anchored onto g-C_3N_4 through strong Mg–N interfacial bonds. These chemical bonds not only created a tightly coupled S-scheme interface that accelerated directional charge migration but also induced abundant oxygen vacancies within MgO, boosting H_2O_2 activation and ROS generation (Fig. 6a). UV–Vis DRS revealed enhanced visible-light absorption (250–450 nm) (Fig. 6b), while suppressed PL intensity and reduced EIS charge-transfer resistance confirmed efficient carrier separation and interfacial electron migration driven by Mg–N bonding, collectively accounting for the superior photo-Fenton degradation performance (Fig. 6c, d). Consequently, the optimized heterojunction achieved markedly higher photo-Fenton degradation efficiency (80% RhB removal) compared to pristine g-C_3N_4 (28%) and MgO (56%), demonstrating how vacancy engineering combined with interfacial S-scheme charge transfer significantly enhances photocatalytic performance.[84]

In the Cu^0@Cu-zeolite system reported by Zhang et al.[104], Vo synergistically cooperate with plasmonic Cu^0 nanoparticles to enhance visible-light harvesting and accelerate charge utilization. The vacancy sites preferentially trap photogenerated electrons and facilitate their directional transfer to Cu^{2+} species, thereby expediting the Cu^{2+}/Cu^+ redox cycle that governs Fenton-like activity. Simultaneously, oxygen vacancies lower the activation energy for H_2O_2 adsorption and, if recovery and dissociation, promote sustained •OH generation under visible light. This dual-channel electron-transfer pathway, mediated by Vo and Cu^0, ensures rapid redox cycling, suppresses charge recombination, and underpins the exceptionally high degradation kinetics observed. These findings highlight oxygen vacancy engineering as a

View Article Online
DOI: 10.1039/D6LF00096G

powerful and generalizable strategy for boosting non-ferrous photo-Fenton efficiency beyond conventional metal-centre control.

In Co/Ni co-doped ZnO nanorods, aliovalent substitution of Zn^{2+} by Co^{2+} and Ni^{2+} induces lattice distortion and defect levels that stabilize surface oxygen vacancies (Vo) rather than allowing their rapid annihilation during photocatalysis.[105] These vacancies act as electron-trapping centres that suppress electron–hole recombination and facilitate directional transfer of photogenerated electrons toward surface-adsorbed H_2O_2, thereby accelerating •OH radical generation. Simultaneously, Vo introduce sub-bandgap states that extend visible-light absorption and sustain charge excitation under mild irradiation. The stabilized defect environment enables continuous ROS production and preserves catalytic integrity over repeated cycles, demonstrating that defect-engineered ZnO systems can overcome the intrinsic instability of vacancy-rich oxides in photo-Fenton reactions. This work highlights oxygen-vacancy stabilization, rather than mere vacancy creation, as a key design principle for long-term, neutral-pH photo-Fenton catalysis.

Oxygen vacancies play a decisive role in amplifying Ce-based photo-Fenton activity by coupling redox cycling with charge-carrier regulation. In Bi-doped CeO_2 nanorods derived from bimetallic-organic frameworks, aliovalent Bi^{3+} incorporation induces a high density of adaptive oxygen vacancies without phase segregation, even at high doping levels.[39] These vacancies act as electron-trapping centres that suppress electron–hole recombination and promote directional electron transfer toward surface-adsorbed H_2O_2, thereby accelerating •OH and $•O_2^-$ generation. In situ Ce 3d XPS fitting (Fig. 6e) revealed a markedly higher light-induced Ce^{3+} fraction in 10Bi–CeO_2 (5.90%) than in pristine CeO_2 (3.02%), indicating that oxygen-vacancy–enhanced visible-light excitation promotes efficient Ce^{4+}→Ce^{3+} reduction and sustains continuous Ce^{3+}/Ce^{4+} redox cycling for photo-Fenton activation. PL spectra reveal that optimal Bi doping (10Bi–CeO_2) suppresses charge recombination relative to CeO_2, while

View Article Online
DOI: 10.1039/D6LF00096G

excessive Bi loading (13Bi–CeO_2) enhances recombination and weakens photo-Fenton activity (Fig. 6f). Photocurrent and EIS analyses as shown in Fig. 6g,h reveal that 10Bi–CeO_2 exhibits a higher photocurrent density and smaller charge-transfer resistance than pristine CeO_2, confirming oxygen-vacancy-assisted Bi doping enhances charge separation, accelerates interfacial electron transport, and thereby improves photo-Fenton degradation efficiency. The synergistic interaction between vacancy-mediated charge separation and cerium redox shuttling endows the Bi-CeO_2 system with exceptional photo-Fenton efficiency and durability, underscoring oxygen-vacancy engineering as a central design principle for advanced non-iron Fenton catalysts.

Oxygen vacancies play a central mechanistic role in enabling efficient photo-Fenton activity in Cu-modified MgO systems by coupling charge separation with Cu redox cycling.[76] In Cu-deposited MgO nanosheets, UV photodeposition induces abundant surface oxygen vacancies that act as electron-trapping centres, suppressing electron–hole recombination and extending visible-light absorption. These vacancies stabilize high-valence Cu species (Cu^{3+}/Cu^{2+}) and facilitate rapid interconversion among $Cu^0/Cu^+/Cu^{2+}/Cu^{3+}$, thereby sustaining continuous H_2O_2 activation under illumination. Moreover, oxygen-vacancy-rich sites promote the accumulation and directional transfer of photogenerated electrons toward Cu centres, accelerating the Cu^{2+}/Cu^+ redox cycle and enhancing $\bullet O_2^-$ and •OH generation. The synergistic interaction between oxygen vacancies and multivalent Cu species enables efficient photo-Fenton degradation across a broad pH range, highlighting oxygen-vacancy engineering as a powerful strategy for activating wide-bandgap oxides in non-iron Fenton-like systems. Overall, Oxygen vacancy and defect engineering at interfaces play a decisive role in expanding light absorption, steering charge transfer, and increasing surface reactive sites. This strategy is especially crucial for Ce- and Bi-based systems, where these OV-mediated pathways rather

View Article Online
DOI: 10.1039/D6LF00096G

than classical Fenton chemistry, dominate H_2O_2 activation and govern the efficiency of visible-light-assisted reactions.

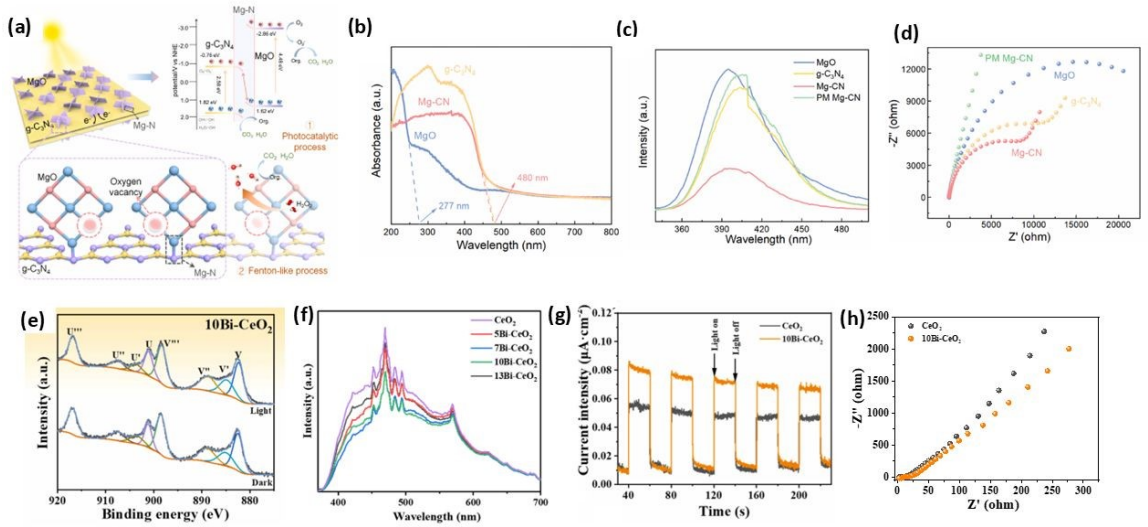

Fig. 6 (a) A schematic illustration showing Oxygen vacancy mediated photo-Fenton degradation of Rhodamine by the Mg–CN, (b) UV–visible diffuse-reflectance spectra, (c) photoluminescence spectra, (d) electrochemical impedance spectra of MgO, g-C_3N_4, Mg–CN, and PM Mg–CN. Reproduced from ref. 84 with permission from Elsevier, Gao, M.; Li, Z.; Su, X.; Zhang, X.; Chang, J.; Geng, D.; Lu, Y.; Zhang, H.; Wei, T.; Feng, J. *Chemosphere* **2023**, *343*, 140285. Copyright 2023. (e) High resolution XPS spectra of Ce 3d of 10Bi-CeO_2 photocatalyst dark and light reaction, (f) PL spectra of CeO_2 and Bi-CeO_2, (g) transient photocurrent response of CeO_2 and 10Bi-CeO_2. (h) EIS Nyquist plots of CeO_2 and 10Bi-CeO_2. Reproduced from ref. 39 with permission from Elsevier, Zhang, X.; Zhang, L.; Ye, H.; Zeng, Z.; Yang, J.; Han, C.; Liang, Y. *J. Environ. Chem. Eng.* **2025**, 117489. Copyright 2025.

3.4 Integration with Porous Scaffolds (MOFs, LDHs, Biochar)

Coupling non-ferrous photo-Fenton catalysts with porous supports such as metal–organic frameworks (MOFs), layered double hydroxides (LDHs), mesoporous carbons, and biochar

View Article Online
DOI: 10.1039/D5LF00096G

has emerged as an effective strategy to enhance surface reactivity, increase active-site density, and improve H_2O_2 utilization. These porous architectures provide high surface areas, abundant anchoring sites, and tunable pore networks that facilitate mass transport, pollutant adsorption, and dispersion of catalytic species. The resulting interfacial synergy significantly accelerates visible-light-driven Fenton-like processes.

Porous carbonaceous materials such as biochar, activated carbon, and mesoporous carbon not only offer large accessible surface areas but also contain oxygen- and nitrogen-functional groups that anchor transition-metal centres. Biochar-derived porous scaffolds play a multifunctional role in photo-Fenton catalysis, serving simultaneously as catalyst supports, electron mediators, and adsorption platforms. Mansoori et al.[56] reported a CuO_x–MnO_y@biochar catalyst in which FESEM images (Fig. 7a) show spherical CuO_x-MnO_y nanoparticles (10–100 nm) well dispersed on a rough, mesoporous biochar surface derived from rice straw. This carbon framework ensures high dispersion and stabilization of Cu and Mn oxide nanodomains while providing abundant surface sites for pollutant enrichment, and its conductive network with persistent free radicals facilitates interfacial electron transfer under visible light, thereby promoting rapid Cu^{2+}/Cu^{+} and Mn^{3+}/Mn^{2+} redox cycling and efficient H_2O_2 activation. ESR analysis (Fig. 7b) confirmed persistent free radical–mediated •OH generation in the biochar/H_2O_2 system, and this synergistic coupling between the porous biochar scaffold and Cu-Mn bimetallic active centres enabled sustained ROS production over a wide pH range, leading to near-complete metronidazole degradation with appreciable mineralization. These results highlight biochar as an effective porous scaffold for integrating adsorption, charge mediation, and Fenton-like redox chemistry in sustainable photo-Fenton systems.

In another study, Wang et al.[106] prepared CuO/Cu_2O/Cu–N–codoped biochar (Cu–N–C-700) by pyrolyzing a chitosan–Schiff-base–Cu precursor, enabling the in-situ formation of CuO,

View Article Online
DOI: 10.1039/D5FF00096G

Cu_2O, metallic Cu, and N-doped carbon within a conductive biochar matrix. The resulting mesoporous biochar (21 nm average pore size) provided high surface area, strong adsorption affinity, and efficient electron transport, which collectively enhanced the interaction between pollutants and catalytic sites. Benefiting from multiple Cu redox centres and the adsorption–activation synergy of the biochar scaffold, the Cu–N–C-700/H_2O_2 system achieved 98.5% tetracycline degradation within 15 min and maintained stable performance over five cycles. The study highlights how embedding multi-valent copper species into N-doped biochar frameworks enables robust, pH-tolerant photo-Fenton catalysis.[106]

In the Cu/HAP-sBC system reported by Wang et al.[50], straw-derived biochar provides a hierarchically porous carbon matrix that anchors hydroxyapatite-stabilized Cu species, ensuring uniform metal dispersion while suppressing Cu leaching and acid etching. The large surface area of the biochar scaffold enhances pollutant enrichment near active sites, while the conductive carbon framework promotes interfacial electron transfer, facilitating continuous Cu^{2+}/Cu^{+} redox cycling and effective H_2O_2 activation under near-neutral conditions. This adsorption–catalysis synergy enables sustained •OH generation and rapid p-nitrophenol mineralization, demonstrating that biochar scaffolds are not passive supports but active structural components that stabilize metal centres, broaden operational pH windows, and enhance the durability of heterogeneous photo-Fenton systems.

MOF-based supports (e.g., ZIF-67, MIL-88, UiO-66) also provide well-defined pore channels and uniform metal sites that assist in dispersing non-ferrous catalytic centres. Upon partial pyrolysis, MOFs can generate highly porous carbon–metal composites that combine conductive frameworks with abundant active sites, resulting in enhanced photo-Fenton activity.

View Article Online
DOI: 10.1039/D6LF00096G

Wang et al.[107] developed self-supported 2D TCPP-MOF arrays vertically grown on conductive copper foam via a hydrothermal route, forming an integrated heterointerface that significantly boosts photo-Fenton-like catalysis. The honeycomb MOF architecture provided a large accessible surface area and rapid mass transfer, while the uniformly dispersed M–N_4 active sites enabled efficient visible-light harvesting and charge separation. Incorporating bimetallic centres further strengthened interfacial redox activity, enhancing electron–hole utilization for ROS generation. Benefiting from the intimate MOF–substrate contact and fast interfacial carrier transport, the catalyst achieved robust mineralization of diverse organic pollutants and exhibited excellent recyclability due to its mechanically stable, self-supported structure. This work highlights the power of MOF interface engineering in designing high-efficiency, recoverable photo-Fenton-like catalysts.[107]

Abdelhaleem et al.[108] synthesized a Cu-based MOF-derived CuO@C catalyst via direct pyrolysis, forming a tightly integrated CuO–carbon interface that enhanced H_2O_2 activation under visible LED irradiation. TEM and HR-TEM analyses (Fig. 7c,d) confirm that CuO nanoparticles are uniformly embedded within the MOF-derived carbon matrix with exposed CuO (111) facets, which ensures homogeneous dispersion, suppresses Cu leaching via in situ redeposition, and facilitates rapid interfacial electron transfer during the photo-Fenton-like process. Control studies (Fig. 7e) demonstrate that the CuO@C/H_2O_2/visible LED system achieves 95% paracetamol degradation within 60 min, far surpassing CuO@C/H_2O_2 (47%) and H_2O_2/LED (26%), thereby underscoring the dominance of synergistic heterogeneous photo-Fenton catalysis enabled by the robust interfacial architecture. TBA quenching (Fig. 7f) confirmed •OH dominated degradation, underscoring that MOF-derived CuO@C provides a conductive and stable scaffold for efficient H_2O_2 activation and sustained photo-Fenton catalysis.[108]

View Article Online
DOI: 10.1039/D6LF00096G

In the POM-incorporated MOF Cu(I)W–DPNDI reported by Chen et al.[109], the ordered porous architecture aligns Cu(I) Fenton-active centers, polyoxometalate (POM) oxidation sites, and photoactive DPNDI ligands at molecular proximity, facilitating efficient interfacial electron transfer and reactive oxygen species generation. The confinement effect of the MOF pores suppresses radical over-diffusion and promotes controlled ROS utilization, which is critical for achieving high selectivity in oxidation reactions. Meanwhile, the rigid MOF scaffold stabilizes Cu(I) species and POM polyanions, enabling sustained redox cycling under light irradiation while preventing catalyst deactivation. This work demonstrates that MOF porosity is not merely structural but functionally decisive, allowing the integration of light harvesting, charge transport, and Fenton-like redox chemistry into a single, highly selective photo-Fenton catalytic platform.

It was reported that porous self-supported scaffolds play a decisive role in enhancing photo-Fenton-like catalysis by simultaneously governing mass transfer, active-site accessibility, and charge transport. In vertically aligned 2D porphyrinic MOF arrays grown on conductive copper foam, the open honeycomb architecture provides interconnected meso-macroporous channels that enrich organic pollutants and H_2O_2 at catalytic interfaces while minimizing diffusion resistance.[107] The rigid, porous scaffold enables uniform exposure of M-N_4 active sites, promoting efficient light harvesting and rapid separation of photogenerated charge carriers. Moreover, the conductive and self-standing framework facilitates directional electron transport and suppresses catalyst aggregation or leaching during redox cycling. This integrated porous-scaffold design demonstrates that architectural engineering, beyond chemical composition, is critical for sustaining high ROS flux, long-term stability, and efficient mineralization in advanced photo-Fenton systems.

In multivariate Cu-ZIF-9-ica frameworks reported by Sánchez et al.[54], the intrinsic microporous ZIF scaffold concentrates organic pollutants and H_2O_2 within confined pores,

View Article Online
DOI: 10.1039/D6LF00096G

enhancing local reactant availability and accelerating interfacial ROS generation. The open framework ensures uniform dispersion of Cu redox centres and mixed-ligand environments, shortening charge-migration pathways and suppressing recombination of photogenerated carriers. Moreover, the rigid porous architecture stabilizes the catalytic sites against leaching during repeated Cu^{2+}/Cu^{+} cycling, enabling sustained photo-Fenton activity under neutral pH and low oxidant dosage. These findings highlight that porous scaffold engineering in MOFs is not merely structural but mechanistically integral to achieving high efficiency, stability, and practical applicability in visible-light-driven photo-Fenton systems.

Layered double hydroxides (LDHs) offer well-ordered two-dimensional galleries, tunable metal compositions, and abundant surface hydroxyl groups that enable uniform dispersion of non-ferrous catalytic centres and facilitate H_2O_2 adsorption and activation. Upon thermal transformation or partial reduction, LDHs can evolve into porous mixed-metal oxides or metal/oxide–carbon hybrids with enlarged surface area, enhanced electrical conductivity, and stabilized multivalent redox sites, collectively leading to accelerated charge transfer and improved photo-Fenton efficiency under visible light.

Ultrathin LDH nanosheets provide an effective porous scaffold for photo-Fenton catalysis by combining high surface area, short carrier diffusion lengths, and uniformly distributed multivalent metal centres. For example, He et al.[110] reported ultrathin ternary CuZnCr-LDH nanosheets in which the layered porous architecture facilitates rapid charge migration and exposes abundant redox-active Cu and Cr sites. The LDH scaffold promotes efficient Cu^{+}/Cu^{2+} and Cr^{3+}/Cr^{6+} cycling under light irradiation, thereby accelerating H_2O_2 activation and sustaining continuous •OH and $\bullet O_2^-$ generation. Benefiting from the synergistic coupling of photocatalysis and Fenton chemistry enabled by the ultrathin LDH framework, the catalyst achieved high degradation and mineralization efficiencies for ciprofloxacin and methylene

View Article Online
DOI: 10.1039/D6LF00096G

blue, highlighting the critical role of LDH porous scaffolds in stabilizing metal redox cycles and enhancing photo-Fenton performance.

Zhu et al.[111] reported an ultrathin engineered $CuNi_2Al$-LDH nanosheet as a porous layered scaffold to accelerate electron transport and enrich redox-active sites. The brucite-like LDH framework enabled intimate spatial proximity between Cu and Ni ions, where Ni acted as an internal electron mediator to continuously shuttle electrons to Cu centres, generating a high proportion of Cu(I) required for efficient H_2O_2 activation. The porous LDH nanosheet architecture simultaneously enhanced visible-light harvesting through Cu/Ni d–d transitions and provided abundant exposed active sites. This synergistic scaffold-induced electron transfer dramatically boosted Cu^{2+}/Cu^{+} cycling and promoted rapid ROS generation, enabling complete degradation of phenol, tetracycline, and dyes within 30 min. Their work highlights how integrating bimetallic centres within a high-surface-area LDH scaffold offers an effective pathway to strengthen charge separation and Fenton-like redox dynamics in non-ferrous systems.

Overall, the integration of non-ferrous catalysts with porous supports strengthens adsorption activation processes, improves charge mobility, and offers structural stability, ultimately leading to faster reaction kinetics and higher pollutant removal efficiencies in visible-light-assisted Fenton-like systems.

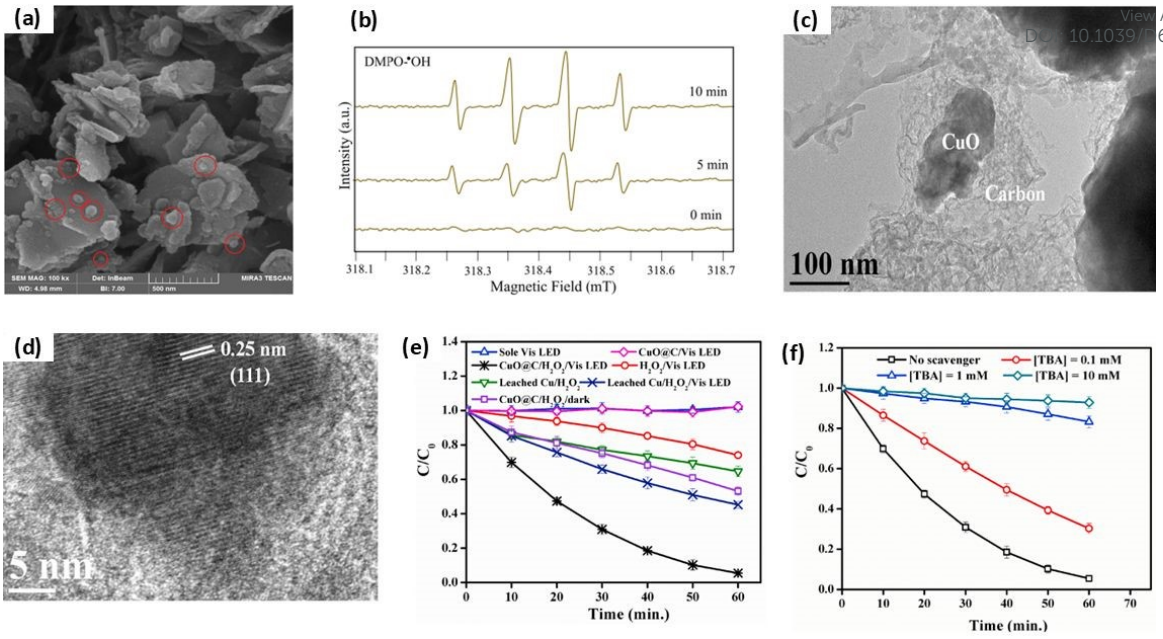

Fig. 7 (a) FESEM image of CuO_x-MnO_y@BC, and (b) ESR spectra of DMPO-OH for BC. Reproduced from ref 56 Mansoori, S.; Ozumchelouei, E. J.; Davarnejad, R.; Zahrani, A. A. *Catal. Commun.* **2022**, 171, 106517. *under the terms of the Creative Commons CC-BY license.* (c) TEM of CuO@C, (d) HR-TEM of CuO@C, (e) Role of various processes for PCM photodegradation, and (f) effect of radical scavengers on PCM photodegradation by CuO@C. Reproduced from ref.108 with permission from Elsevier, Abdelhaleem, A.; Abdelhamid, H. N.; Ibrahim, M. G.; Chu, W. *J. Clean. Prod.* **2022**, *379*, 134571. Copyright 2022.

3.5 Atomically Dispersed Metal Sites on Interfaces

Atomically dispersed metal sites represent a cutting-edge strategy in the design of highly efficient non-ferrous photo-Fenton catalysts. By distributing metal atoms as isolated single-site centres (e.g., M–N_x, M–O_x coordination environments), the maximum atomic utilization is achieved while preventing metal agglomeration and leaching, two major challenges in conventional heterogeneous Fenton systems. These atomic-scale active centres provide well-

View Article Online
DOI: 10.1039/D5LF00096G

defined coordination environments that promote uniform H_2O_2 activation, enhanced charge transfer, and improved catalytic selectivity.

Dong et al.[112] constructed atomically dispersed Cu-N_4 sites on g-C_3N_4, with SEM and TEM confirming the preservation of the wrinkled nanosheet architecture (Fig. 8a,b). These isolated Cu–N_4 centres enable efficient H_2O_2 activation and accelerated charge separation, thereby overcoming sluggish redox kinetics in non-ferrous photo-Fenton systems. The optimized Cu–C_3N_4 achieved nearly 99% ciprofloxacin removal within 30 min, far outperforming pristine g-C_3N_4 and all control systems due to efficient H_2O_2 activation at Cu–N_4 single-atom sites, with the degradation kinetics following a pseudo-first-order model as shown in Fig. 8c. Spectroscopic analyses (EPR and XAFS) revealed that Cu–N_4 sites mediate a nonradical H_2O_2 activation pathway via O═Cu–N_4 and O═Cu–N_4═O intermediates, consistent with the weak •OH signals observed by Scavenger study (Fig 8d). This atomic-scale dispersion maximized the catalytic utilization of Cu, enabled fast electron mobility across the interface, and established a robust platform for next-generation non-ferrous Photo-Fenton catalysts.[112]

Guo et al.[52] developed hydrangea-like carbon nitride decorated with atomically dispersed Cu–N_4 sites, forming a strong metal–support interaction that markedly enhanced photo-Fenton efficiency. The Cu–N_4 coordination created intermediate electronic states that accelerated the Cu^{2+}/Cu^{+} redox cycle and increased the binding affinity of Cu d orbitals (especially d_{xz}) toward H_2O_2 by nearly ten-fold, enabling faster peroxide activation. Benefiting from the maximized atomic utilization and rapid carrier transfer, the Cu-SA/CNH catalyst achieved 98.1% tetracycline degradation and complete *E. coli* inactivation within 30 min, outperforming pristine CN. This work highlights the pivotal role of single-atom dispersion in strengthening redox cycling and H_2O_2 activation pathways during photo-Fenton treatment.[52]

View Article Online
DOI: 10.1039/D6LF00096G

Zichao Lian et al.[113] engineered atomically dispersed Ag–Co dual sites on g-C_3N_4 (AgCo–CN), forming densely distributed bimetallic coordination centres that simultaneously promote charge separation and create self-Fenton redox pairs. The isolated Ag and Co atoms act cooperatively, Ag accelerates photoelectron extraction while Co functions as the primary H_2O_2-activating site, enabling efficient in-situ generation of •OH and $^1O_2$ under visible light. Benefiting from this highly dispersed dual-metal interface, AgCo–CN achieved near-complete mineralization of phenol even under harsh conditions and maintained long-term activity in a custom photo-filter reactor. This work highlights how atomic-scale bimetallic dispersion can unlock self-driven photo-Fenton pathways for degrading recalcitrant pollutants.[113]

In the CuN_x–carbon nitride catalyst reported by Zhang et al.[114], isolated CuN_x moieties embedded within a porous C–N matrix function as well-defined single-atom-like active centres for H_2O_2 activation. Such high-density atomic dispersion prevents Cu aggregation and leaching while enabling efficient Cu^{2+}/Cu^{+} redox cycling under visible light. The strong metal–nitrogen coordination modulates the local electronic structure of Cu, lowers the activation barrier for H_2O_2 dissociation, and promotes selective •OH generation, as corroborated by DFT calculations. Simultaneously, the conductive carbon nitride framework facilitates charge separation and transport, allowing photogenerated electrons to be efficiently funnelled toward CuN_x sites. This work highlights that atomic-scale metal dispersion is not merely a stabilization strategy but a decisive design principle for synchronizing charge transport, oxidant activation, and redox durability in high-performance photo-Fenton catalysts.

This concept extends across a diverse spectrum of the non-ferrous family. Single-atom Ce sites, for example, leverage the Ce^{3+}/Ce^{4+} redox couple at the atomic level to enhance oxygen vacancy-mediated turnover, while atomic Bi sites create unique, highly localized charge centres to promote specific photocatalytic pathways.[115] These single-atom sites effectively modulate the local electronic structure of the host material, creating localized charge-density

View Article Online
DOI: 10.1039/D6LF00096G

regions that accelerate light-driven redox reactions. Overall, atomic dispersion of non-ferrous metals provides a powerful avenue for designing highly active, durable, and structurally uniform photo-Fenton catalysts. By combining biomimetic site architecture with strong interfacial bonding, single-atom catalysts (SACs) offer enhanced catalytic precision and significantly improved pollutant degradation efficiency under visible-light-assisted conditions.

3.6 Bimetallic and Multicomponent Interfaces

Bimetallic and multicomponent interface engineering has emerged as a powerful strategy for significantly improving the catalytic efficiency of non-ferrous photo-Fenton systems. By integrating two or more metal species with complementary redox behaviours, it is possible to create synergistic reaction pathways, broaden light absorption, and optimize H_2O_2 activation. Such interfaces fine-tune electronic structures, promote multivalent cycling, and offer multiple active sites for simultaneous radical generation. Dai et al.[35] synthesized Mn-doped cobalt silicate@diatomite (Co–MnSi@DE) composites to enhance Fenton-like oxidation via synergistic bimetallic interactions. The introduction of Mn into the Co-silicate framework enlarged surface area, narrowed the band gap, and created a more redox-active Co–Mn interface that accelerated H_2O_2 activation. DFT analysis confirmed that Mn incorporation lowered the reaction energy barrier for peroxide cleavage, while ESR revealed that the Co/Mn dual sites enabled the concurrent formation of •OH and $\bullet O_2^-$ under UV light. Benefiting from these cooperative interfacial effects, the optimized $Co_{0.25}$MnSi@DE achieved >95% degradation of methyl orange and maintained stability over repeated cycles, demonstrating the strong performance advantages of bimetallic interface engineering in non-ferrous photo-Fenton catalysis.[35]

Xiong et al.[94] constructed a CNNS/Ni–Ag heterostructure in which bimetallic Ni/Ag sites and an interfacial built-in electric field cooperatively boosted photo-self-Fenton reactivity. The

View Article Online
DOI: 10.1039/D6LF00096G

LSPR-induced hot electrons from Ag and photogenerated electrons from CNNS were directionally driven toward Ni centres, where Ni acted as the primary electron mediator to accelerate O_2 adsorption and the two-electron ORR pathway. This dual-metal synergy enabled high in-situ H_2O_2 generation (1541.3 μmol g^{-1} h^{-1} with IPA) and rapid metronidazole removal (92.9% in 60 min), outperforming single-metal or external-H_2O_2 systems. The study highlights how bimetallic interfaces can simultaneously enhance light harvesting, carrier separation, and surface redox kinetics to realize efficient non-ferrous self-Fenton catalysis.

Hu et al.[96] constructed a Cu-decorated carbon@Bi/Bi_2MoO_6 plasmonic heterojunction derived from a MOF precursor, in which metallic Cu, in situ generated Bi, and Bi_2MoO_6 formed an integrated dual-metal interface. UV–Vis DRS and Tauc analyses (Fig. 8e,f) show that the Cu/Bi bimetallic coupling with Bi_2MoO_6 introduces SPR-enhanced visible-light absorption (~580 nm) and narrows the bandgap (2.58 → 1.48 eV), thereby promoting charge generation and synergistic photo-Fenton activity. Transient photocurrent and EIS analyses (Fig. 8g,h) reveal that the Cu/Bi–carbon coupled BC300–30 heterojunction exhibits the highest photocurrent density and the smallest charge-transfer resistance confirming that bimetallic interfaces, carbon skeletons, and oxygen vacancies synergistically enhance charge separation and migration, thereby boosting photo-Fenton activity. This work highlights that rational engineering of bimetallic and carbon-coupled interfaces is a powerful strategy to amplify interfacial charge dynamics and ROS productivity in non-ferrous photo-Fenton catalysts.

In the rhombohedral AlMnCuZnBi HEA reported by Anuraag et al.[116], the homogeneous atomic-level mixing of Mn, Cu, Zn, Al, and Bi generates a complex electronic landscape with diverse local coordination environments that collectively facilitate H_2O_2 activation and charge transfer. The coexistence of multiple transition and post-transition metals enables parallel redox pathways, enhancing electron availability for Fenton-like reactions while suppressing metal leaching commonly observed in single-metal systems. Such multicomponent interfaces

View Article Online
DOI: 10.1039/D6LF00096G

promote synergistic interactions among different metal centres, improving electron delocalization and sustaining catalytic activity under photo-assisted conditions. This study highlights HEAs as an emerging class of photo-Fenton catalysts, where compositional complexity and interfacial synergy replace conventional heterojunction design to achieve robust and durable pollutant degradation.

In the ternary selenide nanocomposite $Co_9Se_8/Ni_3Se_4/Cu_2Se$ reported by Mohapatra et al.[117], the intimate interfacial coupling among Co, Ni, and Cu-based selenides establishes multiple electron-transfer pathways under visible light, promoting efficient separation and migration of photogenerated charge carriers. These heterogeneous interfaces facilitate cooperative redox cycling (Cu^{2+}/Cu^{+}, Co^{3+}/Co^{2+}, Ni^{3+}/Ni^{2+}), which accelerates H_2O_2 activation and sustains continuous ROS generation during photo-Fenton reactions. Moreover, the multinary junctions broaden light absorption and provide abundant interfacial active sites, enabling high degradation efficiencies for both cationic and anionic dyes. This study highlights that interface-driven electronic synergy in multicomponent catalysts is a powerful strategy for overcoming kinetic limitations in conventional single-metal photo-Fenton systems.

These hybrid structures often operate through dual or cooperative pathways, including simultaneous radical and non-radical oxidation, broadening the scope of degradable pollutants.

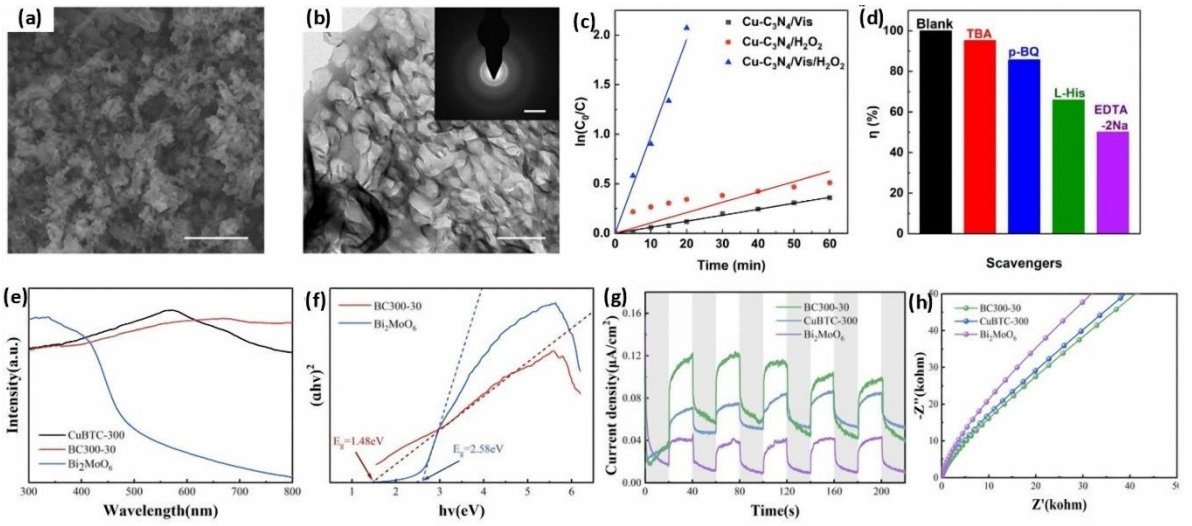

View Article Online
DOI: 10.1039/D6LF00096G

Fig. 8 (a) SEM, (b) TEM (inset SAED) results of Cu–C_3N_4, (c) Pseudo-first-order kinetic plots for CIP degradation in Cu–C_3N_4/Vis, Cu–C_3N_4/H_2O_2, and Cu–C_3N_4/Vis/H_2O_2 systems, and (d) The relative contributions of different scavengers over the Cu–C_3N_4/Vis/H_2O_2 system. Reproduced from ref. 112 with permission from American Chemical Society, S. Dong, X. Chen, L. Su, Y. Wen, Y. Wang, Q. Yang, L. Yi, W. Xu, Q. Yang, P. He, ACS ES&T Engineering, **2022**, 3, 150–164. Copyright 2022. (e) UV-vis diffuse reflectance spectra of CuBTC-300, Bi_2MoO_6 and BC300–30, (f) corresponding $(\alpha h\nu)^2$ or $(\alpha h\nu)^{1/2}$ plots versus photon energy (hν), (g) Instantaneous time-response current of Bi_2MoO_6, CuBTC-300 and BC300-30, and (h) EIS Nyquist plots of Bi_2MoO_6, CuBTC-300 and BC300-30. Reproduced from ref. 96 with permission from Elsevier, Hu, Y.; Ke, J.; Yan, Z.; Zhao, L.; Liu, J. *Colloids Surf. A Physicochem. Eng. Asp.* **2025**, 137409. Copyright 2025.

Overall Integration of Interface Strategies

Interface engineering has evolved into a foundational design principle for next-generation non-ferrous photo-Fenton catalysts. Through the rational construction of semiconductor junctions, cocatalyst decoration, oxygen-vacancy engineering, atomic dispersion of metal centres, and multicomponent design, catalytic efficiency has been dramatically improved. These interfacial strategies synergistically enhance charge separation, strengthen ROS generation, increase pollutant affinity, and improve structural durability. Consequently, multicomponent and interface-engineered catalysts represent the most promising direction for developing advanced, sustainable oxidation systems for water purification.

Table 3. Representative photo-Fenton-like degradation performance of non-ferrous catalysts with different interface-engineering strategies

Interface Engineering Strategy	Catalyst	Pollutant	Light Source	H2O2	Stability & Leaching Assessment	Efficiency / Time	Ref
Heterojunctions (Type II)	$Cu_2(OH)_3F/BiOBr$	TC-HCl	300W Xe Lamp 400 ≥ λ	40mM	5 cycles / 89.8% retention / Structurally stable	98.8% / 60 min	43
	$CuCo_2S_4/Bi_2WO_6$	TC-HCl	300W metal halide Lamp	100µL, 30wt%	4 cycles / High activity maintained /Crystalline structure preserved (XRD)	80% / 60 min	78
	Cu_2ZnSnS_4/Bi_2WO_6	RhB	300W metal halide Lamp	-	4 cycles / High activity / Crystalline stability (XRD)	94% / 50 min	79
	CeO_{2-x}/Bi_2MoO_6	OFX	5W Visible LED	1.5mM	5 cycles / Nearly unchanged / Structurally stable (XRD/XPS); stable redox cycle with low leaching.	97.64% / 120 min	38
Heterojunctions (Z-Scheme)	$CPDs/CuBi_2O_4$	CIP	Visible LED Lamp 420 ≥ λ	0.5 mL	5 cycles / >79.3% removal / High structural stability (XRD/XPS/TEM/FT-IR confirmed); Z-scheme durability	92.3% / 30 min	51
	MnO_2/CNK-OH-Mn	TC	300W Xe Lamp	10 mM	-	96.7% / 120 min	81
	$CDs/CuO/gC_3N_4$	MB	VIS Lamp	5mM	6 cycles / High retention / Excellent universality	100% / 40 min	40
	$gC_3N_4/ZnCo_2O_4$	RhB	40 W Visible LED	1mL (30wt%)	5 cycles / 79% retention / Structurally stable (XRD constant)	94% / 80 min	49
Heterojunctions (S-Scheme)	$CuInS_2/WO_3$	TCH	300W Xe Lamp	50µL	5 cycles / Stable activity / Structural and compositional integrity (XRD confirmed)	42.7% / 6 h	85
	Bi_2WO_6/CoAl LDH	OTC	300W Xe Lamp 420 ≥ λ	50mM	4 cycles / 88.74% retention / Structurally stable (XRD);	98.47% / 60 min	41

View Article Online
DOI: 10.1039/D6LF00095G

					Co^{2+} leaching <1.0 mg/L		
	$C_3N_{4x}/AgO_y@Co_{1-x}Bi_{1-y}O_7$	OTC	100W tungsten bulb	-	4 cycles / 75–78% retention	93% / 160 min	83
	MgO/gC_3N_4	RhB	30W Xenon Lamp	2 mL	-	80% / 60 min	84
Cocatalyst & Electron Mediators	$Cu\text{-}Bi_2O_2S$	TCH	Visible Lamp	30µL	5 cycles / >50% retention / Moderate stability; decline due to Cu nanoparticle peeling and Cu^0 surface oxidation (XPS/SEM confirmed).	77.76% / 60 min	46
	CNNS/Ag/Ni Heterostructure	Metronidazole	Visible Lamp	-	5 cycles / 91.7% retention / High structural stability (XRD/SEM/FT-IR confirmed)	92.9% / 60 min	94
	$Cu_2(OH)_3F/CQDs\text{-}BiVO_4$	CIP	300 W Xenon Lamp	0.2mL	5 cycles / ~90% retention / High structural stability (XRD/XPS)	98.1% / 60 min	97
	CuO/gC_3N_4	Dimethyl Phenol (2,4-DMP)	35W Visible LED	0.2mM	High stability / Leaching significantly suppressed by H_2O_2 (<0.085 mg/L); stabilization via CuO_2 intermediate formation.	99% / 120 min	99
Defect & Oxygen Vacancy (OV)	$CeO_2\text{-}Ba_4TaO_8Cl$	OFX	5W LED Lamp	4.5mM	5 cycles / 93.69% retention / High structural stability (XRD confirmed)	98.78% / 40 min	102
	$Cu^o@CuZ$	Phenol	Visible Lamp	-	High reusability / Wide pH tolerance / Excellent stability in actual complex wastewater	100% / 15 min	104
	Cu-MgO	Rhodamine B (RhB)	Xe Lamp 400 ≥ λ	20mM		92.8% / 60 min	76
Porous Scaffolds (BC/MOFs/LDHs)	$CuO_x/MnO_y@BC$	Metronidazole (MNZ)	300W Xe Lamp	20mM	5 cycles / 85.7% retention / High stability	99.7% / 120 min	56
	Bi/Ce-BMOFs	TC	5W Visible LED	10mM	4 cycles / High retention / Structurally and chemically	83% / 60 min	39

View Article Online
DOI: 10.1039/D6LF00095G

					stable (XRD/SEM/XPS confirmed)		
	$CuNi_2Al$-LDH	Phenol	30W Xenon Lamp	6mM	4 cycles / High retention / High stability; Cu leaching (0.73 ppm)	100% / 30 min	111
Atomically Dispersed Sites	Cu-C_3N_4	CIP	30W Xenon Lamp	-	5 cycles / ~100% retention / Exceptional stability; universal degradation	99% / 30 min	112
	CuCN	TC	300W Xenon Lamp	80mM	5 cycles / 83.3% retention / High stability; Cu leaching <30 µg/L (ICP confirmed)	93.6% / 60 min	114
	Cu-SA/CNH/PF	TC	Visible Xe Lamp $420 \geq \lambda$	160mM	5 cycles / 80.3% retention / Excellent stability; Cu leaching <25 µg/L (ICP-MS)	98.1% / 30 min	52
Bimetallic/Multi component	Mn-doped Cobalt silicate@diamoite	MO	UV Lamp	25mM	5 cycles / >90% efficiency	95% / 90 min	35
	AlMnCuZnBi Alloy	MO	White LED Lamp	0.5mM	5 cycles / ~94% retention / High stability; High-entropy effect prevents significant active site leaching.	100% / 170 min	116
	$Co_9Se_8/Ni_3Se_4/Cu_2Se$	RhB	LED Lamp	-	-	97.14% / 120 min	117

4. Mechanistic Insights into Reactive Oxygen Species (ROS) Generation in Non-Iron Photo-Fenton Catalysts

The performance of non-ferrous photo-Fenton catalysts is governed by the generation and management of reactive oxygen species (ROS), including hydroxyl radicals (•OH), superoxide anions ($•O_2^-$), hydroperoxyl radicals (•OOH), and singlet oxygen ($^1O_2$). In contrast to classical Fe-based systems that require acidic pH, the combination of visible-light-responsive semiconductors with redox-active metals such as Cu, Co, Mn, Bi, and Ce enables efficient

View Article Online
DOI: 10.1039/D6LF00096G

H_2O_2 activation under near-neutral conditions. These processes are strongly influenced by metal valence transitions, semiconductor band alignment, interfacial charge separation, and the presence of oxygen vacancies or other defect sites. Rational interface engineering via heterojunctions, cocatalyst deposition, or atomic dispersion, therefore plays a central role in steering electron flow, stabilizing intermediates, and enhancing ROS productivity in non-ferrous systems.

4.1 Copper-Based Catalysts: Redox Cycling and Enhanced Charge Transfer

Copper-based catalysts exhibit some of the most efficient non-ferrous photo-Fenton activity due to the favourable redox potential of the Cu^+/Cu^{2+} pair (+0.17 V), which enables rapid and reversible electron transfer. The core mechanism consists of two interconnected steps:

(1) Cu^+-driven H_2O_2 decomposition

$$Cu^+ + H_2O_2 \rightarrow Cu^{2+} + \bullet OH + OH^-$$

This reaction is thermodynamically favored and proceeds quickly, generating •OH radicals as the primary oxidant.

(2) Photoreduction of Cu^{2+} to regenerate Cu^+

$$Cu^{2+} + e^-_{(photo)} \rightarrow Cu^+$$

The integration of Cu species with semiconductors significantly enhances this redox cycle by providing a continuous supply of photogenerated electrons. Zhang et al.[114] developed a Cu-doped carbon nitride catalyst featuring highly dispersed CuN_x single sites that markedly strengthened H_2O_2 activation in a photo-Fenton system. Embedding CuN_x centres into the porous C_3N_4 framework enhanced visible-light absorption and accelerated charge transport, enabling rapid generation of •OH, $\bullet O_2^-$, h^+, and $^1O_2$. The optimized CuCN catalyst achieved 93.6% tetracycline degradation within 60 min, with strong performance even in real water matrices. DFT calculations confirmed that CuN_x moieties lower the

View Article Online
DOI: 10.1039/D6LF00096G

energy barrier for H_2O_2 adsorption and cleavage, thereby boosting the Cu^{2+}/Cu^{+} redox cycle and sustaining active radical formation. This work highlights the pivotal role of atomically dispersed Cu centres in accelerating charge transfer and maximizing non-ferrous photo-Fenton reactivity.[114]

Rozmyślak et al.[118] prepared $Cu_3(PO_4)_2$ by a simple precipitation route and demonstrated its strong potential as an iron-free Fenton-like catalyst for ciprofloxacin degradation. Owing to the redox-active Cu^{2+}/Cu^{+} couple and favourable surface adsorption, Cu(II) phosphate delivered a ~7-fold higher Fenton-like degradation rate than commercial CuO and markedly higher activity than Fe_2O_3, CeO_2, and other metal phosphates. Under visible-light assistance, the catalyst further accelerated CIP oxidation ($k = 0.00445\ min^{-1}$), confirming enhanced charge excitation and faster $Cu^{2+} \rightarrow Cu^{+}$ cycling. Radical-quenching and EPR analyses identified •OH as the dominant reactive species, underscoring the key role of copper sites in H_2O_2 activation. Collectively, the strong redox flexibility of Cu species, together with efficient photo-activation, make Cu(II) phosphate a promising copper-based platform for photo-Fenton degradation of antibiotics.

Almahri et al.[119] synthesized hexahydroxy copper–stannate ($CuSn(OH)_6$) and demonstrated its strong sunlight-driven Fenton-like degradation of Rh6G and tetracycline, highlighting the crucial role of Cu-based redox centres in ROS generation. The well-defined cubic CuHS particles (150–300 nm) possessed abundant surface Cu^{2+}/Cu^{+} sites and oxygen-defect-rich domains, which significantly enhanced H_2O_2 activation and visible-light electron transfer, enabling rapid pollutant removal with maximum activity at alkaline pH. Mechanistic analyses confirmed that Cu sites facilitated efficient charge separation and promoted the production of •OH and $•O_2^-$, driving chromophore cleavage in Rh6G and multistep hydroxylation and ring fragmentation in TC. Overall, the study establishes

View Article Online
DOI: 10.1039/D6LF00096G

$CuSn(OH)_6$ as an efficient Cu-driven Fenton-like photocatalyst, where copper redox cycling and defect-assisted ROS generation govern its high degradation performance.[119]

Zhang et al.[104] developed a Cu-doped zeolite catalyst (Cu^0@CuZ) featuring synergistic metallic Cu^0 nanoparticles and abundant oxygen vacancies, which together enabled exceptional photo-Fenton-like performance. The dual-channel electron-transfer pathway, where oxygen vacancies trap photogenerated electrons and plasmonic Cu^0 rapidly donates them to Cu(II), greatly accelerated the Cu^{2+}/Cu^+ redox cycle and boosted H_2O_2 activation. Benefiting from enhanced visible-light harvesting and rapid charge transport, Cu^0@CuZ completely degraded phenol (20 mg/L) within 15 min, with rate constants 40–65 times higher than Cu_2O, CuO, and Cu^0 alone. This work demonstrates how coupling Cu^0 with vacancy-rich zeolite frameworks provides a powerful strategy to maximize Cu-based photo-Fenton reactivity.[104]

In the plasmon-driven V_O-Cu_2O@Cu/CN_x heterojunction reported by Wang et al.[45], mixed-valence $Cu^0/Cu^+/Cu^{2+}$ sites act as dynamic redox mediators that couple visible-light excitation with sustained Cu^+/Cu^{2+} cycling. Metallic Cu^0 and Cu_2O serve as electron-rich reservoirs that harvest plasmon-induced hot electrons, while interfacial Cu^+ sites directly participate in H_2O_2 activation. Notably, the deprotonated H_2O_2 species (HO_2^-) accelerates reversible Cu^+ disproportionation, stabilizing the catalytic cycle and suppressing metal deactivation. This copper-centred dual-channel mechanism enables both radical-assisted (•OH, $•O_2^-$) and non-radical ($^1O_2$, electron-transfer) oxidation pathways, imparting high reaction robustness over a wide pH range. These findings underscore that precise engineering of copper oxidation states and interfacial Cu environments is pivotal for achieving efficient, stable, and interference-resistant photo-Fenton catalysis beyond conventional Fe-based systems.

View Article Online
DOI: 10.1039/D6LF00096G

Copper nanoparticles act as highly effective noble-metal-free cocatalysts in photo-Fenton-like systems by simultaneously enhancing charge transfer and accelerating Cu-mediated H_2O_2 activation. In the Cu-modified Bi_2O_2S nanosheets reported by Guo et al.[46], surface-anchored Cu nanoparticles function as electron sinks, facilitating rapid extraction of photogenerated electrons from Bi_2O_2S and suppressing electron–hole recombination. The accumulated electrons promote the reduction of Cu^{2+} to Cu^{+}, which serves as the key active species for catalytic H_2O_2 decomposition into highly oxidative •OH radicals. This Cu-assisted redox cycling not only increases reactive oxygen species generation but also stabilizes the photo-Fenton process under visible light. Meanwhile, the intimate Cu–Bi_2O_2S interface improves charge carrier mobility and adsorption affinity toward pollutants, collectively leading to markedly enhanced tetracycline degradation kinetics. These results highlight that judicious incorporation of metallic Cu nanoparticles provides a cost-effective strategy to boost photo-Fenton efficiency by coupling semiconductor photoexcitation with sustained Cu^{+}/Cu^{2+} redox catalysis.

Copper species act as the pivotal redox mediators in piezo-photo-Fenton systems by enabling efficient Cu^{2+}/Cu^{+} cycling and sustained H_2O_2 activation. In the $Bi_4Ti_3O_{12}$-$CuBi_2O_4$ p–n heterojunction, interfacial electric fields and piezoelectric polarization continuously drive photogenerated electrons toward Cu^{2+} sites, accelerating their reduction to Cu^{+}.[88] This rapid Cu redox turnover enhances H_2O_2 decomposition into reactive oxygen species, thereby coupling mechanical–photonic charge separation with Cu-centred Fenton chemistry. The results highlight that copper not only serves as the active Fenton centre but also dynamically links interfacial charge transport with oxidant activation, leading to markedly improved degradation kinetics.

In the Cu@MoS_2/PAAm/CA double-network hydrogel, Cu sites immobilized within the 3D polymer matrix catalyze •OH generation, while MoS_2 and the hydrogel scaffold

View Article Online
DOI: 10.1039/D6LF00096G

promote charge transfer and pollutant enrichment.[120] The spatial confinement of Cu species suppresses leaching and enables stable Cu-mediated Fenton reactions even under dark conditions, highlighting copper's decisive role in coupling adsorption-assisted enrichment with durable photo-Fenton degradation. Copper centres act as the decisive photo-Fenton active sites in ligand-engineered Cu-MOFs by enabling efficient Cu^{2+}/Cu^{+} redox cycling and H_2O_2 activation under visible light**.** In secondary-ligand-modulated Cu-MOFs, tetranuclear Cu cluster configurations provide abundant coordinatively unsaturated Cu sites that promote photoinduced charge separation and accelerate interfacial electron transfer to H_2O_2, thereby boosting •OH and $\bullet O_2^-$ generation. This work highlights that precise ligand control over Cu coordination environments directly governs photo-Fenton efficiency, stability, and pH tolerance in Cu-MOF catalysts.[18]

Overall, copper-based catalysts benefit from rapid Cu^{+}/Cu^{2+} cycling, strong visible-light absorption when coupled with semiconductors, and accelerated interfacial charge transfer in engineered heterojunctions. These features enable Cu-based systems to outperform classical Fe-based catalysts, especially under environmentally relevant pH conditions.

4.2 Cobalt-Based Catalysts: Multivalent Redox Mediation

Cobalt-based photo-Fenton catalysts derive their activity from the reversible Co^{2+}/Co^{3+} redox couple ($E° \approx +1.81$ V vs NHE), which enables rapid H_2O_2 activation and efficient •OH generation under mild conditions. The Fenton-like reaction proceeds through the oxidation of Co^{2+} by H_2O_2, followed by the reduction of Co^{3+} to regenerate catalytically active Co^{2+}:

$$Co^{2+} + H_2O_2 \rightarrow Co^{3+} + \bullet OH + OH^-$$

$$Co^{3+} + e^-_{(photo)} \rightarrow Co^{2+}$$

View Article Online
DOI: 10.1039/D5LF00096G

This redox cycling can be significantly accelerated under visible-light irradiation, especially when cobalt is integrated into semiconductor interfaces that promote directional electron transfer. Tang et al.[121] developed a cobalt-based ZIF-67/defective TiO_{2-x} heterostructure (B–TiO_{2-x} @ZIF-67) to enhance visible-light-driven photo-Fenton-like degradation of bisphenol A. The intimate coupling between oxygen-vacancy-rich TiO_{2-x} and Co-containing ZIF-67 constructed an efficient charge-transfer interface, where TiO_{2-x} vacancies trapped electrons to accelerate carrier separation, while Co(II) sites served as active Fenton centres for rapid H_2O_2 decomposition to •OH. Benefitting from the synergistic roles of vacancy-mediated charge migration and Co-induced ROS generation, the B–TiO_{2-x}@ZIF-67/H_2O_2/Vis system achieved ~95% BPA removal and maintained stable activity over repeated cycles. This work highlights the critical role of Co-based centres integrated within MOF–oxide interfaces in promoting peroxidative pathways for efficient photo-Fenton-like oxidation.[121]

Li et al.[122] constructed a Co-POM/N-TiO_2 heterostructure in which cobalt polyoxometalate clusters acted as an efficient cocatalyst to mediate electron transfer during the photo-Fenton-like reaction. Decorating Co-POM onto N-doped TiO_2 not only broadened visible-light absorption but also established a favourable interfacial pathway that accelerated electron migration from TiO_2 to the Co-POM sites, where Co(II) species activated H_2O_2 to generate •OH. Benefiting from this cobalt-driven interfacial charge-transfer mechanism, the hybrid catalyst achieved rapid RhB degradation (~97% within 40 min at neutral pH), exhibiting a rate constant nearly nine times higher than N-TiO_2 alone. The strong Co–TiO_2 electronic coupling and efficient Co^{2+}/Co^{3+} redox cycling underpin the markedly enhanced photo-Fenton-like activity.[122]

Cobalt nodes in ZIF-9 frameworks act as the primary photo-Fenton catalytic centres by facilitating visible-light-driven charge separation and promoting ROS generation under neutral conditions. In multivariate Co-based MOFs, electronic modulation via mixed ligands lowers

View Article Online
DOI: 10.1039/D6LF00096G

the band gap and enhances carrier mobility, enabling efficient interaction between photogenerated electrons and H_2O_2 to produce •OH and $•O_2^-$.[54] This study demonstrates that cobalt-centred MOF scaffolds provide structurally stable, pH-flexible platforms for heterogeneous photo-Fenton reactions, where ligand engineering further amplifies Co-mediated redox activity without metal leaching.[54]

Zhou et al.[123] reported a Pt/$CoAl_2O_4$ heterostructured catalyst derived from spent Pt/γ-Al_2O_3 exhibited highly efficient visible-light-driven photo-Fenton-like degradation of malathion. In this system, $CoAl_2O_4$ acts as the primary Fenton-active phase, where continuous Co^{2+}/Co^{3+} redox cycling governs H_2O_2 activation and •OH generation, while epitaxially grown Pt nanocrystals enhance light absorption and suppress electron–hole recombination. The interfacial charge transfer from Pt to $CoAl_2O_4$ accelerates cobalt redox turnover, thereby sustaining ROS production under mild conditions. This work highlights that cobalt-based spinel oxides provide robust and recyclable photo-Fenton centres, with noble metals mainly serving as photonic and electronic promoters rather than active Fenton sites.

Zhu et al.[124] reported that an amorphous–crystalline CoS_x@TiO_2 heterointerface bridged by S–O bonds markedly accelerates photo-Fenton degradation of ciprofloxacin. In this system, CoS_x serves as the cobalt-based photo-Fenton centre, enabling efficient Co^{2+}/Co^{3+}-mediated H_2O_2 activation and abundant •OH generation, while S–O interfacial bridges promote directional electron transfer and in situ H_2O_2 formation under light irradiation. Consistently, EPR spectroscopy (Fig. 9a,b) detected strong •OH and $•O_2^-$ signals after light irradiation, while radical quenching experiments (Fig. 9c) showed that isopropanol markedly suppressed ciprofloxacin degradation (from 100% to 47%), collectively confirming •OH as the dominant oxidative species with minor contributions from electrons, holes, and $•O_2^-$. These results demonstrate that cobalt sulphide heterointerfaces effectively couple photocatalytic charge

View Article Online
DOI: 10.1039/D6LF00096G

transport with cobalt redox cycling to drive •OH-dominated photo-Fenton oxidation without the need for noble metals.

Overall, cobalt-based catalysts offer high intrinsic oxidizing power through Co^{2+}/Co^{3+} transitions, efficient H_2O_2 activation at near-neutral pH, strong compatibility with Z-scheme and defect-engineered systems, and improved ROS generation through oxygen-vacancy-enabled pathways. These characteristics make Co an exceptionally potent non-ferrous metal for advanced photo-Fenton applications.

4.3 Manganese-Based Catalysts: Valence Versatility and Defect Engineering

Manganese-based catalysts leverage the rich redox chemistry of $Mn^{2+}/Mn^{3+}/Mn^{4+}$ to activate H_2O_2 and dissolved oxygen for ROS production. The multivalent nature of Mn enables both radical and non-radical oxidation pathways, making manganese oxides particularly attractive for visible-light-assisted Fenton-like reactions, especially under neutral or slightly alkaline conditions.

The primary Fenton-like step involves the oxidation of Mn^{2+} by H_2O_2 to produce •OH, followed by the photoreduction of Mn^{3+} to sustain the cycle:

$$Mn^{2+} + H_2O_2 \rightarrow Mn^{3+} + \bullet OH + OH^-$$

$$Mn^{3+} + e^-_{(photo)} \rightarrow Mn^{2+}$$

Meanwhile, higher-valent Mn^{4+} species commonly present in MnO_2 can participate in surface redox reactions that facilitate the production of •OOH and $\bullet O_2^-$, especially when oxygen vacancies (OVs) are present. These OVs promote electron trapping, enhance Mn valence cycling, and improve adsorption of H_2O_2 and O_2.

Mansoori et al.[56] reported a biochar-supported CuO_x-MnO_y nanocatalyst, highlighting the key role of manganese redox chemistry in visible-light-driven photo-Fenton degradation of

View Article Online
DOI: 10.1039/D6LF00096G

metronidazole. In this system, Mn^{2+} acts as an efficient H_2O_2 activator, promoting sustained •OH generation under near-neutral pH, while Cu species and biochar-derived persistent free radicals synergistically facilitate electron transfer and Mn redox regeneration. The Mn-centred Fenton-like pathway dominates ROS production, enabling almost complete MNZ removal with high stability and recyclability, underscoring manganese oxides as robust, non-iron active sites for practical photo-Fenton applications.

Dai et al.[35] synthesized Mn-doped cobalt silicate@diatomite (Co-MnSi@DE) composites via a hydrothermal route, where Mn incorporation enhances synergistic Co/Mn redox cycling; as shown in Fig. 9d, MO degradation proceeds via UV-driven Co/Mn Fenton-like pathways that continuously generate •OH radicals following initial pollutant adsorption. The introduction of Mn increased surface area, narrowed the band gap, and strengthened H_2O_2 adsorption/activation, which DFT confirmed by showing a much lower H_2O_2 adsorption energy on Mn-doped surfaces. Benefiting from this bimetallic synergy, the optimized $Co_{0.25}$MnSi@DE achieved >95% methyl orange degradation under UV/H_2O_2, significantly outperforming Mn-free counterparts. Radical quenching experiments (Fig. 9e,f) revealed that both •OH and •OOH contribute to methyl orange degradation in the $Co_{0.25}$MnSi@DE/H_2O_2-UV system, with a much stronger inhibition observed upon •OH scavenging (k = 0.0033) than •OOH scavenging (k = 0.008), indicating that hydroxyl radicals play the dominant role in the catalytic process. The catalyst remained reusable and structurally stable, underscoring Mn doping as a potent strategy to boost cobalt-based photo-Fenton activity.

Zhang et al.[81] reported that a porous Z-scheme MnO_2/Mn-modified alkalinized g-C_3N_4 heterojunction exhibits outstanding Mn-driven photo-Fenton performance for pharmaceutical degradation. In this system, multivalent Mn species (Mn^{4+}/Mn^{3+}/Mn^{2+}) act as the core Fenton-like active centres, efficiently activating H_2O_2 to generate abundant •OH, while the Z-scheme charge transfer preserves strong redox ability and suppresses charge recombination. The

View Article Online
DOI: 10.1039/D6LF00096G

synergistic coupling of Mn redox cycling, surface hydroxyl groups, and Z-scheme photocatalysis enables deep mineralization of tetracycline and high TOC/COD removal, highlighting manganese oxides as robust, iron-free photo-Fenton catalysts.

Singh et al.[57] reported that a Cu-Mn codoped $BiVO_4$ demonstrates efficient Mn-driven photo-Fenton degradation of ciprofloxacin by exploiting the multivalent $Mn^{2+}/Mn^{3+}/Mn^{4+}$ redox cycle. In this system, Mn acts as the primary Fenton-like centre, facilitating rapid H_2O_2 activation to generate •OH radicals, while Cu serves as an electron mediator that regenerates lower-valence Mn species and stabilizes the redox cycle. The coexistence of Mn multivalence with oxygen vacancies and favourable band alignment prolongs charge-carrier lifetimes, enabling sustained •OH production and high photocatalytic stability, underscoring the critical role of manganese redox chemistry in non-iron photo-Fenton systems.

Overall, manganese-based photo-Fenton catalysts benefit from multi-valence redox flexibility ($Mn^{2+}/Mn^{3+}/Mn^{4+}$), Oxygen-vacancy-enhanced H_2O_2 and O_2 activation, Strong synergy with carbonaceous and semiconductor supports, and robust performance over a wider pH window than classical Fe-based systems. These advantages position Mn-based catalysts as promising candidates for energy-efficient and environmentally compatible advanced oxidation processes.

4.4 Bismuth-Based Catalysts: Surface Coordination and Interfacial Activation

Bismuth-based materials represent a distinct class of non-ferrous photo-Fenton catalysts, primarily due to their layered structures, strong internal electric fields (IEFs), and intrinsic ability to form oxygen vacancies (OVs). Unlike transition metals such as Cu, Co, or Mn, bismuth does not undergo classical multivalent Fenton cycling. Instead, its catalytic activity arises from photocatalytic activation of H_2O_2 and interfacial charge modulation, both of which are strongly influenced by crystal anisotropy and defect engineering.

View Article Online
DOI: 10.1039/D6LF00096G

Layered bismuth oxyhalides (BiOX, X = Cl, Br, I) and oxides (Bi_2O_3, $BiVO_4$) possess unique (001) or (010) facets that exhibit strong IEFs, which promote spatial charge separation and directional electron migration.[64] Upon visible-light excitation, photogenerated electrons can reduce H_2O_2 to $\bullet O_2^-$, while valence-band holes oxidize surface hydroxyls or H_2O to yield •OH. This dual-pathway ROS formation compensates for the absence of classical Bi redox cycling. The presence of oxygen vacancies significantly enhances these processes. OVs act as electron-trapping sites, prolong photocarrier lifetime, and facilitate the adsorption and activation of H_2O_2 and O_2.

Guo et al.[46] constructed a noble-metal-free Cu-modified Bi_2O_2S nanosheet photocatalyst (Cu–Bi_2O_2S), where Cu nanoparticles act as an efficient cocatalyst to accelerate charge transfer and H_2O_2 activation. The optimized 13 wt% Cu–Bi_2O_2S showed a 3.95-fold increase in the TCH photo-Fenton-like degradation rate compared to pristine Bi_2O_2S, attributed to enhanced electron mobility, higher ROS generation, and stronger pollutant adsorption. Importantly, Bi_2O_2S served as the high-responsivity visible-light absorber, while Cu introduction markedly boosted interfacial electron extraction and surface redox activity. Beyond pollutant degradation, the Cu–Bi_2O_2S catalyst also achieved significantly higher CO_2 photoreduction performance (CH_4 formation rate: 2.27 μmol g^{-1} h^{-1}, 7× higher than Bi_2O_2S), demonstrating the strong synergy between Bi-based layered structure and Cu cocatalyst. This work highlights Bi-based hosts as versatile platforms where cocatalyst engineering can simultaneously enhance photo-Fenton activity and solar-fuel conversion.[46]

Hu et al.[96] constructed a dual-metal plasmonic heterojunction (Cu-decorated C@Bi/Bi_2MoO_6) by carbonizing CuBTC and subsequently introducing Bi_2MoO_6 with in-situ reduced metallic Bi. The Bi/Bi_2MoO_6 interface played a central role in boosting the photo-assisted Fenton process by providing plasmon-active Bi sites and forming an efficient charge-transfer

View Article Online
DOI: 10.1039/D6LF00096G

heterojunction that accelerated electron–hole separation. Coupled with Cu-derived SPR enhancement, the catalyst achieved rapid tetracycline degradation (96.1% in 5 min) with excellent pH tolerance and recyclability. Mechanistic studies confirmed •OH as the dominant ROS, with metallic Bi enabling fast O_2 reduction and ROS generation, thereby driving the superior Fenton activity.

Zhang et al.[39] fabricated ultra-high Bi-doped CeO_2 nanorods by pyrolyzing Bi/Ce-BMOFs, achieving uniform Bi incorporation (up to 20 mol%) without phase segregation. The Bi doping, together with abundant oxygen vacancies, markedly enhanced visible-light absorption and accelerated the Ce^{3+}/Ce^{4+} redox cycling, enabling fast H_2O_2 activation. The resulting Bi–CeO_2 catalyst delivered outstanding photo-Fenton activity for tetracycline removal across a broad pH range (2-9). Mechanistic investigations confirmed $\bullet O_2^-$ and •OH as dominant species, with OVs serving as electron-trapping sites to promote charge separation. Overall, the study highlights how Bi doping effectively modulates the electronic structure of CeO_2, strengthens redox cycling, and boosts photo-Fenton efficiency, offering a robust strategy for MOF-derived Bi-modified catalysts.

Reported by Wang et al.[78], the 2D/2D $CuCo_2S_4/Bi_2WO_6$ heterojunction underscores the active role of the Bi_2WO_6 host in photo-Fenton catalysis. The layered Bi–O–W framework of Bi_2WO_6 serves as a robust visible-light absorber and hole-rich oxidation platform, while its suitable band structure enables directional charge transfer in the type-II heterojunction. Coupling with $CuCo_2S_4$ primarily accelerates electron extraction and Fenton redox cycling, whereas Bi_2WO_6 preserves strong oxidative holes and stabilizes interfacial charge separation, promoting sustained •OH and $\bullet O_2^-$ generation. This study highlights that bismuth-based oxides are not passive supports but key photoredox backbones that govern light harvesting, hole-driven oxidation, and interfacial stability in non-ferrous photo-Fenton systems.

View Article Online
DOI: 10.1039/D5LF00096G

Overall, the superior performance of Bi-based photo-Fenton catalysts arises from strong internal electric fields that promote charge separation, oxygen-vacancy-mediated H_2O_2 and O_2 activation, broad visible-light absorption across layered BiOX structures, and enhanced interfacial charge migration in Z/S-scheme heterojunctions. These attributes allow Bi-based materials to generate ROS effectively without relying on classical redox cycling, making them highly promising for visible-light-driven pollutant degradation in aqueous environments.

4.5 Cerium-Based Catalysts: Redox Buffering and Oxygen Vacancy-Mediated ROS Generation

Cerium-based catalysts occupy a unique position among non-ferrous photo-Fenton systems due to the exceptional redox flexibility of the Ce^{3+}/Ce^{4+} couple and the strong tendency of CeO_2 to form oxygen-deficient structures (CeO_{2-x}). Unlike classical Fenton catalysts, Ce does not rely primarily on direct homogeneous H_2O_2 activation; instead, its catalytic behaviour is governed by oxygen-vacancy (OV)-mediated electron transfer, surface Ce^{3+} enrichment, and interfacial photoreduction pathways.

Oxygen vacancies in CeO_2 create localized Ce^{3+} sites that serve as active centres for H_2O_2 adsorption and electron transfer. The Ce^{3+}/Ce^{4+} shuttle facilitates redox cycling under illumination:

$$Ce^{3+} + H_2O_2 \rightarrow Ce^{4+} + \bullet OH + OH^-$$

$$Ce^{4+} + e^-_{(photo)} \rightarrow Ce^{3+}$$

Although this reaction proceeds more slowly than Cu or Co-based Fenton pathways, the high OV concentration is significantly compensated for by enhancing H_2O_2 activation efficiency. In addition to •OH formation, CeO_{2-x} surfaces promote $\bullet O_2^-$ and $^1O_2$ generation through electron transfer to dissolved O_2, enabling both radical and non-radical oxidation routes.

View Article Online
DOI: 10.1039/D6LF00096G

Several interfacial engineering strategies have been reported to substantially enhance Ce-based photo-Fenton performance. Yang et al.[38] constructed a cerium-rich CeO_{2-x}/Bi_2MoO_6 heterojunction in which abundant oxygen-deficient CeO_{2-x} nanodots were uniformly anchored onto Bi_2MoO_6 nanosheets. The introduction of non-stoichiometric CeO_{2-x} proved crucial: oxygen vacancies accelerated the Ce^{4+}/Ce^{3+} self-circulating redox cycle, markedly enhancing H_2O_2 activation and preventing metal sludge formation typically seen in stoichiometric CeO_2. Benefiting from this rapid Ce-centred redox cycling and the intimate heterojunction interface, the optimized CEO/BIM-3 catalyst achieved >97% degradation of ofloxacin under only 5 W visible LED irradiation, far surpassing pristine CeO_{2-x} and Bi_2MoO_6. The catalyst also efficiently removed norfloxacin and ciprofloxacin with similarly high efficiencies. Mechanistic studies confirmed that the accelerated Ce^{3+} regeneration boosted •OH production, while the Bi_2MoO_6 component enhanced visible-light absorption and charge separation. Overall, the work highlights cerium's pivotal role as a self-renewing Fenton cocatalyst, enabling highly stable, efficient, and sludge-free photo-Fenton degradation of fluoroquinolone antibiotics.[38]

Peng et al.[125] engineered Ce-induced lattice distortion and oxygen vacancies to generate surface FLP sites (Ce^{4+}-Ov-O^{2-}), which strengthened Lewis acidity/basicity and promoted interfacial adsorption/activation of both H_2O_2 and escaped O_2. This FLP-mediated $O_2/•O_2^-/^1O_2/H_2O_2$ redox cycling enabled highly efficient ROS generation, giving Ce-BMO a 2.15-fold activity boost over pristine BMO for tetracycline degradation. EPR and quenching tests confirmed $^1O_2$ and $•O_2^-$ as dominant species. Overall, Ce doping establishes an FLP-driven catalytic environment that maximizes H_2O_2 utilization and accelerates photo-Fenton pathways.[125]

An iron-free Ce-Ag nano-Fenton catalyst (ZY@(CeAg)) was green-synthesized by anchoring Ce and Ag nanoparticles onto a zeolite-Y matrix using papaya-leaf phytochemicals.[126] The introduction of Ce, supported by XPS and XRD evidence of reduced Ce species, significantly

View Article Online
DOI: 10.1039/D6LF00096G

narrowed the band gap of zeolite Y (4.2 → 3.0 eV) and created abundant redox-active Ce^{3+}/Ce^{4+} sites that accelerated H_2O_2 activation and ROS generation. The resulting heterojunction exhibited strong photo-Fenton-like degradation of tetracycline and ciprofloxacin (≈87% removal under UV-A), with •OH radicals identified as the dominant oxidants. Benefiting from Ce-driven redox cycling, stable surface dispersion, and minimal Ce leaching, ZY@(CeAg) maintained high activity over multiple cycles and displayed consistent performance in natural waters, highlighting cerium's pivotal role in enabling robust, iron-free Fenton catalysis.[126]

Hu et al.[127] constructed ZIF-67–derived Co_3O_4-CeO_2 nanocage micromotors, where CeO_2 nanoparticles uniformly anchored on Co_3O_4 created abundant Ce^{3+}/Ce^{4+} redox sites that enhanced peroxide-like activity and accelerated ROS generation. The Ce-modified nanocages enabled rapid self-propulsion in H_2O_2, providing efficient mass transfer and boosted photo-Fenton-like degradation, achieving 98.2% hydroquinone removal. The CeO_2 contribution, strong redox cycling, oxygen-vacancy–mediated activation, and reinforced catalytic centres, was pivotal to both sensitive colorimetric detection and high-efficiency pollutant oxidation.

Overall, cerium-based catalysts benefit from OV-rich structures, enabling efficient H_2O_2 and O_2 activation, Ce^{3+}/Ce^{4+} redox shuttling under visible light, compatibility with Z-scheme and S-scheme heterojunctions, and broad pH stability and high structural durability. These properties allow CeO_2-based systems to operate as robust, versatile photo-Fenton catalysts capable of engaging both radical and non-radical oxidation pathways, making them particularly valuable for the treatment of persistent pollutants in realistic water conditions.

View Article Online
DOI: 10.1039/D5LF00096G

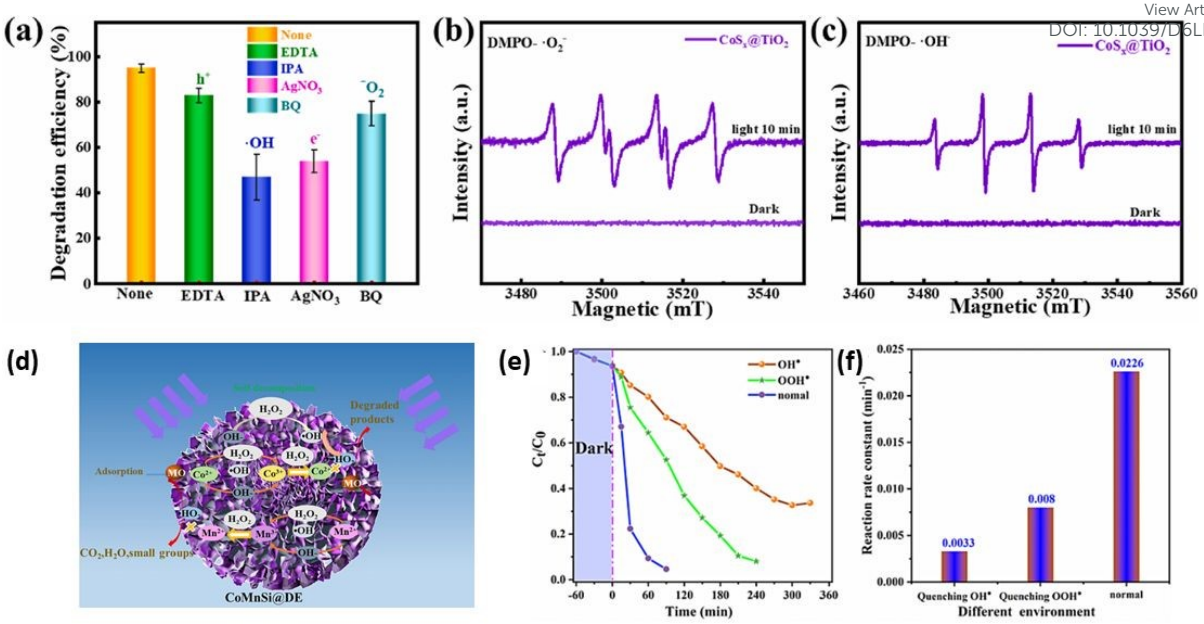

Fig. 9 (a) CIP removal efficiency over $CoS_x@TiO_2$ in the presence of radical quenchers and (b) the ESR of $•O_2^-$, and (c) •OH. Reproduced from ref. 124 with permission from Elsevier, Zhu, Y.; Li, J.; Lai, Y.; Cao, Y.; Li, J.; Wei, Z.; Yang, L.; Chen, Z.; Zou, J. *Environ. Res.* **2025**, *279*, 121785. Copyright 2025. (d) Schematic diagram of the possible degradation mechanism of dye wastewater degradation in the $Co_{0.25}MnSi@DE/H_2O_2$-UV system, (e) The effects of quenching of different radicals on MO degradation, and (f) The corresponding reaction constant. Reproduced from ref. 35 with permission from Elsevier, Dai, N.; Yang, L.; Liu, X.; Gao, L.; Zheng, J.; Zhang, K.; Song, D.; Sun, T.; Luo, S.; Liu, X. *J. Colloid Interface Sci.* **2023**, *652*, 1812–1824. Copyright 2023.

4.6 Emerging Paradigms: Non-Radical Pathways and Surface-Activated Complexes

In addition to conventional radical pathways dominated by •OH, increasing evidence indicates that non-radical oxidation mechanisms play a pivotal role in non-ferrous photo-Fenton systems, particularly in interface-engineered catalysts. Importantly, these processes should not be interpreted within a binary framework of radical presence or absence; rather, they involve a dynamic interplay between radical and non-radical pathways. Non-radical routes include

View Article Online
DOI: 10.1039/D6LF00096G

singlet oxygen ($^1O_2$) generation and surface-activated complex-mediated electron transfer, both of which exhibit higher selectivity and enhanced resistance to matrix interference.

Interface features such as oxygen vacancies (OVs), defect-rich surfaces, and specific exposed crystal facets significantly facilitate these pathways. Oxygen vacancies act as electron-rich centres that promote the adsorption and activation of dissolved O_2 or H_2O_2, leading to the formation of surface-bound superoxide intermediates ($\bullet O_2^-$), which can subsequently convert into $^1O_2$ via energy-transfer processes. Unlike free •OH radicals, these reactions predominantly occur at the catalyst surface, thereby minimizing non-selective oxidation and reducing oxidant loss.

Furthermore, facet engineering (e.g., BiOBr (010) or CeO_2 (111)) modulates local electronic structure and adsorption configurations, enabling selective electron transfer to oxygen species rather than homolytic H_2O_2 cleavage. In parallel, interfacial electric fields in S-scheme and Z-scheme heterojunctions drive directional charge migration, enriching electrons at specific active sites that favour O_2 activation and $^1O_2$ formation.

Notably, these non-radical pathways are especially prominent in Cu–N_4 coordinated systems and oxygen-vacancy-rich Bi and Ce-based catalysts. In such systems, the pollutant and H_2O_2 can form a metastable surface-activated ternary complex with the catalytic site, enabling direct and localized electron transfer without the involvement of freely diffusing radicals. This surface-complex-mediated mechanism provides enhanced selectivity, improved resistance to scavenging effects, and superior catalytic stability, thereby underpinning the high performance observed in interface-engineered composites.

4.7 Delineation of Oxidative Pathways and Practical Implications

View Article Online
DOI: 10.1039/D6LF00096G

In photo-Fenton systems, it is essential to distinguish between different oxidation pathways, as they have significant implications for catalytic selectivity and performance in real water matrices. Free •OH radicals generated in solution are highly reactive and non-selective; however, they are readily scavenged by co-existing ions and natural organic matter, which can significantly reduce their effectiveness in practical applications. In contrast, surface-bound •OH species are localized at the catalyst interface and participate in more controlled oxidation processes with reduced susceptibility to scavenging.

Furthermore, direct interfacial electron transfer represents a distinct non-radical pathway, wherein pollutants are oxidized through interaction with catalyst-bound activated species without the involvement of freely diffusing radicals. This mechanism, commonly observed in defect-rich and single-atom catalytic systems, offers enhanced selectivity, improved resistance to matrix interference, and greater stability under realistic conditions. Therefore, understanding and differentiating these pathways is crucial for the rational design of efficient and application-oriented photo-Fenton catalysts.

Table 4 Recent non-ferrous photo-Fenton-like catalytic systems and their degradation performance toward organic pollutants

Catalyst	Target pollutant	Light source	Operational conditions	K (min^{-1})	Degradation efficiency (%)	Main ROS	Ref.
$Cu(OH)_3F/Cu_2O$	Tetracycline (TCH)	300W Xe Lamp $400 \geq \lambda$	Catalyst dosage: 0.6g/L, C_0: 20 mg/L, $[H_2O_2]$: 40mM, pH: 7, 30 min	0.212	99.93	•OH	89
Cu-MgO	Rhodamine B (RhB)	Xe Lamp $400 \geq \lambda$	Catalyst dosage: 0.05g/L, C_0: 50 mg/L, $[H_2O_2]$: 20mM, 60 min	0.0435	92.8	$•O_2^-$	76
Vo- Cu_2O@Cu/CN_x	Tetracycline (TC)	Visible LED Lamp	Catalyst dosage: 0.2g/L, C_0: 20 mg/L, $[H_2O_2]$: 20mM, pH: 7, 30 min	0.2	100	$^1O_2$	45

Ag-doped CuS	Rhodamine (RhB)	UV Lamp	Catalyst dosage: 15 mg, C_0: 30 mg/L, pH: 5	-	94.9	$^1O_2$ •OH	128
Mesoporous CuO nanoplate	Sulfathiazole (STZ)	Visible LED Lamp	$[H_2O_2]$: 20mM, 90 min	0.0547	100	•OH	129
Cu nanoparticles modified Bi_2O_2S	TC HCL	Visible LED Lamp	Catalyst dosage: 0.75g/L, C_0: 50 mg/L, $[H_2O_2]$: 30µL, pH: 4, 60 min	0.243	77.76	•OH	46
$Cu_{2-x}S$/g-C_3N_4	RhB	300W Xe Lamp	Catalyst dosage: 0.4g/L, C_0: 30 mg/L, $[H_2O_2]$: 0.5mL, 30 min	0.172	99.6	$O_2•^-$	47
Cu@MoS_2/PAAm/CA NCDN	TC	300W Xe Lamp	Catalyst dosage: 1g/L, C_0: 200 mg/L, $[H_2O_2]$: 1.5mM, pH: 5	-	90	$•O_2^-$	120
$CuSn(OH)_6$	Rh6G	500W Xe Lamp	Catalyst dosage: 30mg, C_0: 20 mg/L, $[H_2O_2]$: 20mM, pH: 11, 50 min	0.084	99	•OH	119
(Cu_2O/CFYO)	MO	Visible Xe Lamp	$[H_2O_2]$: 1mM, 60 min	0.0474	97	•OH , $•O_2^-$	130
BiOBr/Co_3O_4	MB	500W Xe Lamp	C_0: 10 mg/L, $[H_2O_2]$: 50µL, 60 min	-	96	•OH , $•O_2^-$	131
Pt-Cu BTC	RhB	Near IR Light	Catalyst dosage: 1g/L, pH: 7, 120 min	-	99	•OH	132
CPDS/$CuBiO_4$	CIP	Visible LED Lamp 420 ≥ λ	Catalyst dosage: 0.5g/L, C_0: 10 mg/L, $[H_2O_2]$: 0.5 mL, 30 min	-	92.3	•OH , $O_2•^-$, $^1O_2$	51
CuO/gC_3N_4	TC	400W Na Lamp 400 ≥ λ	Catalyst dosage: 0.2g/L, C_0: 10 mg/L, $[H_2O_2]$: 300µL/L, 15 min	0.1254	99	•OH , $O_2•^-$	133
Basalt powder	Attrazzine (ATZ)	UV C Lamp	Catalyst dosage: 0.5g/L, C_0: 5 mg/L, $[H_2O_2]$: 1.6mM, pH: 6, 180 min	-	96	•OH	134
$Cu_2(OH)_3F$/BiOBr	TC-HCl	300W Xe Lamp 400 ≥ λ	Catalyst dosage: 0.3g/L, C_0: 20 mg/L, $[H_2O_2]$: 40mM, pH: 5, 60 min	0.0635	98.8	•OH , $O_2•^-$	43
Cu-decorated C@Bi/Bi_2MoO_6	TC	VIS Lamp 400 ≥ λ	Catalyst dosage: 0.16g/L, C_0: 50 mg/L, $[H_2O_2]$: 10µL (20 wt%), 5 min	-	96.12	•OH	96
HOFs/Cu/gCN	TC	500W Xe Lamp 420 ≥ λ	Catalyst dosage: 0.3g/L, C_0: 20 mg/L, $[H_2O_2]$: 150µL (30 wt%), 20 min	-	96	•OH	135
Cu mesh/Cu_7S_4	MB	VIS Lamp	C_0: 10 mg/L, $[H_2O_2]$: 5mL (30 wt%), 140 min	-	98.4	•OH	136

$CuLPMo_{12}$	RhB	300W Hg Lamp	Catalyst dosage: 0.136g/L, C_0: 4.8 mg/L, $[H_2O_2]$: 10mM, pH: 7	-	99.1	•OH, $^1O_2$	137
Cu-ZIF-9-ica	MB	24 W LED Lamp	Catalyst dosage: 0.5g/L, C_0: 5 mg/L, $[H_2O_2]$: 35µL, 45 min	0.0475	94	•OH	54
Posnjakite (CP)	MB	Vis Xe Lamp	Catalyst dosage: 30 mg, C_0: 20 mg/L, $[H_2O_2]$: 0.2M, 20 min	0.638	97	•OH	138
Mn-doped Cobalt silicate@diamoite	MO	UV Lamp	Catalyst dosage: 0.2g/L, C_0: 20 mg/L, $[H_2O_2]$: 25mM, pH: 2.88, 90 min	0.0226	95	•OH	35
$CDs/CuO/gC_3N_4$	MB	VIS Lamp	Catalyst dosage: 0.6g/L, C_0: 20 mg/L, $[H_2O_2]$: 5mM, 40 min	0.198	100%	•OH, $O_2•^-$	40
Cu-N/C-500	CR	300 W Xenon Lamp	Catalyst dosage: 0.8g/L, C_0: 10 mg/L, 60 min	0.041	91.8	•OH	98
$Cu_2(OH)_3F/CQDs-BiVO_4$	CIP	300 W Xenon Lamp	Catalyst dosage: 0.2g/L, C_0: 20 mg/L, $[H_2O_2]$: 0.2 mL, pH: 7, 60 min	0.0642	98.1	•OH	97
Cu-SA/CNH/PF	TC	Visible Xe Lamp $420 \geq \lambda$	Catalyst dosage: 0.2g/L, C_0: 10 mg/L, $[H_2O_2]$: 160mM, 30 min	0.121	98.1	•OH, $^1O_2$	52
CeO_{2-x}/Bi_2MoO_6	OFX	5W Visible LED	Catalyst dosage: 0.2g/L, C_0: 20 mg/L, $[H_2O_2]$: 1.5mM, 120 min	0.026	97.64	•OH, $^1O_2$	38
Bi/Ce-BMOFs	TC	5W Visible LED	Catalyst dosage: 0.6g/L, C_0: 20 mg/L, $[H_2O_2]$: 10mM, 60 min	-	83	•OH, $O_2•^-$	39
Co_3O_4-CeO_2	Hydroquinone (HQ)	500W Xe Lamp	Catalyst dosage: 30 mg, C_0: 33 mg/L, $[H_2O_2]$: 3 mL (30 wt%),	-	98.21	•OH, $O_2•^-$	127
Ce-BMO	TC	Visible LED Lamp	$[H_2O_2]$: 9.5mM, 40 min	0.0487	90.7	$O_2•$, $^1O_2$	38
CeO_2-Ba_4TaO_8Cl	OFX	5W LED Lamp	Catalyst dosage: 0.2g/L, C_0: 20 mg/L, $[H_2O_2]$: 4.5mM	0.096	98.78	•OH, $O_2•^-$	102
Mesoporous Ceria nanoparticles	AO7	LED Lamp	Catalyst dosage: 1g/L, C_0: 70 mg/L, 3 min	-	90	•OH	73
Ce_4O_7/Bi_4MoO_9	TC	5W Visible LED Lamp	Catalyst dosage: 0.4g/L, C_0: 10 mg/L, $[H_2O_2]$: 3mM, 120 min	0.036	99.8	•OH, $O_2•^-$	59
$Cu-Bi_2O_2S$	TCH	Visible Lamp	Catalyst dosage: 0.75g/L, C_0: 50 mg/L, $[H_2O_2]$: 30µL, pH: 4, 60 min	0.0243	77.76	•OH	46
$Pt/CoAl_2O_4$	Malathion	300 W Xe Lamp	Catalyst dosage: 1g/L, C_0: 10 mg/L, $[H_2O_2]$: 4mM, pH: 8	-	94.61	•OH, $O_2•^-$	123
$ZnCo_2O_4$–ZnO $Li(Mn_{0.75}Ni_{0.25})_2O_4$ mixed oxide	MB	20W UV Lamp	Catalyst dosage: 0.4g/L, C_0: 20 mg/L, $[H_2O_2]$: 19 mM, 90 min	-	93	•OH	139
B-TiO2@ZIF-67	Bisphenyl-A	Visible Lamp	Catalyst dosage: 0.5g/L, C_0: 50 mg/L, $[H_2O_2]$: 16mM, 6 min	0.045	95.30	$O_2•^-$	121
$CoS_x@TiO_2$	CIP	300W Xe Lamp	C_0: 10 mg/L, pH: 5, 100 min	0.0356	100	•OH, $O_2•^-$	124

View Article Online
DOI: 10.1039/D6LF00096G

Cu-ZBP	MO	72W UV A Lamp	C_0: 3 mg/L, $[H_2O_2]$: 22mM, pH: 6.12, 60 min	-	90	$O_2•^-$	140
Bi_2WO_6/CoAl LDH	OTC	300W Xe Lamp 420 ≥ λ	Catalyst dosage: 1g/L, C_0: 10 mg/L, $[H_2O_2]$: 50mM, 60 min	-	98.47	•OH , $O_2•^-$	41
Co-POM/N-TiO_2	RhB	300W Xe Lamp	Catalyst dosage: 0.8g/L, $[H_2O_2]$: 2µL (30 wt%), pH: 7, 40 min	0.092	97.47	•OH , $O_2•^-$	83
BiOBr/Co_3O_4	MB	500W Xenon Lamp	C_0: 10 mg/L, $[H_2O_2]$: 50µL, 60 min	-	96	•OH , $O_2•^-$	131
$Zn_{0.96}Co_{0.03}Ni_{0.01}O$ nanorods	Chloramphenicol (CAP)	Visible Lamp	Catalyst dosage: 0.05g/L, $[H_2O_2]$: 100µL, 500 min	0.0052	94.2	•OH	105
gC_3N_4/$ZnCo_2O_4$	RhB	40 W Visible LED	Catalyst dosage: 01g/L, C_0: 10 mg/L, $[H_2O_2]$: 1mL (30wt%), pH: 7, 80 min	0.03	94%	•OH	49
C_3N_{4x}/AgO_y@$Co_{1-x}Bi_{1-y}O_7$	OTC	100W tungsten bulb	C_0: 25mM, pH: 7, 160 min	-	93	•OH , $O_2•^-$	83
Co-gC_3N_4/DE	4-Chlorophenol (4CP)	500W Xe Lamp	Catalyst dosage: 0.3g/L, C_0: 10 mg/L, $[H_2O_2]$: 2mM, pH: 3, 100 min	-	85	•OH , $O_2•^-$	37
Ti/TiO_2-$CoWO_4$	MO	100W UV Lamp	C_0: 10 mg/L, $[H_2O_2]$: 10mM, pH: 6.8, 180 min	-	85	•OH	141
Co-SMA	MO	Visible Lamp	Catalyst dosage: 0.029g/L, C_0: 30 mg/L, $[H_2O_2]$: 38mM, pH: 4.31	-	94.79	•OH	142
$ZnAl_2O_4$/$BiPO_4$	MB	100W UV Hg Lamp	Catalyst dosage: 0.8g/L, C_0: 30 mg/L, 180 min	-	92.55	•OH	143
Prussian Blue/Mn_3O_4	Levofloxacin (LVF)	30W LED Lamp	$[H_2O_2]$: 20mM, 60 min	0.076	93.9	$^1O_2$	48
AlMnCuZnBi Alloy	MO	White LED Lamp	Catalyst dosage: 1g/L, C_0: 10 mg/L, $[H_2O_2]$: 0.5M, 170 min	-	100%	•OH	116
Mn_3O_4/ZnO on ACFs	MB	500W Visible Xe Lamp	Catalyst dosage: 0.6g/L, C_0: 5 mg/L, 120 min	0.0328	100	•OH , $O_2•^-$	101
CuO_x/MnO_y@BC	Metronidazole (MNZ)	300W Xe Lamp	Catalyst dosage: 0.75g/L, C_0: 20 mg/L, $[H_2O_2]$: 20mM, pH: 7	0.0216	99.7	•OH	56
Cu (II) Quinoline complex	MB	30W UV Light	Catalyst dosage: 0.2g/L, C_0: 5 mg/L, 150 min	-	95	•OH , $O_2•^-$	144
Al/Cu-PILC	Paracetamol	8W UV C Hg Lamp	Catalyst dosage: 0.5g/L, C_0: 100 mg/L, $[H_2O_2]$: 145µL, pH: 5.8, 120 min	0.231	100	•OH	145
CuSe(Cu_2Se)/g-C_3N_4	MB	Visible Xe Lamp	Catalyst dosage: 0.4g/L, C_0: 30 mg/L, $[H_2O_2]$: 0.1 mL, 60 min	0.083	98.3	•OH	146
Ag/SnO_2	Naproxen (NPS)	18W Visible LED	Catalyst dosage: 0.2g/L, C_0: 40 mg/L, $[H_2O_2]$: 0.2mL, pH: 6, 40 min	0.0946	96.85	•OH	147
Cu-Cu_2O/gC_3N_4	RhB	Visible Lamp	$[H_2O_2]$: 3mM, 50 min	0.041	99	•OH	148
Cu^o@CuZ	Phenol	Visible Lamp	C_0: 20 mg/L, 15 min	-	100	•OH	104
Phosphate doped ZnO	MB	72W Visible LED Lamp	Catalyst dosage: 0.3g/L, C_0:10 mg/L, $[H_2O_2]$: 1.5mL (30wt%), pH: 3, 120 min	0.024	92.35	•OH	149

LMSN	RhB	Sunlight	0.22g/L, C_0:1 mg/L, [H_2O_2]: 0.8mL,105 min	-	97	•OH , $•O_2^-$	150
Copper(II) Phosphate	CIP	200W Visible XE Lamp	C_0: 15 mg/L, [H_2O_2]: 50µL (30 wt%), pH: 6.5, 60 min	0.004	95	•OH	118
$Gd_{2-x}La_xZr_2O_7$	Crystal Violet (CV)	36W UV Lamp	C_0: 10 mg/L, [H_2O_2]: 1mL (33 wt%), 60 min	-	90	•OH , $•O_2^-$	151
CeO_2-MoO_3	RhB	Sunlight	C_0: 1 mg/L, [H_2O_2]: 10mM, pH: 7, 120 min	-	95.36	•OH , $•O_2^-$	152
CuN/C-500	CR	300W Xe Lamp	Catalyst dosage: 0.8g/L, C_0: 10 mg/L, 60 min	0.0418	91.8	•OH , $•O_2^-$	98
$Cu_xMn_{0.03-x}Bi_{1-x}V_{0.97+x}O_4$	CIP	Visible LED	Catalyst dosage: 0.2g/L, C_0: 10 mg/L, [H_2O_2]: 1M, pH: 3, 100 min	-	100	•OH	57
CuO/gC_3N_4	Dimethyl Phenol (2,4-DMP)	35W Visible LED	Catalyst dosage: 0.5g/L, [H_2O_2]: 0.2mM, 120 min	0.0006	99	•OH	99
CNNS/Ag/Ni Heterostructure	Metronidazole	Visible Lamp	Catalyst dosage: 1g/L, C_0: 20 mg/L, 60 min	-	92.9	•OH	94
$CuCo_2S_4/BiWO_4$	TC-HCl	300W metal halide Lamp	Catalyst dosage: 1 g/L, C_0: 40 mg/L, [H_2O_2]: 100µL, pH: 5	-	80	•OH , $•O_2^-$	78
MnO_2/CNK-OH-Mn	Tc	300W Xe Lamp	Catalyst dosage: 0.5g/L, C_0: 10 mg/L, [H_2O_2]: 10 mM	-	96.7	•OH , $•O_2^-$	81
C/N-CCO@AgAu	Ofloxacin (OFX)	Hg Lamp	Catalyst dosage: 1 g/L, C_0: 20 mg/L, 60 min	-	91	•OH , $•O_2^-$	53
Cu_2O/Bi_2MoO_6	CIP	300W Xe Lamp	Catalyst dosage: 0.4g/L, C_0: 50 mg/L, pH: 3, 120 min	-	100	•OH , $•O_2^-$	87
$Ba_4Ti_3O_{12}$-$CuBi_2O_4$	OTC	300W Xe Lamp	Catalyst dosage: 0.4g/L, C_0: 10 mg/L, [H_2O_2]: 0.7mL (30 wt%), pH: 7, 50 min	-	96	•OH , $•O_2^-$	88
Cu^o+Ag^o@Bentonite	AMX	9W UV A Light	C_0: 2 mg/L, [H_2O_2]: 0.2 mL/L, pH: 3, 120 min	0.0095	84	•OH , $•O_2^-$	95
MgO/gC_3N_4	RhB	30W Xenon Lamp	Catalyst dosage: 1g/L, C_0: 100 mg/L, [H_2O_2]: 2mL,	0.0263	80	•OH , $•O_2^-$	84
Cu-N-C-700	TC	30W Xenon Lamp	Catalyst dosage: 0.g/L, C_0: 10 mg/L, [H_2O_2]: 0.2 mL, 15 min	-	98.5	•OH	106
$CuNi_2$Al-LDH	Phenol	30W Xenon Lamp	Catalyst dosage: 0.4g/L, C_0: 20 mg/L, [H_2O_2]: 6mM, pH: 3, 30 min	-	100	•OH , $•O_2^-$	111
CuO@C	Paracetamol	Visible LED Lamp	Catalyst dosage: 1g/L, C_0: 0.008mM, [H_2O_2]: 5mM, 60 min	-	95	•OH	108
Cu-C_3N_4	CIP	30W Xenon Lamp	Catalyst dosage: 0.4g/L, C_0: 10 mg/L, pH: 7, 30 min	0.0978	99	$^1O_2$	112
Ag-Co-CN	Phenol	Visible Lamp	Catalyst dosage: 20mg, C_0: 10 mg/L, 180 min	0.0135	94	•OH , $^1O_2$	113

View Article Online
DOI: 10.1039/D6LF00096G

5. Challenges and Outlook

Despite the impressive progress in the development of non-ferrous photo-Fenton catalysts, particularly Cu, Co, Mn, Bi, and Ce-based systems, several scientific and technological barriers must still be overcome to transition from lab-scale studies to real-world environmental remediation applications. A critical assessment of these challenges is essential to chart a path forward for the design of more efficient, stable, and sustainable systems.

5.1 Catalyst Stability and Leaching: A Quantitative Comparison

A persistent issue across non-iron photo-Fenton systems is the instability of active metal sites under prolonged photocatalytic conditions. For instance, Cu^{+}-based catalysts are prone to oxidation into Cu^{2+}, leading to structural collapse or leaching of active Cu ions into solution.[153] Similarly, Co^{2+} and Mn^{2+} ions can migrate out of the catalyst lattice during cyclic operations, raising concerns about secondary contamination and limiting reusability. Even cerium-based materials, despite the robust Ce^{4+}/Ce^{3+} redox pair, may suffer from partial surface dissolution under highly acidic or oxidative environments. Therefore, designing stable anchoring frameworks, such as mesoporous supports or MOFs with strong metal–ligand bonding, is crucial for minimizing leaching while retaining catalytic activity.

In addition to qualitative stability assessment, recent studies increasingly report quantitative metal leaching data to evaluate catalyst durability. A critical factor in the practical deployment of non-ferrous photo-Fenton systems is the stability of active metal sites and the mitigation of secondary pollution via leaching. A quantitative comparison of modern interface engineering strategies reveals significant variations in metal retention and structural durability after repeated reaction cycles.

- **Atomically Dispersed and Single-Atom Sites:** This paradigm offers the highest degree of metal immobilization. For instance, the CuCN system, featuring atomically

View Article Online
DOI: 10.1039/D6LF00096G

dispersed sites, demonstrated high stability with 83.3% retention after 5 cycles and Cu leaching levels confirmed via ICP at less than 30 μg/L. Similarly, the Cu-SA/CNH/PF architecture maintained excellent stability over 5 cycles (80.3% retention), with extremely low Cu leaching (25 μg/L) as verified by ICP-MS.

- **Bimetallic and High-Entropy Effects:** Multicomponent systems like the AlMnCuZnBi alloy utilize the "high-entropy effect" to prevent significant leaching of active sites. This strategy yielded high structural stability and approximately 94% retention after 5 cycles.

- **Cocatalysts and Intermediate Stabilization:** The use of cocatalysts and electron mediators, such as in the CuO/gC_3N_4 composite, provides a chemical pathway for stabilization. In this system, leaching is significantly suppressed to less than 0.085 mg/L by the presence of H_2O_2, which facilitates the formation of a protective CuO_2 intermediate.

- **Porous Scaffolds and Heterojunction Engineering:** Frameworks that provide lattice anchoring or directional charge dynamics also show promising results. The Bi_2WO_6/CoAl-LDH S-scheme heterojunction remained structurally stable (verified by XRD) after 4 cycles with 88.74 % retention, keeping Co^{2+} leaching below 1.0 mg/L. Porous scaffolds such as $CuNi_2$Al-LDH exhibited high retention over 4 cycles with a reported Cu leaching level of 0.73 ppm.

As summarized in Table 3, the shift toward atomic-level dispersion and high-entropy alloying represents the most effective technical approach for ensuring the long-term environmental safety of non-ferrous catalysts. These quantitative findings provide a robust roadmap for designing interfaces that minimize leaching while maintaining high catalytic flux in complex wastewater matrices.

View Article Online
DOI: 10.1039/D6LF00096G

5.2 Matrix Effects and Practical Adaptability

In practical wastewater treatment, the performance of non-ferrous photo-Fenton catalysts is significantly influenced by the presence of co-existing ions and natural organic matter, collectively referred to as matrix effects. Unlike model laboratory conditions, real water systems contain a complex mixture of inorganic anions (e.g., Cl^-, HCO_3^-, PO_4^{3-}, SO_4^{2-}) and dissolved organic substances such as humic and fulvic acids, which can interfere with catalytic processes.

Among these, chloride ions (Cl^-) can react with hydroxyl radicals (•OH) to form less reactive chlorine-based radicals (Cl•, $Cl_2•^-$), thereby reducing oxidation efficiency. Similarly, bicarbonate (HCO_3^-) and carbonate (CO_3^{2-}) ions act as scavengers of •OH, forming carbonate radicals ($CO_3•^-$) with lower oxidation potential. Phosphate ions (PO_4^{3-}), on the other hand, can strongly adsorb onto catalyst surfaces, blocking active sites and inhibiting H_2O_2 activation. In addition, natural organic matter such as humic acids can compete with target pollutants for adsorption sites, alter surface charge properties, and even quench reactive oxygen species.

Importantly, the extent of matrix interference depends on the dominant reaction pathway. Radical-based systems relying on free •OH are highly susceptible to scavenging by co-existing species, whereas non-radical pathways, such as singlet oxygen ($^1O_2$) generation and surface-mediated electron transfer, exhibit greater selectivity and resistance to interference. Interface engineering plays a crucial role in mitigating matrix effects by promoting selective adsorption, enhancing charge separation, and favouring localized reaction pathways. For example, oxygen-vacancy-rich surfaces and S-scheme heterojunctions can facilitate controlled ROS generation and reduce undesired side reactions with background ions.

Overall, understanding and addressing matrix effects is essential for translating laboratory-scale catalytic performance to real-world wastewater treatment applications.

View Article Online
DOI: 10.1039/D6LF00096G

5.3 Quantitative Benchmarking and Performance Metrics

A significant challenge in evaluating the performance of non-ferrous photo-Fenton systems is the lack of standardized experimental protocols across the literature. Direct comparison of pseudo-first-order rate constants (k, min^{-1}) is often misleading, as k is highly sensitive to parameters such as catalyst dosage (C_{cat}), initial pollutant concentration (C_0), light intensity, and reactor configuration.

To enable more meaningful comparison, normalized performance descriptors can be considered. One such parameter is the mass-normalized rate constant (k□), defined as:

$$k_m = \frac{k}{C_{cat}}$$

where k□ is expressed in L g^{-1} min^{-1}. This metric accounts for variations in catalyst loading and provides a more representative indication of intrinsic catalytic activity.

However, it is important to note that even normalized parameters may be influenced by additional experimental factors, including light intensity and solution chemistry. Therefore, such metrics should be interpreted cautiously and used primarily to identify general performance trends rather than for strict quantitative comparison across different studies.

Overall, the development of standardized testing protocols and reporting guidelines will be essential for enabling reliable benchmarking and accelerating the rational design of high-performance photo-Fenton catalysts.

5.4 H_2O_2 Consumption and Economic Viability

While degradation efficiency is the most frequently reported metric in photo-Fenton studies, the utilization efficiency of H_2O_2 is also a critical factor in determining the economic and environmental feasibility of the process. In many systems, a significant fraction of H_2O_2 may

View Article Online
DOI: 10.1039/D6LF00096G

be lost through non-productive pathways, including self-decomposition and scavenging reactions with excess oxidant. From a practical perspective, inefficient H_2O_2 utilization leads to increased operational costs and reduced process sustainability. Therefore, it is essential to evaluate how effectively H_2O_2 is converted into reactive oxygen species (ROS) for pollutant degradation.

Interface engineering provides an effective strategy to improve H_2O_2 utilization efficiency. By modulating surface electronic structure and adsorption behaviour, engineered interfaces can promote selective activation of H_2O_2 toward ROS generation while suppressing unproductive decomposition pathways. For example, defect-rich catalysts, heterojunction systems, and atomically dispersed metal sites can enhance controlled H_2O_2 activation and improve oxidant efficiency.

In this context, metrics such as H_2O_2 consumption efficiency (η) can be considered for a more realistic assessment of catalytic performance. These parameters are particularly important for bridging the gap between laboratory-scale studies and practical wastewater treatment applications.

5.5 Interface Engineering Complexity

The creation of efficient heterojunctions or atomically precise interfaces remains synthetically challenging, particularly for large-scale production. Techniques such as atomic layer deposition (ALD), electrospinning, or solvothermal synthesis often require stringent control over temperature, pH, or precursor ratios to maintain desired morphology and interface composition. Moreover, ensuring reproducibility and uniform dispersion of active sites is still difficult in batch-to-batch synthesis. Scalable and green fabrication methods like mechanochemical synthesis or bio-templating need to be developed to make such advanced materials industrially viable.

View Article Online
DOI: 10.1039/D6LF00096G

5.6 Narrow Light Absorption Range and Photocorrosion

Although visible-light-responsive materials like g-C_3N_4, BiOBr, and Co_3O_4 have expanded the working wavelength of photo-Fenton catalysts, many systems still suffer from limited light absorption or rapid electron–hole recombination. Additionally, photocorrosion of materials such as Bi-based catalysts under high-flux light can compromise long-term durability. Incorporating plasmonic nanoparticles (e.g., Ag, Au) or constructing broadband absorbers via doped semiconductors offers a potential path to widen spectral absorption while suppressing photocorrosion.

5.7 ROS Selectivity and Byproduct Toxicity

Current systems often rely on nonspecific ROS such as •OH and $\bullet O_2^-$, which indiscriminately attack organic pollutants. However, this lack of selectivity may lead to incomplete mineralization or the formation of toxic intermediates, particularly in pharmaceutical degradation. Advanced characterization techniques and LC-MS studies have shown accumulation of quinolone or aromatic byproducts even at high degradation percentages. Future systems should aim to steer ROS pathways using ligand-functionalized surfaces or microenvironment engineering (e.g., acidic/basic zones) to maximize pollutant selectivity and safety.

5.8 Real-World Wastewater Complexity

While the specific effects of co-existing ions and natural organic matter on catalytic activity have been discussed in Section 5.2, additional challenges arise when translating non-ferrous photo-Fenton systems from controlled laboratory conditions to real wastewater environments. Most reported studies rely on model pollutants (e.g., rhodamine B, tetracycline) in deionized or simplified aqueous systems, which do not adequately represent the complexity of real wastewater. In practical scenarios, wastewater streams typically contain diverse pollutant

mixtures, including pharmaceuticals, dyes, and industrial organics, along with fluctuating pH, variable ionic strength, and suspended solids. These factors can significantly alter catalyst surface properties, light penetration, and mass transfer dynamics.

Furthermore, the presence of turbidity and coloured dissolved organic matter can reduce photon utilization efficiency by attenuating light intensity, thereby limiting photocatalytic activation. In addition, competitive adsorption among multiple pollutants may reduce the effective availability of active sites, leading to decreased degradation efficiency compared to single-component systems. From an operational perspective, real-world implementation also requires consideration of catalyst recovery, long-term stability under continuous flow conditions, and scalability of synthesis methods. The transition from batch laboratory experiments to pilot-scale or continuous-flow reactors introduces additional constraints related to hydrodynamics, catalyst dispersion, and reactor design.

Importantly, the impact of real wastewater matrices varies significantly depending on the nature of the metal system and its dominant reaction pathway. Cu and Co-based catalysts, which often rely on radical-driven mechanisms, are more susceptible to inhibition by common anions such as Cl^- and HCO_3^- due to scavenging of •OH radicals. In contrast, Bi and Ce-based systems, particularly those with abundant oxygen vacancies, tend to operate via non-radical pathways (e.g., $^1O_2$ or surface-mediated electron transfer), which exhibit greater resistance to such interference. Mn-based catalysts typically display intermediate behaviour, where both radical and non-radical pathways may coexist, leading to variable sensitivity depending on surface structure and oxidation state. Additionally, natural organic matter (e.g., humic substances) can compete for active sites and modify surface charge, further influencing catalyst performance in a system-dependent manner.

View Article Online
DOI: 10.1039/D6LF00096G

Therefore, future research should prioritize testing under realistic wastewater matrices, integrating continuous-flow systems, and conducting pilot-scale studies to bridge the gap between laboratory-scale performance and practical environmental applications.

5.9 The Environmental Trade-off: Secondary Toxicity and Regulatory Compliance

A significant hurdle for the large-scale transition from iron-based Fenton processes to non-ferrous systems is the inherent toxicity of the metals themselves. While iron is an environmentally benign baseline, transition metals such as Cu, Co, and Mn possess complex toxicity profiles that can lead to secondary contamination if leaching is not strictly controlled. This creates a "dual challenge" where the catalyst must maintain high interfacial activity while ensuring metal dissolution remains below stringent parts-per-billion (ppb) levels.

- **Regulatory Thresholds and Metal-Specific Risks:** The environmental impact varies significantly across different metal systems. For instance, Cobalt (Co) is a high-priority concern due to its potential bioaccumulation and carcinogenicity, with industrial discharge often capped at 1.0 mg/L.[154] Copper (Cu), while less toxic to humans, exhibits high aquatic toxicity to invertebrates and fish, with WHO and EPA limits set between 1.3 and 2.0 mg/L.[155] Excessive Manganese (Mn) is associated with neurotoxicity. Health-based limits are generally set around 0.4 mg/L.[156]

- **The "Green" Alternative Gap:** Bismuth (Bi) and Cerium (Ce) are frequently proposed as "greener" alternatives due to their low systemic toxicity. However, their catalytic turnover frequencies often lag behind Cu or Co-based systems, requiring more intensive interface engineering to reach competitive degradation rates.

View Article Online
DOI: 10.1039/D6LF00096G

- **Long-term Operational Stability:** A major challenge remains in assessing "real-world" leaching over hundreds of hours. Most current studies report stability over only 5 to 10 cycles, which is insufficient to guarantee that metal-N_x sites or high-entropy alloys will remain leaching-free under the continuous oxidative stress of industrial-scale H_2O_2 activation.

To overcome this, future research must prioritize quantitative mass-balance studies and standardized leaching protocols that test catalysts in complex wastewater matrices where competing anions (like Cl^- or PO_4^{3-}) might accelerate metal dissolution. Ensuring that treated water meets both organic pollutant limits and heavy metal safety standards is the final bridge that non-ferrous photo-Fenton technology must cross.

Outlook

(1) Atomic-Level Engineering of Active Sites.

Although atomically dispersed catalysts offer maximum atom efficiency and tunable electronic properties, their controlled synthesis and long-term stability under reaction conditions remain challenging. Most current methods for anchoring single or dual metal atoms (e.g., Cu, Co, Mn) on supports such as g-C_3N_4 or graphene suffer from aggregation and metal leaching. Future strategies should focus on stabilizing metal-N/O coordination environments using defect-rich or heteroatom-doped carbon frameworks, as well as in situ/operando spectroscopy to track coordination dynamics during catalysis.

(2) Design of Multimodal Interface Architectures.

While individual interfaces like Type-II or Z-scheme heterojunctions have shown promise, hybrid systems integrating multiple interfacial types (e.g., Type-II with atomically

View Article Online
DOI: 10.1039/D5FF00096G

dispersed metals or embedded in porous frameworks) remain underexplored. Developing composite catalysts with synergistic interfaces can enhance directional charge transfer and suppress ROS recombination. Rational design of such architectures requires integrated synthetic computational approaches to optimize spatial configurations and electron pathways at the nano–micro scale.

(3) Surface Functionalization and Charge Regulation via Metal Nanoparticles. Noble and transition metal nanoparticles (e.g., Ag, Cu, Pt) can act as electron sinks or plasmonic sensitizers, but their catalytic role in non-ferrous photo-Fenton systems often lacks mechanistic clarity. Future studies should explore size-dependent effects, support-metal interactions, and plasmon-induced hot carrier dynamics through advanced characterization and theoretical modelling. Tailoring interfacial charge densities and local electric fields will be key to enhancing H_2O_2 activation and ROS selectivity.

(4) Scaffolded Interfaces with Porous Frameworks.

Despite the success of MOFs, COFs, and porous carbon materials in pollutant capture and dispersion of active species, their integration with photo-Fenton centres is still in its infancy. The development of hierarchically structured supports with controlled pore size distribution, hydrophilicity, and functional anchoring groups is crucial. Additionally, structure-activity correlations between support chemistry and catalytic efficiency should be systematically studied using DFT and experimental mapping techniques.

(5) Mechanistic Exploration of ROS Pathways.

The true identity and interplay of ROS (•OH, $•O_2^-$, $^1O_2$) in Cu, Co, Mn, Bi, and Ce-based systems remain ambiguous due to overlapping generation mechanisms. Although scavenger tests and EPR studies are widely used, they often provide indirect or incomplete evidence. Time-resolved spectroscopy, isotope labelling, and operando techniques (e.g.,

XAS, TRPL) are necessary to delineate the ROS evolution kinetics, charge transfer routes, and interfacial energy band modulations during light-assisted H_2O_2 activation.

(6) AI/ML-Driven Catalyst Discovery and Design

The integration of artificial intelligence and machine learning (AI/ML) with materials chemistry offers a powerful strategy to bypass the traditional "trial-and-error" bottleneck in non-ferrous photo-Fenton catalyst design. ML models can be trained on Density Functional Theory (DFT)-derived datasets to predict key physicochemical descriptors that govern the catalytic cycle at the interface.

A primary challenge in photo-Fenton-like systems is optimizing the adsorption energy of H_2O_2. If the binding is too weak, the activation is inefficient; if too strong, the active sites become poisoned by intermediates. ML algorithms can rapidly screen metal-support combinations and defect structures to identify the "volcano plot" peak for H_2O_2 binding, promoting efficient reactive oxygen species (ROS) generation. Similarly, band alignment is a crucial descriptor for heterojunction engineering. ML models trained on electronic structure data can predict the Fermi levels and band edge positions of new semiconductor pairs, enabling the rational construction of S-scheme or Z-scheme systems with maximized redox potential.

Furthermore, ML can predict defect formation energies, particularly for oxygen vacancies, which are vital for tuning charge density. By combining these computational descriptors with experimental datasets through Active Learning loops, researchers can establish quantitative structure–activity relationships (QSAR). This data-driven approach facilitates the high-throughput screening of interfacial architectures, ultimately accelerating the discovery of optimized catalysts with enhanced H_2O_2 activation efficiency and long-term operational stability.

View Article Online
DOI: 10.1039/D6LF00096G

(7) Bifunctional Systems for In Situ H_2O_2 Generation

A major limitation in the practical deployment of photo-Fenton systems is the reliance on externally added H_2O_2. A promising high-risk research direction involves the development of bifunctional catalytic interfaces capable of driving the two-electron oxygen reduction reaction ($2e^-$ ORR) for in situ H_2O_2 generation.

It is hypothesized that coupling plasmonic nanoparticles (e.g., Ag, Au) with Cu–N_x coordinated sites or oxygen-vacancy-rich Bi-based surfaces can enable simultaneous generation and activation of H_2O_2 at the same interface. Such a synergistic system could facilitate localized oxidant production from dissolved O_2, thereby minimizing mass transport limitations and improving overall process efficiency. This self-sustaining catalytic cycle has the potential to significantly reduce chemical input requirements and enhance the economic feasibility of photo-Fenton processes.

(8) Pulsed-Light Operation and Time-Resolved Catalytic Dynamics

Most reported photo-Fenton systems operate under continuous irradiation, which can lead to inefficient charge utilization due to the mismatch between photogenerated charge carrier flux and the intrinsic kinetics of surface redox cycles (e.g., Co^{2+}/Co^{3+}).

An emerging hypothesis is that pulsed-light irradiation, employing microsecond (μs) or millisecond (ms) timescales, can be used to better synchronize charge carrier generation with catalytic turnover processes. By temporally modulating light input, this approach may reduce charge recombination and allow active sites to undergo complete redox cycling between pulses. Such dynamic operation could enhance quantum efficiency and provide new insights into time-resolved catalytic mechanisms in non-ferrous photo-Fenton systems.

6. Conclusion

View Article Online
DOI: 10.1039/D6LF00096G

The development of non-ferrous photo-Fenton catalysts has unlocked new possibilities in sustainable water remediation by expanding the catalytic toolbox beyond traditional iron-based systems. Transition metals such as Cu, Co, Mn, Bi, and Ce have demonstrated remarkable redox activity under visible light in the presence of H_2O_2, facilitating the generation of reactive oxygen species (ROS) essential for efficient pollutant degradation. Recent advances in interface engineering, ranging from Type-II and Z-scheme heterojunctions, p-n junctions, to atomically dispersed metal sites and bimetallic interfaces, have significantly enhanced charge separation, optimized band alignment, and improved H_2O_2 activation kinetics. These tailored architectures have also shown superior selectivity, faster degradation rates, and better adaptability to diverse water matrices. Nonetheless, challenges persist, particularly regarding catalyst leaching, limited reusability, and incomplete understanding of ROS formation mechanisms across various interfacial configurations. Furthermore, real-world water treatment often involves complex mixtures, variable pH, and interfering species, which are underexplored in current lab-scale studies. Future efforts should focus on (i) integrating machine learning and theoretical modelling to guide rational interface design, (ii) advancing operando characterization tools to capture transient species during photocatalysis, and (iii) scaling up these systems through green synthesis, stable supports, and reactor design optimization. By addressing these aspects, non-iron photo-Fenton-like systems with engineered interfaces can transition from promising academic discoveries to practical solutions for global water pollution challenges.

Data availability

This article is based on an analysis of previously published data. All relevant data supporting the findings of this study are included within the article. Original sources of the data are cited throughout the manuscript.

View Article Online
DOI: 10.1039/D6LF00096G

Conflicts of interest

The authors declare that they have no conflict of interest.

List of Abbreviations

AI/ML – Artificial Intelligence / Machine Learning

AOPs – Advanced Oxidation Processes

BiOX – Bismuth Oxyhalides (X = Cl, Br, I)

CB – Conduction Band

g-C_3N_4 – Graphitic Carbon Nitride

DIET – Direct Interfacial Electron Transfer

DFT – Density Functional Theory

ECs – Emerging Contaminants

EPR – Electron Paramagnetic Resonance

H_2O_2 – Hydrogen Peroxide

CNT– Carbon Nanotubes

rGO – Reduced Graphene Oxide

IEFs – Internal Electric Fields

LDHs – Layered Double Hydroxides

LMCT – Ligand-to-Metal Charge Transfer

MOFs – Metal–Organic Frameworks

View Article Online
DOI: 10.1039/D6LF00096G

NHE – Normal Hydrogen Electrode

NOM – Natural Organic Matter

OVs – Oxygen Vacancies

PPCPs – Pharmaceuticals and Personal Care Products

QSAR – Quantitative Structure–Activity Relationships

ROS – Reactive Oxygen Species

SACs – Single-Atom Catalysts

VB – Valence Band

XPS – X-ray Photoelectron Spectroscopy

References

(1) Montgomery, M. A.; Elimelech, M. Water and Sanitation in Developing Countries: Including Health in the Equation. *Environ. Sci. Technol.* **2007**, *41* (1), 17–24.

(2) Shannon, M. A.; Bohn, P. W.; Elimelech, M.; Georgiadis, J. G.; Mariñas, B. J.; Mayes, A. M. Science and Technology for Water Purification in the Coming Decades. *Nature* **2008**, *452* (7185), 301–310.

(3) Ramesha, G. K.; Kumara, A. V.; Muralidhara, H. B.; Sampath, S. Graphene and Graphene Oxide as Effective Adsorbents toward Anionic and Cationic Dyes. *J. Colloid Interface Sci.* **2011**, *361* (1), 270–277.

(4) Pan, C.; Zhu, Y. New Type of $BiPO_4$ Oxy-Acid Salt Photocatalyst with High Photocatalytic Activity on Degradation of Dye. *Environ. Sci. Technol.* **2010**, *44* (14), 5570–5574.

(5) Xu, J.; Wang, L.; Zhu, Y. Decontamination of Bisphenol A from Aqueous Solution by Graphene Adsorption. *Langmuir* **2012**, *28* (22), 8418–8425.

(6) Liang, F.; Zhu, Y. Enhancement of Mineralization Ability for Phenol via Synergetic Effect of Photoelectrocatalysis of G-C_3N_4 Film. *Appl. Catal. B* **2016**, *180*, 324–329.

View Article Online
DOI: 10.1039/D6LF00096G

(7) Ghorbani, P.; Hassani, A.; Eghbali, P.; Abbasi, A. Activated carbon-based photocatalysts for the removal of pesticides. In *Pesticide Removal Methods from Wastewater: Proactive Approaches and Future Trends*; Hassani, A., Ed.; CRC Press, **2025**; pp 203–236.

(8) Wang, J.; Zhuan, R. Degradation of Antibiotics by Advanced Oxidation Processes: An Overview. *Science of the Total Environment* **2020**, *701*, 135023.

(9) Calvete, M. J. F.; Piccirillo, G.; Vinagreiro, C. S.; Pereira, M. M. Hybrid Materials for Heterogeneous Photocatalytic Degradation of Antibiotics. *Coord. Chem. Rev.* **2019**, *395*, 63–85.

(10) Hassani, A.; Pourshirband, N.; Sayyar, Z.; Eghbali, P. Fenton and Fenton-like-based advanced oxidation processes. In *Innovative and Hybrid Advanced Oxidation Processes for Water Treatment*; Hamdaoui, O., Ed.; Elsevier, **2025**; pp 171–203.

(11) Bai, X.; Sun, C.; Liu, D.; Luo, X.; Li, D.; Wang, J.; Wang, N.; Chang, X.; Zong, R.; Zhu, Y. Photocatalytic Degradation of Deoxynivalenol Using Graphene/ZnO Hybrids in Aqueous Suspension. *Appl. Catal. B* **2017**, *204*, 11–20.

(12) Deng, Y.; Ezyske, C. M. Sulfate Radical-Advanced Oxidation Process (SR-AOP) for Simultaneous Removal of Refractory Organic Contaminants and Ammonia in Landfill Leachate. *Water Res.* **2011**, *45* (18), 6189–6194.

(13) Deng, Y.; Zhao, R. Advanced Oxidation Processes (AOPs) in Wastewater Treatment. *Curr. Pollut. Rep.* **2015**, *1* (3), 167–176.

(14) Ribeiro, J. P.; Marques, C. C.; Portugal, I.; Nunes, M. I. Fenton Processes for AOX Removal from a Kraft Pulp Bleaching Industrial Wastewater: Optimisation of Operating Conditions and Cost Assessment. *J. Environ. Chem. Eng.* **2020**, *8* (4), 104032.

(15) Miklos, D. B.; Remy, C.; Jekel, M.; Linden, K. G.; Drewes, J. E.; Hübner, U. Evaluation of Advanced Oxidation Processes for Water and Wastewater Treatment–A Critical Review. *Water Res.* **2018**, *139*, 118–131.

(16) Peng, G.; Gao, F.; Zou, J.; Wang, X.; Gao, Y.; Zhou, H.; Liu, S.; Li, M.; Lu, L. One-Step Electrochemical Synthesis of Tremella-like Co-MOFs/Carbon Nanohorns Films for Enhanced Electrochemical Sensing of Carbendazim in Vegetable and Fruit Samples. *Journal of Electroanalytical Chemistry* **2022**, *918*, 116462.

(17) Zhou, Y.; Zhou, L.; Zhou, Y.; Xing, M.; Zhang, J. Z-Scheme Photo-Fenton System for Efficiency Synchronous Oxidation of Organic Contaminants and Reduction of Metal Ions. *Appl. Catal. B* **2020**, *279*, 119365.

(18) Duan, W.-L.; Li, Y.-X.; Li, W.-Z.; Luan, J. Controllable Synthesis of Copper-Organic Frameworks via Ligand Adjustment for Enhanced Photo-Fenton-like Catalysis. *J. Colloid Interface Sci.* **2023**, *646*, 107–117.

(19) Zhang, M.; Dong, H.; Zhao, L.; Wang, D.; Meng, D. A Review on Fenton Process for Organic Wastewater Treatment Based on Optimization Perspective. *Science of the Total Environment* **2019**, *670*, 110–121.

(20) Ribeiro, J. P.; Nunes, M. I. Recent Trends and Developments in Fenton Processes for Industrial Wastewater Treatment–A Critical Review. *Environ. Res.* **2021**, *197*, 110957.

(21) Li, L.; Yin, Z.; Cheng, M.; Qin, L.; Liu, S.; Yi, H.; Zhang, M.; Fu, Y.; Yang, X.; Zhou, X. Insights into Reactive Species Generation and Organics Selective Degradation in Fe-Based Heterogeneous Fenton-like Systems: A Critical Review. *Chemical Engineering Journal* **2023**, *454*, 140126.

(22) Cleveland, V.; Bingham, J.-P.; Kan, E. Heterogeneous Fenton Degradation of Bisphenol A by Carbon Nanotube-Supported Fe_3O_4. *Sep. Purif. Technol.* **2014**, *133*, 388–395.

(23) Lv, H.; Zhao, H.; Cao, T.; Qian, L.; Wang, Y.; Zhao, G. Efficient Degradation of High Concentration Azo-Dye Wastewater by Heterogeneous Fenton Process with Iron-Based Metal-Organic Framework. *J. Mol. Catal. A Chem.* **2015**, *400*, 81–89.

(24) Cheng, M.; Lai, C.; Liu, Y.; Zeng, G.; Huang, D.; Zhang, C.; Qin, L.; Hu, L.; Zhou, C.; Xiong, W. Metal-Organic Frameworks for Highly Efficient Heterogeneous Fenton-like Catalysis. *Coord. Chem. Rev.* **2018**, *368*, 80–92.

(25) De Urzedo, A. P. F. M.; Nascentes, C. C.; Augusti, R. Degradation of the Insecticides Thiamethoxam and Imidacloprid in Aqueous Solution as Promoted by an Innovative Fe^o/Fe_3O_4 Composite. *J. Braz. Chem. Soc.* **2009**, *20*, 51–56.

(26) Du, D.; Shi, W.; Wang, L.; Zhang, J. Yolk-Shell Structured Fe_3O_4@ Void@TiO_2 as a Photo-Fenton-like Catalyst for the Extremely Efficient Elimination of Tetracycline. *Appl. Catal. B* **2017**, *200*, 484–492.

(27) Li, X.; Liu, J.; Rykov, A. I.; Han, H.; Jin, C.; Liu, X.; Wang, J. Excellent Photo-Fenton Catalysts of Fe–Co Prussian Blue Analogues and Their Reaction Mechanism Study. *Appl. Catal. B* **2015**, *179*, 196–205.

(28) Guo, T.; Wang, K.; Zhang, G.; Wu, X. A Novel α-Fe_2O_3@ g-C_3N_4 Catalyst: Synthesis Derived from Fe-Based MOF and Its Superior Photo-Fenton Performance. *Appl. Surf. Sci.* **2019**, *469*, 331–339.

(29) Ma, B.; Zha, Y.; Shi, H.; Qin, Y.; Zhao, M.; Li, J.; Wang, S.; Yan, B.; Zhao, B.; Ma, Y. Enhanced Photocatalysis-Fenton Degradation of Levofloxacin by Fe Doped BiOCl Microspheres with Rich Surface Oxygen Vacancies: The Accelerated Redox Cycle Of≡ Fe (III)/≡ Fe (II). *Sep. Purif. Technol.* **2025**, *354*, 129086.

(30) Wang, X.; Wu, L.; Wang, J.; Zhou, Y.; Wang, Y.; Wu, W. D.; Li, W.; Wu, Z. Oxygen Vacancies and Interfacial Iron Sites in Hierarchical BiOCl Nanosheet Microflowers Cooperatively Promoting Photo-Fenton. *Chemosphere* **2022**, *307*, 135967.

(31) Liu, J.; Wu, H.; Sun, J.; Li, S.; Hassani, A.; Zhou, M. Non-TiO_2-based photoanodes for photoelectrocatalytic wastewater treatment: electrode synthesis, evaluation, and characterization. *EES Catalysis* **2025**, *3*(5), 921–942.

(32) Tian, Y.; Jia, N.; Ma, H.; Liu, G.; Xiao, Z.; Wu, Y.; Zhou, L.; Lei, J.; Wang, L.; Liu, Y. 0D/3D Coupling of g-C_3N_4 QDs/Hierarchical Macro-Mesoporous CuO-SiO_2 for High-Efficiency Norfloxacin Removal in Photo-Fenton-like Processes. *J. Hazard. Mater.* **2021**, *419*, 126359.

(33) Li, J.; Pham, A. N.; Dai, R.; Wang, Z.; Waite, T. D. Recent Advances in Cu-Fenton Systems for the Treatment of Industrial Wastewaters: Role of Cu Complexes and Cu Composites. *J. Hazard. Mater.* **2020**, *392*, 122261.

(34) Tian, H.; Zhang, M.; Jin, G.; Jiang, Y.; Luan, Y. Cu-MOF Chemodynamic Nanoplatform via Modulating Glutathione and H_2O_2 in Tumour Microenvironment for Amplified Cancer Therapy. *J. Colloid Interface Sci.* **2021**, *587*, 358–366.

(35) Dai, N.; Yang, L.; Liu, X.; Gao, L.; Zheng, J.; Zhang, K.; Song, D.; Sun, T.; Luo, S.; Liu, X. Enhanced Photo-Fenton-like Performance of Biotemplated Manganese-Doped Cobalt Silicate Catalysts. *J. Colloid Interface Sci.* **2023**, *652*, 1812–1824.

(36) Mokoba, T.; Li, Z.; Zhang, T. C.; Yuan, S. Superwetting Sea Urchin-like BiOBr@Co_3O_4 Nanowire Clusters-Coated Copper Mesh with Efficient Emulsion Separation and Photo-Fenton-like Degradation of Soluble Dye. *Appl. Surf. Sci.* **2022**, *594*, 153497.

(37) Zhang, L.-M.; Lv, X.-X.; Shu, A.-L.; Lu, X.-Z.; Chen, X. Insight on the Degradation of P-Chlorophenol Based on the Co-g-C_3N_4/Diatomite Composite Photo-Fenton Process. *Journal of Industrial and Engineering Chemistry* **2024**, *136*, 305–316.

(38) Yang, G.; Liang, Y.; Zheng, H.; Yang, J.; Guo, S.; Yu, H. A Self-Circulating Cerium-Rich CeO_{2-x}/Bi_2MoO_6 Heterojunction Catalyst for Boosting Photo-Fenton Degradation of Fluoroquinolone Antibiotics. *Sep. Purif. Technol.* **2023**, *309*, 123084.

(39) Zhang, X.; Zhang, L.; Ye, H.; Zeng, Z.; Yang, J.; Han, C.; Liang, Y. Bimetallic-Organic Frameworks Derived Bi-Doped CeO_2 Nanorods with Oxygen Vacancies for Boosted Photo-Fenton Activity. *J. Environ. Chem. Eng.* **2025**, 117489.

(40) Wu, X.; Zhao, Q.; Zhang, J.; Li, S.; Liu, H.; Liu, K.; Li, Y.; Kong, D.; Sun, H.; Wu, M. 0D Carbon Dots Intercalated Z-Scheme CuO/g-C_3N_4 Heterojunction with Dual Charge Transfer Pathways for Synergetic Visible-Light-Driven Photo-Fenton-like Catalysis. *J. Colloid Interface Sci.* **2023**, *634*, 972–982.

(41) Shao, B.; Liu, Z.; Tang, L.; Liang, Q.; He, Q.; Wu, T.; Pan, Y.; Cheng, M.; Liu, Y.; Tan, X. Construction of Bi_2WO_6/CoAl-LDHs S-Scheme Heterojunction with Efficient Photo-Fenton-like Catalytic Performance: Experimental and Theoretical Studies. *Chemosphere* **2022**, *291*, 133001.

View Article Online
DOI: 10.1039/D6LF00096G

(42) Yang, B.; Li, J.; Li, Y.; Zhang, M.; Zhu, J.; Zhou, T.; Deng, J. Electrochemical Post-Treatment of Bimetallic-ICP/RGO Precursor for Z-Scheme CuO_x·Ag_2O/RGO Hetero-Structure with Catalytic Activity Enhancement for Visible-Light-Driven Photo-Fenton Degradation of Tetracycline. *Sep. Purif. Technol.* **2022**, *299*, 121741.

(43) Guo, Y.; Liu, Y.; Hao, S.; Zhang, X.; Yu, Y. In-Situ Decoration of $Cu_2(OH)_3F$ on BiOBr with Exposed (010) Facets: Heterojunctions and Photo-Fenton-like Synergistic Promote Cu^+/Cu^{2+} Circulation. *Journal of Water Process Engineering* **2023**, *55*, 104140.

(44) Bokare, A. D.; Choi, W. Review of Iron-Free Fenton-like Systems for Activating H_2O_2 in Advanced Oxidation Processes. *J. Hazard. Mater.* **2014**, *275*, 121–135.

(45) Wang, Y.; Hu, C.; Gan, Y.; Sun, Z.; Deng, Y.; Xie, M.; Wang, Y.; Xie, J.; Zhang, W.; Huang, L. Plasmon-Drive Multi-Channel Hot Electron Transfer in VO-Cu_2O@ Cu/CN_x Heterojunction for Enhanced Photo-Fenton-Like Reaction: Critical Roles of Copper Species and H_2O_2. *Applied Catalysis B: Environment and Energy* **2025**, 125500.

(46) Guo, Y.; Han, T.; Luo, Y.; Xing, J.; Jia, Y. Noble Metal-Free Cu Nanoparticles Modified Bi_2O_2S Nanosheets for Enhanced Photo-Fenton-Like Degradation and CO_2 Photoreduction. *Available at SSRN 5229724*.

(47) Kang, Z.; Ren, X.; Wang, Y.; Li, J.; Ma, Y.; Feng, Z.; Sun, T. In-Situ Stripping Synthesis of $Cu_{2-X}S$/g-C_3N_4 Heterojunction with Feeble Nitrogen Vacancy Sites for Constructing Complementary Enhanced Photo-Fenton-like Systems. *Journal of Water Process Engineering* **2025**, *69*, 106876.

(48) Xi, F.; Yue, M.; Zhao, J.; Xie, K.; Ma, J.; Song, X.; Liang, L.; Hou, A. Photo-Fenton Enhanced Self-Floating Z-Scheme Prussian Blue/Mn_3O_4 Heterojunction for Efficient Levofloxacin Degradation: Mechanism, Pathway and DFT Analysis. *Colloids Surf. A Physicochem. Eng. Asp.* **2025**, 138653.

(49) Palanivel, B.; Hossain, M. S.; Reddy, I. N.; Al-Enizi, A. M.; Ubaidullah, M.; Macadangdang Jr, R. R.; Shim, J. Chemical Oxidants (H_2O_2 and Persulfate) Activated Photo-Fenton like Degradation Reaction Using Sol-Gel Derived g-C_3N_4/$ZnCo_2O_4$ Nanocomposite. *Diam. Relat. Mater.* **2022**, *130*, 109413.

(50) Wang, Z.; Ren, D.; Chi, R. Synthesis of Copper-Based Fenton-like Catalyst (Cu/HAP-SBC) for Oxidative Degradation of p-Nitrophenol in Aqueous Solution. *J. Mol. Struct.* **2025**, *1339*, 142383.

(51) Lu, S.; Zhang, X.; Wang, M.; Huang, Y.; Yin, S.; Wang, B.; Xia, J.; Li, H. Ball-Milling Synthesis of CPDs/$CuBi_2O_4$ Z-Scheme Heterojunction Photocatalysis for Photofenton Antibiotic Wastewater Treatment. *J. Environ. Chem. Eng.* **2025**, 118820.

(52) Guo, Z.; Wei, W.; Li, Y.; Niu, X.; Hou, F.; Li, J.; Zhang, X.; Zhang, X.; Wei, A. Cu Single Atoms Anchored on Hydrangea-like Carbon Nitride for Facilitating Photo-Fenton: Role of Cu^{2+}/Cu^+ Cycle. *Sep. Purif. Technol.* **2024**, *344*, 127290.

(53) Panda, J.; Priyadarshini, N.; Mansingh, S.; Parida, K. Ce/Cu-MOF-Derived AgAu–C/N–CeO_2@ C/N–CuO S-Scheme Nanohybrids for Photocatalytic H_2O_2 Production and Photo-Fenton Antibiotic Degradation. *Langmuir* **2025**.

(54) Rodríguez-Sánchez, N.; Bhattacharya, B.; Emmerling, F.; Prinz, C.; Prieto-Laria, P.; Ruiz-Salvador, A. R.; Ballesteros, M. Engineering a Multivariate Cobalt Metal–Organic Framework for High Photocatalytic Activity: The Impact of Mixed Ligands and Metal Incorporation in a Visible Light-Driven Heterogeneous Photo-Fenton Reaction for Water Treatment. *Nanoscale Adv.* **2025**, *7* (8), 2255–2265.

(55) Jia, X.; Xie, L.; Li, Z.; Li, Y.; Ming, R.; Zhang, Q.; Mi, X.; Zhan, S. Photo-Electro-Fenton-like Process for Rapid Ciprofloxacin Removal: The Indispensable Role of Polyvalent Manganese in Fe-Free System. *Science of the Total Environment* **2021**, *768*, 144368.

(56) Mansoori, S.; Ozumchelouei, E. J.; Davarnejad, R.; Zahrani, A. A. CuO_x-MnO_y@ Biochar Nanocatalyst Synthesis for Heterogeneous Visible-Light-Driven Fenton-like: A Resistant Antibiotic Degradation. *Catal. Commun.* **2022**, *171*, 106517.

(57) Singh, N.; Sinha, I. Development of Cu, Mn Codoped $BiVO_4$ ($Cu_xMn_{0.03-X}Bi_{1-x}V_{0.97+\ x}\ O_4$) Photocatalyst for Photo-Fenton Degradation of Ciprofloxacin. *Langmuir* **2025**.

(58) Campagnoli, E.; Tavares, A.; Fabbrini, L.; Rossetti, I.; Dubitsky, Y. A.; Zaopo, A.; Forni, L. Effect of Preparation Method on Activity and Stability of $LaMnO_3$ and $LaCoO_3$ Catalysts for the Flameless Combustion of Methane. *Appl. Catal. B* **2005**, *55* (2), 133–139.

(59) Yang, G.; Liang, Y.; Xiong, Z.; Yang, J.; Wang, K.; Zeng, Z. Molten Salt-Assisted Synthesis of Ce_4O_7/Bi_4MoO_9 Heterojunction Photocatalysts for Photo-Fenton Degradation of Tetracycline: Enhanced Mechanism, Degradation Pathway and Products Toxicity Assessment. *Chemical Engineering Journal* **2021**, *425*, 130689.

(60) Gao, B.; Pan, Y.; Yang, H. Enhanced Photo-Fenton Degradation of Fluoroquinolones in Water Assisted by a 3D Composite Sponge Complexed with a S-Scheme MoS_2/Bi_2S_3/$BiVO_4$ Ternary Photocatalyst. *Appl. Catal. B* **2022**, *315*, 121580.

(61) Liu, R.; Li, R.; Yang, L.; Wang, R.-X.; Chen, H.-Y.; Wang, N.; Li, Z.; Chen, Y.-Q.; Ramakrishna, S.; Long, Y.-Z. FeOOH Quantum Dot-Coupled Z-Scheme $BiVO_4$/g-C_3N_4 Heterojunction for Enhancing Photo-Fenton Reactions. *ACS Appl. Nano Mater.* **2023**, *6* (18), 17009–17020.

(62) Zhou, Q.; Xing, A.; Li, J.; Zhao, D.; Zhao, K.; Lei, M. Synergistic Enhancement in Photoelectrocatalytic Degradation of Bisphenol A by CeO_2 and Reduced Graphene Oxide Co-Modified TiO_2 Nanotube Arrays in Combination with Fenton Oxidation. *Electrochim. Acta* **2016**, *209*, 379–388.

(63) Suryaa, K. V.; Balakrishnan, A.; Chinthala, M.; Devi, K. B.; Tripathy, H.; Kumar, A.; Aminabhavi, T. M.; Rtimi, S. Photocatalytic Self-Fenton Degradation of Tetracycline over Z-Scheme Functionalized g-C_3N_4/CeO_2/Bi_2S_3 Hydrogel Beads: Dynamics, Mechanism, Degradation Pathways and Toxicity Analysis. *Chemical Engineering Journal* **2025**, *505*, 159470.

(64) Liang, L.; Gao, S.; Zhu, J.; Wang, L.; Xiong, Y.; Xia, X.; Yang, L. The Enhanced Photocatalytic Performance toward Carbamazepine by Nitrogen-Doped Carbon Dots Decorated on BiOBr/CeO_2: Mechanism Insight and Degradation Pathways. *Chemical Engineering Journal* **2020**, *391*, 123599.

(65) Liu, Y.; Wang, J. Multivalent Metal Catalysts in Fenton/Fenton-like Oxidation System: A Critical Review. *Chemical Engineering Journal* **2023**, *466*, 143147.

(66) Prajapati, J.; Maharana, N.; Bhoi, B.; Badola, A.; Chaturvedi, S.; Chandra, V. Solar-Powered Degradation of Malachite Green Dye via α-MnO_2 Nanorods with CTAB-Mediated Electron Trapping. *Next Materials* **2026**, *10*, 101511.

(67)Anitha, T. V; Menon, K. G.; Venugopal, K.; Vimalkumar, T. V. Investigating the Role of Film Thickness on the Physical Properties of Sol-Gel Coated CuO Thin Films: Discussing Its Potentiality in Optoelectronic Applications. *Materials Science and Engineering: B* **2024**, *299*, 116960.

(68)Aktas, S.; Hasanli, I. S.; Demiroglu, A.; Caglar, M. Band Gap Tunability and Optical Properties of Sol-Gel Derived Fe-Doped CeO_2 Films. *Physica B Condens. Matter* **2024**, *675*, 415621.

(69) Li, F.; Wu, W.; Liu, G.; Liu, X.; Dong, L.; Wang, D.; Huang, Y.; Zhang, J.; Yang, Z.; Yang, W. Synergistical Promotion of Carrier Separation of Z-Scheme BiOBr/Bi_2O_3 Heterojunctions with Band-Gap Design and Oxygen Defects for Co-Catalysis of CIP and Cr (VI). *J. Alloys Compd.* **2025**, 181810.

(70) Ahamed, M.; Ali, S. M.; Lateef, R.; Dotto, G. L.; Alhadlaq, H. A. Oxygen-Vacancy Engineering and Junction Design in CeO_2 Nanomaterials for Photocatalysis and Antibacterial Action: A Review. *Results in Engineering* **2025**, 108076.

(71) Wang, A.; Zheng, Z.; Wang, H.; Chen, Y.; Luo, C.; Liang, D.; Hu, B.; Qiu, R.; Yan, K. 3D Hierarchical H2-Reduced Mn-Doped CeO_2 Microflowers Assembled from Nanotubes as a High-Performance Fenton-like Photocatalyst for Tetracycline Antibiotics Degradation. *Appl. Catal. B* **2020**, *277*, 119171.

(72) Kumar, S. R. A.; Mary, D. V.; Josephine, G. A. S.; Sivasamy, A. Hydrothermally Synthesized WO_3: CeO_2 Supported GC_3N_4 Nanolayers for Rapid Photocatalytic Degradation of Azo Dye under Natural Sunlight. *Inorg. Chem. Commun.* **2024**, *164*, 112366.

(73) Liu, Q.; He, J.; Yang, W.; Wu, Q.; Zou, L.; Wu, Y.; Yang, L.; Shi, G.; Yang, X. Mesoporous Ceria Nanoparticles for Ultra-Fast and Highly Flexible Photo-Fenton Catalytic Reaction. *J. Photochem. Photobiol. A Chem.* **2023**, *435*, 114309.

(74) Hassani, A.; Eghbali, P.; Ghanbari, F. Layered double hydroxide (LDH)-based materials applied in advanced photocatalytic oxidation of pharmaceuticals. In *Advanced materials for pharmaceutical wastewater treatment*; Hassani, A., Ed.; CRC Press, **2024**; pp 147–171.

(75) Huang, R.; Liang, D.; Zhang, W.; Gan, T.; Hu, H.; Huang, Z.; Zhang, Y. Hydrogen Bond-Induced Supramolecular Self-Assembly Strategy to Fabricate Ultra-Dispersed Cu-Loaded Porous Tubular Graphitic Carbon Nitride with Rich Nitrogen Vacancies and CuN_x Sites for Efficient Photo-Fenton Catalysis. *J. Colloid Interface Sci.* **2025**, *678*, 987–1000.

(76) Zhou, W.; Ding, X.; Li, W.; Zhao, L.; Lu, Y.; Zhao, M.; Ma, F.; Wen, Z.; Zhang, H.; Feng, J. Copper Deposition on MgO Surfaces: Synergistic Effect of Multivalent Cu and Oxygen Vacancies Efficiently Activates H_2O_2 and Enhances Photo-Fenton Efficiency. *Colloids Surf. A Physicochem. Eng. Asp.* **2025**, 139074.

(77) Wang, Y.; Wang, Q.; Zhan, X.; Wang, F.; Safdar, M.; He, J. Visible Light Driven Type II Heterostructures and Their Enhanced Photocatalysis Properties: A Review. *Nanoscale* **2013**, *5* (18), 8326–8339.

(78) Wang, Y.; Yang, C.; Zhang, K.; Guo, L.; Li, R.; Zaheer, A.; Fu, F.; Xu, B.; Wang, D. In-Situ Construction of 2D/2D $CuCo_2S_4/Bi_2WO_6$ Contact Heterojunction as a Visible-Light-Driven Fenton-like Catalyst with Highly Efficient Charge Transfer for Highly Efficient Degradation of Tetracycline Hydrochloride. *Colloids Surf. A Physicochem. Eng. Asp.* **2022**, *634*, 127965.

(79) Guo, L.; Zhang, K.; Han, X.; Zhao, Q.; Zhang, Y.; Qi, M.; Wang, D.; Fu, F. 2D/2D Type-II Cu_2ZnSnS_4/Bi_2WO_6 Heterojunctions to Promote Visible-Light-Driven Photo-Fenton Catalytic Activity. *Chinese Journal of Catalysis* **2020**, *41* (3), 503–513.

(80) Low, J.; Jiang, C.; Cheng, B.; Wageh, S.; Al-Ghamdi, A. A.; Yu, J. A Review of Direct Z-scheme Photocatalysts. *Small Methods* **2017**, *1* (5), 1700080.

(81) Zhang, Q.; Peng, Y.; Deng, F.; Wang, M.; Chen, D. Porous Z-Scheme MnO_2/Mn-Modified Alkalinized g-C_3N_4 Heterojunction with Excellent Fenton-like Photocatalytic Activity for Efficient Degradation of Pharmaceutical Pollutants. *Sep. Purif. Technol.* **2020**, *246*, 116890.

(82) Wang, X.; Sayed, M.; Ruzimuradov, O.; Zhang, J.; Fan, Y.; Li, X.; Bai, X.; Low, J. A Review of Step-Scheme Photocatalysts. *Appl. Mater. Today* **2022**, *29*, 101609.

(83) Kumar, O. P.; Shahzad, K.; Nazir, M. A.; Farooq, N.; Malik, M.; Shah, S. S. A.; ur Rehman, A. Photo-Fenton Activated $C_3N_{4x}/AgO_y@Co_{1-x}Bi_{0.\ 1-Y}O_7$ Dual S-Scheme Heterojunction towards Degradation of Organic Pollutants. *Opt. Mater. (Amst).* **2022**, *126*, 112199.

(84) Gao, M.; Li, Z.; Su, X.; Zhang, X.; Chang, J.; Geng, D.; Lu, Y.; Zhang, H.; Wei, T.; Feng, J. 2D/2D MgO/g-C_3N_4 S-Scheme Heterogeneous Tight with Mg–N Bonds for Efficient Photo-Fenton

Degradation: Enhancing Both Oxygen Vacancy and Charge Migration. *Chemosphere* **2023**, *343*, 140285.

(85) Wang, J.-W.; Chen, W.; Han, D.-M.; Chen, J.-R. S-Scheme $CuInS_2/WO_3$ Hybrid Heterostructures as Catalysts for Visible-Light-Driven Photo-Fenton Degradation of Tetracycline Hydrochloride. *Opt. Mater. (Amst).* **2023**, *138*, 113635.

(86) Sreedhar, A.; Ta, Q. T. H.; Noh, J.-S. Role of P-n Junction Initiated Mixed-Dimensional 0D/2D, 1D/2D, and 2D/2D BiOX (X= Cl, Br, and I)/TiO_2 Nanocomposite Interfaces for Environmental Remediation Applications: A Review. *Chemosphere* **2022**, *305*, 135478.

(87) Wang, J.; Jia, X.; Shang, D.; Xie, L.; Li, Y.; Zhang, H.; Zhan, S.; Hu, W. Constructing Cu_2O/Bi_2MoO_6 p–n Heterojunction towards Boosted Photo-Assisted-Electro-Fenton-like Synergy Degradation of Ciprofloxacin. *Environ. Sci. Nano* **2021**, *8* (12), 3629–3642.

(88) Shi, X.; Chen, Q.; Qin, X.; Rao, X.; Li, S.; Liu, G.; Wang, J.; Dong, X.; Chen, F.; Luo, D. Robust $Bi_4Ti_3O_{12}$-$CuBi_2O_4$ p-n Heterojunction with Enhanced Piezo-Photocatalytic Activity Boosted by Cu (II)-Catalysed Fenton-like Reaction. *J. Alloys Compd.* **2025**, *1020*, 179472.

(89) Liu, K.; Shi, L.; Guo, Y.; Hao, S.; Zhai, Y.; Liu, Y. Construction of a Novel $Cu_2(OH)_3F/Cu_2O$ Np Heterojunction by in-Situ Reduction: Photo-Fenton-like Synergistic Promotion of Efficient Cu^{2+}/Cu^{+} Cycling. *J. Catal.* **2024**, *435*, 115544.

(90) Guo, L.; Zhang, K.; Han, X.; Zhao, Q.; Wang, D.; Fu, F. 2D In-Plane CuS/Bi_2WO_6 P-n Heterostructures with Promoted Visible-Light-Driven Photo-Fenton Degradation Performance. *Nanomaterials* **2019**, *9* (8), 1151.

(91) Kumari, P.; Bahadur, N.; Kong, L.; O'Dell, L. A.; Merenda, A.; Dumée, L. F. Engineering Schottky-like and Heterojunction Materials for Enhanced Photocatalysis Performance–a Review. *Mater. Adv.* **2022**, *3* (5), 2309–2323.

(92) Zhong, Q.; Li, Y.; Liu, J.; Li, J.; Zhang, G. In Situ Construction of Ti^{3+} Self-Doped TiO_2/Ti_3C_2 Schottky Heterojunctions for Highly Selective Photo-Fenton-like Degradation of Organic Pollutants: Surface/Interface Effect and Mechanism Insight. *Appl. Surf. Sci.* **2024**, *667*, 160376.

(93) Wang, Y.; Yang, W.; Ding, K. Synergistic Ag/g–C_3N_4 H_2O_2 System for Photocatalytic Degradation of Azo Dyes. *Molecules* **2024**, *29* (16), 3871.

(94) Xiong, L.; Li, R.; Ba, K.; Chen, L.; Shi, Y.; Yu, Y.; Yang, M. Dual-Metal Synergy and Interfacial Electric Field Engineering in CNNS/Ni-Ag Heterostructure for Sacrificial Agent-Free in-Situ H_2O_2-Enabled Self-Photo-Driven Fenton Degradation. *Applied Catalysis B: Environment and Energy* **2025**, 126032.

(95) Dihingia, H.; Tiwari, D. Green and Facile Synthesis of Heterojunction Nanocatalyst (Cu^0+ Ag^0@ Supported Bentonite): Insights into the Removal of Potential Antibiotics. *Available at SSRN 4193816*.

(96) Hu, Y.; Ke, J.; Yan, Z.; Zhao, L.; Liu, J. Facile Construction of Dual-Metal Modified Bi_2MoO_6 Plasmonic Heterojunction for Enhanced Photo-Assisted Fenton Performances. *Colloids Surf. A Physicochem. Eng. Asp.* **2025**, 137409.

(97) Zhang, X.; Liu, Y.; Zhai, Y.; Yu, Y.; Guo, Y.; Hao, S. An Optimization Strategy for Photo-Fenton-like Catalysts: Based on Crystal Plane Engineering of $BiVO_4$ and Electron Transfer Properties of 0D CQDs. *Environ. Res.* **2023**, *222*, 115347.

(98) Tan, Z.; Wang, R.; Yang, S.; Shi, Z.; Wang, D. Fabrication of Cu-Cu_2ON Doped Carbon with High Photo-Fenton Catalytic Activity Using a Cu-Nicotinic Acid Framework: Insight into Structural Transformation. *J. Mol. Struct.* **2025**, *1337*, 142248.

(99) Sharma, K.; Raizada, P.; Hosseini-Bandegharaei, A.; Thakur, P.; Kumar, R.; Thakur, V. K.; Nguyen, V.-H.; Pardeep, S. Fabrication of Efficient CuO/Graphitic Carbon Nitride Based Heterogeneous Photo-Fenton like Catalyst for Degradation of 2, 4 Dimethyl Phenol. *Process Safety and Environmental Protection* **2020**, *142*, 63–75.

(100) Taha, A. A.; Huang, L.; Ma, H.; Ramakrishna, S.; Liu, Y. Metal-Free Nitrogen-Doped Porous Carbon Nanofiber Catalyst for Solar-Fenton-like System: Efficient, Reusable and Active Catalyst over a Wide Range of pH. *Colloids Surf. A Physicochem. Eng. Asp.* **2023**, *663*, 131021.

(101) Cui, X.; Li, J.; Ng, D. H. L.; Liu, J.; Liu, Y.; Yang, W. 3D Hierarchical ACFs-Based Micromotors as Efficient Photo-Fenton-like Catalysts. *Carbon N. Y.* **2020**, *158*, 738–748.

(102) Guo, Z.; Yang, G.; Wu, Y.; Long, J.; He, H.; Ren, X.; Huang, B.; Pan, X.; Liang, Y. Molten Salt Defect Engineering Regulation of Bi_4TaO_8Cl Perovskite Structure for Boosting Photo-Fenton Degradation of Antibiotics. *Chemical Engineering Journal* **2024**, *496*, 153923.

(103) Zhang, S.; Wang, R.; Wang, K.; Wang, M.; He, Z.; Chen, H.; Ho, S.-H. Aeration-Free in Situ Fenton-like Reaction: Specific Adsorption and Activation of Oxygen on Heterophase Oxygen Vacancies. *Environ. Sci. Technol.* **2024**, *58* (4), 1921–1933.

(104) Zhang, W.; Wang, L.; Hou, C.; Zhu, Z.; Lichtfouse, E.; Trapalis, C.; Wang, C. Combined Effect of Cu^0 and Oxygen Vacancies in Cu-Based Zeolites Enables Highly Efficient Photo-Fenton-like Performance for Water Purification. *Environ. Sci. Nano* **2024**, *11* (6), 2481–2493.

(105) Brindha, B.; Syed, A.; Balakrishnaraja, R.; Elgorban, A. M.; Abid, I.; Wong, L. S.; Khan, S. S. Stabilize the Oxygen Vacancies in ZnO via Altering Local Electronic Structure by Co and Ni Doping: A Novel Strategy for Achieving Durable Visible Light Driven Photo-Fenton Degradation of Chloramphenicol. *Colloids Surf. A Physicochem. Eng. Asp.* **2025**, *707*, 135796.

(106) Wang, D.; Wang, H.; Tan, Z.; Almalki, A. S. A.; Fallatah, A. M.; Yang, S.; Shi, Z. In-Situ Preparation of $CuO/Cu_2O/Cu$/N-Codoped Biochar from Chitosan Derivative: Adsorption Property and Photo-Fenton Catalytic Performance in Removal of Antibiotic. *Adv. Compos. Hybrid Mater.* **2025**, *8* (1), 2.

(107) Wang, S.; Wang, Y.; Cao, L.; Zhang, J.; Liu, Y.; Wang, B.; Li, M. Boosting Photoelectricity Based on Self-Supported Flexible Metal–Organic Framework Arrays for Photo-Fenton-like Degradation of Organic Pollutants. *J. Mater. Chem. C Mater.* **2025**, *13* (11), 5526–5535.

(108) Abdelhaleem, A.; Abdelhamid, H. N.; Ibrahim, M. G.; Chu, W. Photocatalytic Degradation of Paracetamol Using Photo-Fenton-like Metal-Organic Framework-Derived CuO@C under Visible LED. *J. Clean. Prod.* **2022**, *379*, 134571.

(109) Si, C.; Liu, X.; Zhang, T.; Xu, J.; Li, J.; Fu, J.; Han, Q. Constructing a Photocatalyst for Selective Oxidation of Benzyl Alcohol to Benzaldehyde by Photo-Fenton-like Catalysis. *Inorg. Chem.* **2023**, *62* (10), 4210–4219.

(110) He, Z.; Shi, T.; Chen, D.; Wang, Y.; Feng, Y.; Zhou, F.; Li, Y. Ultrathin CuZnCr-LDH Nanosheets for Photo-Fenton Synergistic Degradation of Ciprofloxacin and Methylene Blue. *J. Alloys Compd.* **2025**, *1010*, 177302.

(111) Zhu, Z.; Wang, L.; Zhang, W.; Hou, C.; Wang, C.; Zhao, J. Ultrathin $CuNi_2Al$-LDH Nanosheets with Enhanced Electron Transfer for Visible-Light-Driven Photo-Fenton-like Water Decontamination. *Chemical Engineering Journal* **2024**, *481*, 148313.

(112) Dong, S.; Chen, X.; Su, L.; Wen, Y.; Wang, Y.; Yang, Q.; Yi, L.; Xu, W.; Yang, Q.; He, P. Integration of Atomically Dispersed $Cu–N_4$ Sites with C_3N_4 for Enhanced Photo-Fenton Degradation over a Nonradical Mechanism. *ACS ES&T Engineering* **2022**, *3* (2), 150–164.

(113) Lian, Z.; Gao, F.; Xiao, H.; Luo, D.; Li, M.; Fang, D.; Yang, Y.; Zi, J.; Li, H. Photo-self-Fenton Reaction Mediated by Atomically Dispersed Ag− Co Photocatalysts toward Efficient Degradation of Organic Pollutants. *Angewandte Chemie International Edition* **2024**, *63* (8), e202318927.

(114) Zhang, X.; Xu, B.; Wang, S.; Li, X.; Liu, B.; Xu, Y.; Yu, P.; Sun, Y. High-Density Dispersion of CuN_x Sites for H_2O_2 Activation toward Enhanced Photo-Fenton Performance in Antibiotic Contaminant Degradation. *J. Hazard. Mater.* **2022**, *423*, 127039.

(115) Li, D.; Zhang, Y.; Zhu, H.; Zhu, R.; Bai, X.; Dang, J.; Song, F.; Zhou, J. Investigation on Photo-Assisted Fenton-like Mechanism of Bismuth Single-Atom Charge Transfer Bridge in Bi@g-C_3N_4/CoNi-LDH Step-Scheme Heterojunction. *J. Environ. Chem. Eng.* **2025**, 119483.

(116) Anuraag, N. S.; Kumar, U.; Pradhan, S.; Shaw, S. K.; Sharma, A.; Sinha, I.; Prasad, N. K. Rhombohedral Phase High-Entropy Alloy of AlMnCuZnBi as a Photo-Fenton Catalyst for Methyl Orange Degradation. *J. Alloys Compd.* **2025**, *1010*, 177142.

(117) Mohapatra, S.; Das, H. T.; Tripathy, B. C.; Das, N. Unleashing the Electrochemical/Photocatalytic Activity of $Co_9Se_8/Ni_3Se_4/Cu_2Se$ Ternary Nanocomposites for Sustainable Energy Storage and Photo-Fenton Based Pollutants Degradation. *Adv. Sustain. Syst.* **2024**, *8* (12), 2400405.

(118) Rozmyślak, M.; Walkowiak, A.; Frankowski, M.; Wolski, L. Copper (II) Phosphate as a Promising Catalyst for the Degradation of Ciprofloxacin via Photo-Assisted Fenton-like Process. *Sci. Rep.* **2024**, *14* (1), 7007.

(119) Almahri, A. Fenton-like Photocatalytic Degradation of Rhodamine 6G and Tetracycline under Sunlight Irradiation Using Hexahydroxy Copper-Stannate $CuSn(OH)_6$. *Inorg. Chem. Commun.* **2025**, *177*, 114340.

(120) Qin, G.; Song, X.; Chen, Q.; He, W.; Yang, J.; Li, Y.; Zhang, Y.; Wang, J.; Dionysiou, D. D. Novel Durable and Recyclable $Cu@MoS_2$/Polyacrylamide/Copper Alginate Hydrogel Photo-Fenton-like Catalyst with Enhanced and Self-Regenerable Adsorption and Degradation of High Concentration Tetracycline. *Applied Catalysis B: Environment and Energy* **2024**, *344*, 123640.

(121) Tang, Y.; Li, X.; Zhang, H.; Ouyang, T.; Jiang, Y.; Mu, M.; Yin, X. Cobalt-Based ZIF Coordinated Hybrids with Defective TiO_{2-x} for Boosting Visible Light-Driven Photo-Fenton-like Degradation of Bisphenol A. *Chemosphere* **2020**, *259*, 127431.

(122) Li, S.; Zhang, J.; Cao, Y.; Yang, Y.; Xie, T.; Lin, Y. Visible Light Assisted Heterogeneous Photo-Fenton-like Degradation of Rhodamine B Based on the Co-POM/N-TiO_2 Composites: Catalyst Properties, Photogenerated Carrier Transfer and Degradation Mechanism. *Colloids Surf. A Physicochem. Eng. Asp.* **2022**, *648*, 129248.

(123) Zhou, Q.; Zhang, J.; Shu, Q.; Yu, F.; Guo, Y. Construction of Platinum/Cobalt Aluminate Heterostructured Catalyst via Spent Catalyst Recycling for Photo-Fenton-like Degradation of Malathion. *Journal of Water Process Engineering* **2026**, *81*, 109253.

(124) Zhu, Y.; Li, J.; Lai, Y.; Cao, Y.; Li, J.; Wei, Z.; Yang, L.; Chen, Z.; Zou, J. Accelerated Photo-Fenton Degradation of Ciprofloxacin on CoS_x@ TiO_2 Amorphous-Crystalline Interface with SO Bond Bridging. *Environ. Res.* **2025**, *279*, 121785.

(125) Peng, G.; Xie, Y.; Chen, H.; Zou, J.; Li, L.; Luo, C.; Lu, L.; Mao, G. Frustrated Lewis Pairs Created by Ce-Doped Bi_2MoO_6: A Universal Strategy to Promote Efficient Utilization of H_2O_2 for Fenton-like Photodegradation. *Chemosphere* **2024**, *356*, 141952.

(126) Ralte, L.; Goswami, S.; Tiwari, D.; Jung, J. Novel Iron Free Nano-Fenton-like Catalyst for Sustainable Treatment of Antibiotics and Cyanobacteria. *J. Clean. Prod.* **2025**, *496*, 144982.

(127) Hu, K.; Li, J.; Han, Y.; Ng, D. H. L.; Xing, N.; Lyu, Y. A Colorimetric Detection Strategy and Micromotor-Assisted Photo-Fenton-like Degradation for Hydroquinone Based on the Peroxidase-like Activity of Co_3O_4–CeO_2 Nanocages. *Catal. Sci. Technol.* **2022**, *12* (23), 7161–7170.

(128) Han, C.; Zhou, Q.; Tao, Q.; Li, X.; Zhao, B.; Jing, Q. Photochemical Fabrication of CuS-Based Compounds Driven by UV Irradiation and Their Photo-Fenton-like Catalytic Activity. *J. Alloys Compd.* **2025**, 184749.

(129) Tzvetkov, G.; Tsvetkov, M.; Spassov, T. Self-Sacrificing Template Fabrication of Mesoporous CuO Micro/Nanoplates for Photo-Fenton-like Oxidation of Sulfathiazole. *Mater. Lett.* **2025**, *378*, 137582.

(130) Liu, Q.; Zhou, C.; Li, X.; He, Y.; Fan, Y.; Meng, Y.; Xu, M. Dual-Functional Photocatalytic Composites Featuring Direct Z-Scheme Heterojunctions and Photo-Fenton Reactions. *J. Photochem. Photobiol. A Chem.* **2025**, 116937.

(131) Mokoba, T.; Li, Z.; Zhang, T. C.; Yuan, S. Superwetting Sea Urchin-like BiOBr@Co_3O_4 Nanowire Clusters-Coated Copper Mesh with Efficient Emulsion Separation and Photo-Fenton-like Degradation of Soluble Dye. *Appl. Surf. Sci.* **2022**, *594*, 153497.

(132) Li, J.; Ma, T.; Guo, P.; Zhao, C.; Xu, P.; Luo, D. Octahedral Alloyed PtCu-BTC for Photothermal Synergistic Enhanced Photo-Fenton Degradation of Organic Dye Contaminant. *Environ. Res.* **2025**, 122863.

(133) Imran, M.; Abdullah, A. Z.; Khan, M. E.; Kim, Y.-M.; Khan, F. Excellent Successive Photo-Induced Degradation of Tetracycline Using CuO/g-C_3N_4 Nanocomposites: Synergistic Effects of CuO Integration and H_2O_2 in a Photo-Fenton System. *J. Taiwan Inst. Chem. Eng.* **2025**, *171*, 106068.

(134) da Rocha, A. C.; Dantas, Á. de O. S.; Vieira, P. A.; Cardoso, V. L. Evaluation of Basalt Powder as a Natural Heterogeneous Catalyst in Photo-Fenton-like Treatment of Atrazine. *J. Photochem. Photobiol. A Chem.* **2024**, *446*, 115149.

(135) Liu, Y.; Liu, W.; Du, M.; Li, W.; Masuda, H.; Kang, S. HOFs Structured CN Template Enables the Dual Regulation of Cu–O and Cu–N Active Sites in Porous Cu-g-CN for Synergistic Photo-Fenton Process. *J. Environ. Chem. Eng.* **2024**, *12* (2), 112291.

(136) He, R.-M.; Yang, Y.-L.; Chen, H.-J.; Liu, J.-J.; Sun, Y.-M.; Guo, W.-N.; Li, D.-H.; Hou, X.-J.; Suo, G.-Q.; Ye, X.-H. In Situ Controllable Growth of Cu_7S_4 Nanosheets on Copper Mesh for Catalysis: The Synergistic Effect of Photocatalytic Fenton-like Process. *Colloids Surf. A Physicochem. Eng. Asp.* **2022**, *642*, 128651.

(137) Ji, J.-J.; Cui, Z.-W.; Liu, Q.-Q.; Shi, S.; Long, J.-Y.; Wang, X.-L.; Fei, B.-L. Synthesis, Characterization and Heterogeneous Photo-Fenton-like Catalyst Activity of a Novel Inorganic-

Organic 2D Framework Based on Reduced α-Keggin Phosphomolybdate. *Mater. Chem. Phys.* **2023**, *302*, 127692.

(138) Wen, T.; Zhao, Y.; Jiao, X.; Yang, G.; Zhang, Z.; Wang, W.; Zhang, T.; Zhang, Q.; Song, S. Use of Posnjakite Containing Sludge as Catalyst for Decoloring Dye via Photo-Fenton-like Process. *J. Clean. Prod.* **2021**, *293*, 126184.

(139) Betim, F. S.; Marins, A. A. L.; Coelho, E. L. D.; Lelis, M. F. F.; Freitas, M. Evaluation of Photocatalytic Properties of Zinc and Cobalt Mixed Oxide Recycled from Spent Li-Ion and Zn–MnO_2 Batteries in Photo-Fenton-like Process. *Mater. Res. Bull.* **2023**, *162*, 112179.

(140) Kaewdee, P.; Tupberg, C.; Tandorn, S.; Boontakam, W.; Saenkam, K.; Limpichaipanit, A.; Rujijanagul, G.; Thavornyutikarn, P.; Randorn, C. Redox-Active Shapeable Phosphate-Based Glass Containing CuO for Long-Life Photo-Fenton Catalytic Applications. *Chemical Engineering Journal Advances* **2025**, 100833.

(141) Vasilyeva, M. S.; Lukiyanchuk, I. V; Sergeev, A. A.; Sergeeva, K. A.; Ustinov, A. Y.; Tkachev, V. V; Arefieva, O. D. Plasma Electrolytic Synthesis and Characterization of Oxide Coatings with MWO_4 (M= Co, Ni, Cu) as Photo-Fenton Heterogeneous Catalysts. *Surf. Coat. Technol.* **2021**, *424*, 127640.

(142) Mahamallik, P.; Pal, A. Photo-Fenton Process in Co (II)-Adsorbed Admicellar Soft-Template on Alumina Support for Methyl Orange Degradation. *Catal. Today* **2020**, *348*, 212–222.

(143) Tian, Q.; Ran, M.; Fang, G.; Ding, L.; Pan, A.; Shen, K.; Deng, Y. $ZnAl_2O_4$/$BiPO_4$ Composites as a Heterogeneous Catalyst for Photo-Fenton Treatment of Textile and Pulping Wastewater. *Sep. Purif. Technol.* **2020**, *239*, 116574.

(144) Khudkham, T.; Channei, D.; Pinchaipat, B.; Chotima, R. Degradation of Methylene Blue with a Cu(II)–Quinoline Complex Immobilized on a Silica Support as a Photo-Fenton-like Catalyst. *ACS Omega* **2022**, *7* (37), 33258–33265.

(145) Hurtado, L.; Avilés, O.; Brewer, S.; Donkor, K. K.; Romero, R.; Gómez-Espinosa, R. M.; Alvarado, O.; Natividad, R. Al/Cu-PILC as a Photo-Fenton Catalyst: Paracetamol Mineralization. *ACS Omega* **2022**, *7* (27), 23821–23832.

(146) Liu, C.; Xue, S. Efficient Photo-Assisted Fenton-like Reaction of Yolk–Shell CuSe (Cu_2Se)/GC_3N_4 Heterojunctions for Methylene Blue Degradation. *RSC Adv.* **2023**, *13* (13), 8464–8475.

(147) Hazarika, B.; Hazarika, B. J.; Ahmed, M. J. K. Visible-Light Induced Photo-Fenton-Like Degradation of Pharmaceuticals Via Advanced Oxidation Process Using Ag@SnO_2 Nanocomposite Fabricated Via a Green in-Situ Strategy. *J. Clust. Sci.* **2025**, *36* (6), 233.

(148) Zhou, G.; Yang, F.; Zhu, X.; Feng, W.; Chen, D.; Fang, J. Copper-Copper Oxide Heterostructural Nanocrystals Anchored on g-C_3N_4 Nanosheets for Efficient Visible-Light-Driven Photo-Fenton-like Catalysis. *Molecules* **2025**, *30* (1), 144.

(149) Nehhal, S.; Ben Ali, M.; Abrouki, Y.; Ofqir, K.; Elkahoui, Y.; Labjar, N.; Nasrellah, H.; El Hajjaji, S. Photocatalytic and Photo-Fenton-like Degradation of Methylene Blue Using Green-Synthesized Phosphate-Doped ZnO Under Visible LED Light. *Reactions* **2025**, *6* (4), 64.

(150) Muthusami, R.; Ramachandran, V.; Palaniappan, M.; Arumugam, S.; Palanisamy, K.; Irena, K.; Rangappan, R. Cu (II) Schiff Base Complex Functionalized Mesoporous Silica Nanoparticles as an Efficient Catalyst for the Synthesis of Questiomycin A and Photo-Fenton-like Rhodamine B Degradation. *J. Solid State Chem.* **2021**, *302*, 122429.

(151) Abdelbaky, M.; Abdelghany, A. M.; Oraby, A. H.; Abdelrazek, E. M.; Rashad, M. M. Efficacious Elimination of Crystal Violet Pollutant via Photo-Fenton Process Based on $Gd_{(2-x)}La_{(x)}Zr_2O_7$ Nanoparticles. *Sci. Rep.* **2023**, *13* (1), 7723.

(152) Dhadage, A.; Nagare, A.; Ghare, P.; Athare, A.; Gogoi, P.; Navgire, M. Ultrasonic Wave-Assisted Synthesis of CeO_2-MoO_3 Nanocomposite for Photo-Fenton Degradation of Rhodamine-B Dye. *Chemical Papers* **2024**, *78* (10), 5833–5850.

(153) Santos, A.; Yustos, P.; Quintanilla, A.; Ruiz, G.; Garcia-Ochoa, F. Study of the Copper Leaching in the Wet Oxidation of Phenol with CuO-Based Catalysts: Causes and Effects. *Appl. Catal. B* **2005**, *61* (3–4), 323–333.

(154) Mustapha, L. S.; Obayomi, O. V.; Obayomi, K. S. A comprehensive review on potential heavy metals in the environment: Persistence, bioaccumulation, ecotoxicology, and agricultural impacts. *Ecological Frontiers* **2025**.

(155) Bang, S.; Choi, J. W.; Cho, K.; Chung, C.; Kang, H.; Hong, S. W. Simultaneous reduction of copper and toxicity in semiconductor wastewater using protonated alginate beads. *Chemical Engineering Journal* **2016**, 288, 525–531.

(156) Patil, D. S.; Chavan, S. M.; Oubagaranadin, J. U. K. A review of technologies for manganese removal from wastewaters. *Journal of Environmental Chemical Engineering* **2016**, 4, 468–487.

View Article Online
DOI: 10.1039/D6LF00096G

View Article Online
DOI: 10.1039/D6LF00096G

Data Availability Statement

This article is based on analysis of previously published data. All relevant data supporting the findings of this study are included within the article. Original sources of the data are cited throughout the manuscript.